ZEOLITIC IMIDAZOLE FRAMEWORK ZIF-8 MEMBRANES FOR ENHANCED PROPYLENE/PROPANE SEPARATION

By

ANIL RONTE

Bachelor of Technology in Chemical Engineering

Chaitanya Bharathi Institute of Technology

Hyderabad, Telangana, India

2014

Master of Technology in Chemical Engineering

University College of Technology - Osmania University

Hyderabad, Telangana, India

2017

Submitted to the Faculty of the

Graduate College of the

Oklahoma State University

in partial fulfillment of

the requirements for

the Degree of

DOCTOR OF PHILOSOPHY

May, 2022

ZEOLITIC IMIDAZOLE FRAMEWORK ZIF-8 MEMBRANES FOR ENHANCED PROPYLENE/PROPANE SEPARATION

Dissertation Approved:

Dr. Seokjhin Kim

Dissertation Advisor

Dr. Jeffery L. White

Dr. David N. Mcllroy

Dr. Marimuthu Andiappan

ACKNOWLEDGEMENTS

First, I would like to express my gratitude to my esteemed supervisor, Dr. Seokjhin Kim, for the invaluable tutelage, advice, and support that he provided me throughout my academic research. His constant patience and guidance encouraged me to undertake the necessary research. I want to extend my gratitude to the Faculties of the Department of Chemical Engineering of Oklahoma State University for sharing their immense knowledge through the coursework.

Moreover, along with thanking Dr. Seokjhin Kim, I would also like to thank Dr. Jeff-White, Dr. Mari Andiappan, and Dr. David Mcllroy for their valuable support which has been influential in shaping the experiments I undertook, for critiquing my outcomes, and for agreeing to serve as my thesis committee members. The School of Chemical Engineering of OSU has made it possible for me to pursue a Ph.D. by extending funding opportunities. I am also grateful to Dr. David Mcllroy and his group members Elena Echeverria, Bastatas Lyndon, and Phadindra Wagle, for their suggestions during my Ph.D. study. I would also like to thank Brent Johnson, Lisa-White Worth, Eillen Nelson, Shelley Potter, and Beth Kelley for their continuous help and support.

I would like to thank my ex-lab mate, Shailesh Dangwal, for his continuous support and help which he provided me even after leaving OSU. My current lab mate Diako Mahmoodi constantly provided me with his insights and suggestions, and we cherished the time spent together in Dr. Kim's lab. Further, I would like to express my heartfelt thanks to all my friends namely, Harsha V. R., Aseem P. S., Sundaram B., Bertan O., Raviteja A.T, Sushobhan P, Sri Laxmi V who provided me with their love and companionship. My Special thanks to Mr. Abhiram Pamula for the guidance and support he gave me as a brother during my studies.

I am also pleased to express my gratitude toward Dr. B. Satyavathi, Mr. B. Suresh, Ms. B. Nagabhadra, Mr. G. Mallesh, and Ms. G. Uma are my teachers and mentors and will be forever indebted to them. Without their support, I would not have been able to get this prestigious Doctoral Degree.

Last but not the least; I would like to thank my father, Mr. Ramalaxmulu Ronte, and my mother, Ms. Kalavathi Ronte. I would not have been able to achieve any of my degrees without the immeasurable sacrifices they made and the support they gave to me. Their blessings have lasted with me all my life. They are the reason for all my accomplishments throughout my life. I also want to express my thanks to my siblings, Siva Naga Prasad G, Nanaiah Y, Srinivas Rao K, Rama Krishna S, and Sai Krishna A. They all have contributed emotionally and financially at a great scale all through my life. Being a student from a third-world country and a middle-class family, pursuing a Ph.D. was a distant dream for me in my early life. All my family members made it a reality. It is both a debt, which I will never be able to repay, and a decoration I will always wear as pride.

Name: ANIL RONTE

Date of Degree: MAY, 2022

Title of Study: ZEOLITIC IMIDAZOLE FRAMEWORK ZIF-8 MEMBRANES FOR ENHANCED PROPYLENE/PROPANE SEPARATION

Major Field: CHEMICAL ENGINEERING

Abstract: The separation of propylene/propane is essential in the refineries and most importantly, propylene is used as raw material to produce polymers and other intermediate chemicals. The separation of propylene/propane is challenging due to their similar physical properties. Currently, the separation carried out by the conventional distillation process requires a significant amount of operating energy and high capital cost. Therefore, energy-efficient alternative separation techniques are important in the separation processes. Compared to traditional technologies, membrane-based gas separation is a promising alternative substantial candidate for separation processing applications. However, the energy-efficient membrane-based propylene/propane gas separation was not commercialized due to the limited separation capability of current membrane materials. Zeolitic imidazolate frameworks (ZIFs) are a subclass of metal-organic frameworks that are promising membrane materials due to their well-defined ultra-micropores with superior thermal/chemical stabilities. In particular, a prototypical ZIF-8 has shown the potential separation capability of propylene/propane and received massive interest because of its effective aperture pore size of less than 0.5 nm, which is located in between propylene and propane molecular sizes. However, several challenges hinder their commercial purposes including non-economical ceramic supports, moderate batch process, lack of stability, and general processing methods. Since the microstructure of the membrane is greatly affected by the processing methods, it is important to investigate the optimization of new processing techniques. Moreover, to overcome the challenges in processing methods, a significant improvement is necessary. Therefore, the membrane productivity with separation efficiency can be enhanced by reducing membrane thickness and optimizing the fabrication techniques. This dissertation proposed novel membrane fabrication methods for superior propylene/propane separation efficiency with high flux ZIF-8 membranes for their practical applications. Three different methods were developed and investigated thoroughly including secondary growth, post-synthetic ZnO atomic layer deposition (ALD), and vapor-phase synthesis of ZIF-8. Moreover, the synthesized membranes were tested for propylene/propane separation measurements to optimize the fabrication techniques and the synthesized membranes were analyzed with a series of characterizations. First, secondary growth membranes were synthesized using silicalite nanoparticles as a seed layer. Using silicalite as seed material made it possible to achieve a high packing density of seed crystal layers in a couple of minutes, followed by 10 h of secondary growth method. It enabled us to obtain high-quality propylene selective ZIF-8 membranes with an average propylene/propane separation factor of ~170. Second, post-synthetic ALD treatment of ZnO on as-synthesized secondary grown ZIF-8 membranes was studied to reduce the surface defects and nonselective diffusion paths. The ALD ZIF-8 membranes stabilized effectively and exhibited a significant increase in separation factor up to ~270. Third, ZIF-8 membranes were prepared without using any solvents. The synthesis method was based on vapor-based technology. Initially, we deposited ZnO on the support surface followed by activation treatment with a ligand which was subsequently converted to a ZIF-8 membrane. The unique vapor-phase method was able to produce an ultra-thin ZIF-8 membrane with a thickness of ~400 nm. The resulting ultra-thin membranes showed significant improvement in propylene/propane membrane separation performance.

TABLE OF CONTENTS

Chapter Page

Chapter Page

LIST OF TABLES

LIST OF FIGURES

Figure Page

Figure Page

CHAPTER I

INTRODUCTION

Petrochemical industries use separation and purification processes for light olefins such as ethylene and propylene. The traditional separation process involves an energy-intensive distillation process which is expected to increase energy consumption. In the US, almost 15% of total energy consumption involves chemical separations in chemical/petrochemical industries [1]. The high energy demand for chemical separations also results in high operating costs and increases greenhouse gas emissions due to fossil fuel combustion [2-4]. Therefore, both from an economic and environmental standpoint, it is critical to investigate alternative methods for chemical separations. Recently, membrane-based gas separations have gained momentum in the area of chemical engineering as an alternative separation process [5, 6]. Membrane-based gas separations heavily rely on different membrane materials, and therefore researchers have investigated several materials to improve the efficiency of the gas separations. For propylene/propane gas separations, membrane materials that have been studied previously include polymers, carbon molecular sieves, and zeolites [7]. However, membrane technology has not yet been commercially available to separate light olefin/paraffin chemicals like ethylene and propylene. The main reason membranes lack commercial efficacy is because there are limitations in the separation capability of available membrane materials [8, 9]. Therefore, it is important to investigate the available membrane materials and improve the separation process efficiency of olefins/paraffin. Polymeric membranes are being tested for gas separation applications [10, 11]. However, one major limitation of polymeric membranes is the trade-off between permeability and selectivity. These polymeric membranes have plasticization and swelling issues at high pressure which reduces the selectivity of these membranes in gas separation applications [12]. One

promising membrane material candidate is an inorganic crystalline compound such as Metal-Organic Framework (MOF). Zeolitic-imidazole frameworks (ZIFs) are a subclass of MOFs consisting of multivalent metal cations and bidentate imidazolates. These ZIF-based membranes have well-defined micropores which make them useful for propylene/propane separation applications and have the potential to be used commercially [13, 14]. ZIFs have unique zeolite topologies because they have a metal-ligand-metal bond angle (145^{o}) which is similar to the Si-O-Si bond angle in zeolites [13]. In addition, ZIF-8 is formed as a membrane layer that consists of zinc cations coordinated with 2-methylimidazole (2-mIm) forming a metal topology that is promising for propylene/propane separation [15-17]. The current work deals with preparing ZIF-8 membranes using commercially available anodic aluminum oxide (AAO) substrates. In Aim I, The ZIF-8 membranes were fabricated using secondary growth on a silicalite-seeded AAO substrate to increase the membrane-substrate bonding. Other seeding materials were also investigated for ZIF-8 membrane fabrications. The effects of synthesis time and Zn source on silicalite-seeded AAO supports were investigated to improve the inter-crystalline growth between the support surface and ZIF-8 membranes. The synthesized ZIF-8 membranes were assessed for propylene/propane gas separations. In Aim II, the research on ZIF-8 membrane synthesis involves improving the separation efficiency of the membranes using ZnO-ALD treatment. In addition, the separation performance of ZIF-8 membranes was evaluated before and after ZnO-ALD treatment in Aim II. The vapor-phase method was used to fabricate ultra-thin propylene selective ZIF-8 membranes in Aim III. The ZIF-8 membranes synthesized from mentioned synthesis techniques in Aims I, II, and III were characterized using Scanning Electron Microscope (SEM), X-Ray Diffraction (XRD), Energy Dispersive X-Ray (EDX), X-ray photoelectron spectroscopy (XPS), Brunauer–Emmett–Teller (BET), and Fourier-Transform Infrared (FT-IR) Spectroscopy. All the dissertation goals and objectives are described in Aims I, II, and III, respectively.

Objectives

Aim I: Development of secondary grown ZIF-8 membranes on silicalite-seeded supports.

Significance: We plan to perform propylene/propane binary gas separation under Aim I. For this, we plan to design a secondary growth synthesis process by varying different parameters and developing seed material to fabricate ZIF-8 membranes. The purpose is to develop ZIF-8 membranes that efficiently separate the propylene/propane binary gas mixture. Developing and optimizing the synthesis process tasks were listed below followed by an illustration of the seeded secondary growth method on porous support shown in Figure 1.1.

Task A: Synthesis of ZIF-8 membranes using different seeding techniques

Task B: Investigation of the effects of parameters such as the Zn source, synthesis time, and seeding materials on ZIF-8 membrane performance

Task C: Evaluation of the membrane performance in propylene/propane separation

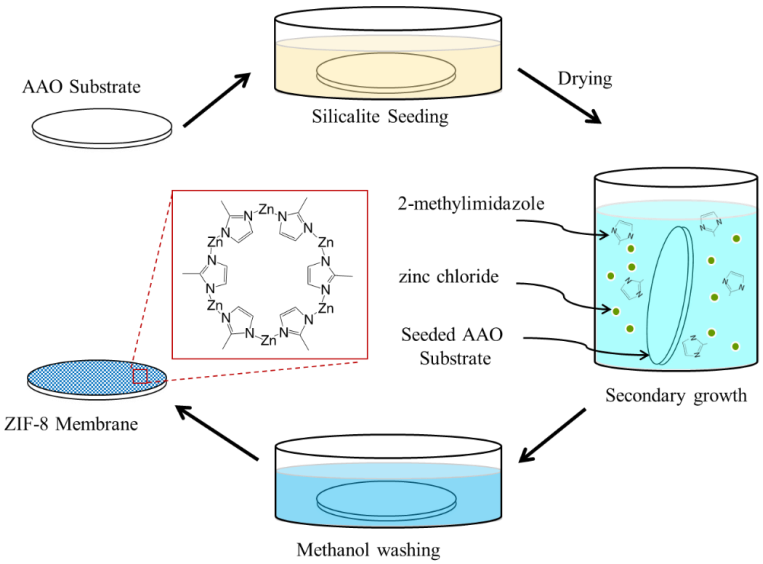

Figure 1.1: Schematic illustration of secondary growth synthesis on porous AAO support.

Aim II: Modification of as-synthesized ZIF-8 membrane surface by depositing ZnO using atomic layer deposition.

Significance: We plan to develop a post-synthetic metal treatment method to reduce the non-selective defects on the ZIF-8 membrane surface based on Aim I results and analysis observations. We plan to perform ZnO coating on the synthesized ZIF-8 membrane surface to enhance membrane separation efficiency by modifying the ZIF-8 membrane surface using atomic layer deposition (ALD). Investigation and optimization of ZnO coating on ZIF-8 membrane tasks were listed below followed by the schematic representation of the ZnO ALD process illustrated in Figure 1.2.

Task A: ZnO deposition on the ZIF-8 membranes for pore structure modification and reducing non-selective defects

Task B: Characterization of the ZIF-8 membranes using ALD to investigate the structural morphology

Task C: Evaluation of ZIF-8 and ZnO ALD ZIF-8 membranes in propylene/propane separation

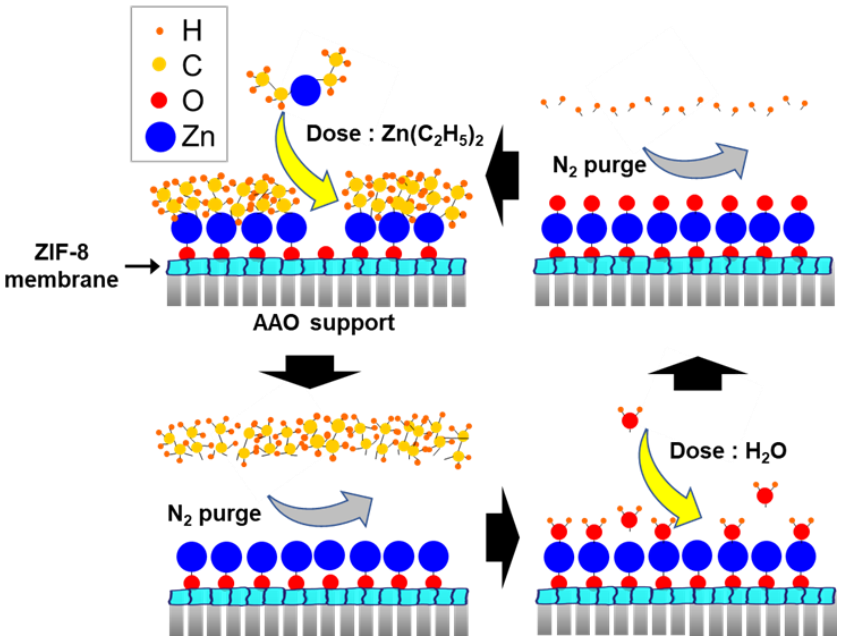

Figure 1.2: Schematic illustration of ZnO deposition on ZIF-8 membrane surface.

Aim III: Enhancement of the ZIF-8 membrane performance by reducing membrane thickness via vapor phase synthesis techniques.

Significance: We plan to develop high flux propylene selective ZIF-8 membranes under Aim III. To produce an ultra-thin ZIF-8 membrane to improve membrane productivity we plan to design a vapor-phase method to reduce the membrane thickness. Based on the understanding gained from Aim II, we plan to perform ZnO coating using ALD as a metal precursor and design the vapor phase synthesis process to synthesize the ZIF-8 membrane. The ZnO ALD investigation and optimization of vapor-phase treatment process tasks were listed below followed by an illustration of vapor-phase synthesis as shown in Figure 1.3.

Task A: Reduction of the membrane thickness by varying the deposition of ZnO-ALD cycles

Task B: Optimization of the vapor phase synthesis for the operating conditions of temperature, synthesis time, and the number of ALD cycles

Task C: Evaluation of the ZIF-8 membranes obtained by the vapor phase synthesis for propylene/propane separation.

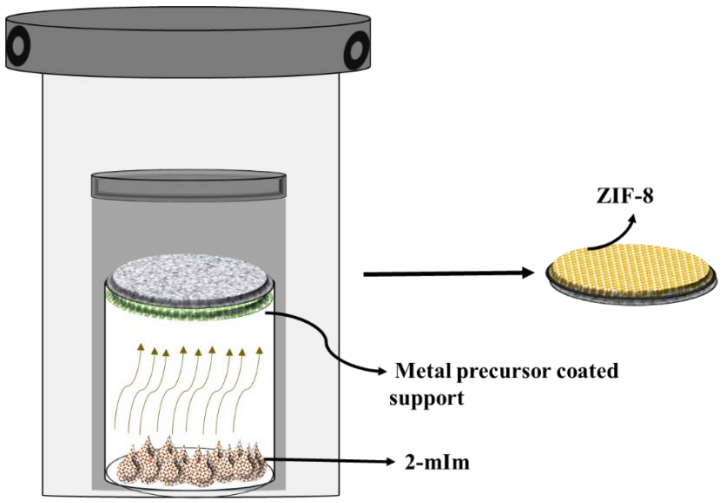

Figure 1.3: Schematic representation of the vapor-phase synthesis.

CHAPTER II

LITERATURE REVIEW

Summary

This chapter introduces the propylene/propane separation and its energy demand through conventional technologies. We discuss alternative technologies of propylene/propane separation and offer a recent literature review about membrane materials. We explain several synthesis approaches and different types of supports used for ZIF-8 membrane fabrication which are explored in the literature.

2.1. Olefin market

Light olefins such as ethylene and propylene are widely used as raw materials in the petrochemical industry. Propylene is the second most important material after ethylene and global demand is estimated to be ~120 million tons in 2021 [18, 19]. It can be used as a feedstock to produce polypropylene, cumene, and propylene oxide which are widely used in the industrial sectors. Traditionally, propylene is obtained as a byproduct of gasoline and ethylene by steam cracking of naphtha or catalytic cracking of heavy oils in refineries. These two traditional production processes of propylene cover 90% of the current market requirements [20, 21]. However, due to the high increase in propylene demand, the balance between supply and demand is not being met. Moreover, industries moving to lighter feedstocks such as natural gas liquid (NGL) for the cracking process due to large natural gas reserves in the U.S. These light feedstocks mainly

produce ethylene and lesser amounts of propylene containing by-products. The U.S. is one of the countries in the world that is consuming a large amount of propylene and the transition to NGL can affect the global markets. Figure 2.1 shows the increasing production and consumption demand for propylene in recent years [22].

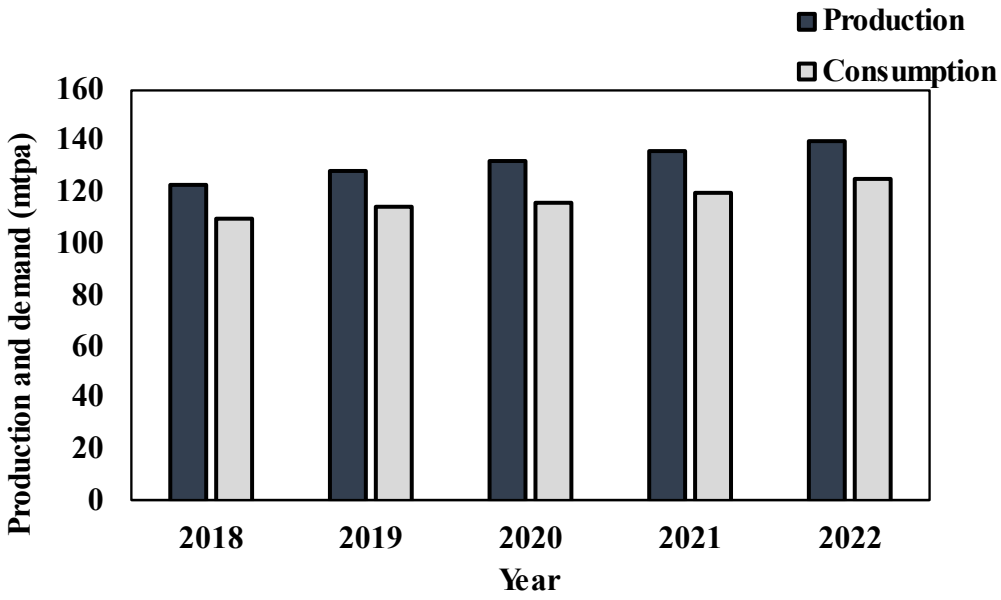

Figure 2.1: Production and consumption of propylene in million tonnes per annum (mtpa).

Observing the supply/demand dynamics and changes in the unstable price of propylene, producers are seeking alternative production methods to stabilize the current imbalanced market. Currently, three technologies serve the purpose of quenching the market demand including propane dehydrogenation (PDH), olefin metathesis, and methanol to propylene (MTP) conversion processes [23]. These technologies of propylene production are marginal, and they are economical due to the rise in propylene demand. While both PDH and MTP are economical because the raw materials used in these processes are of low cost, olefin metathesis is comparatively expensive because of the use of 2-butene. Therefore, alternative methods to produce propylene are needed to explore which are economical and energy-efficient.

2.2. Separation of propylene/propane

Propylene produced from traditional routes including steam cracking and fluid catalytic cracking (FCC) always co-exists with propane. Since industrially pure propylene with chemical and polymer grades required further chemical processing of the co-existing propylene/propane is necessary and both are needed to be separated. The separation of propylene/propane is quite challenging but commercially very important [24, 25]. The thermally driven distillation process is traditionally used to separate propylene/propane, but the capital costs involved are high and the energy consumption in the separation process is enormous [26, 27]. Moreover, the similar volatilities of both the gases require a change from gas to the liquid stage in the distillation process, which makes the whole separation operation energy-intensive. Based on the estimation from the U.S. Department of Energy (DOE), the cryogenic distillation process consumes energy over 120 TBtu (Tera British thermal units) per year for propylene/propane separations [28]. To reduce the energy footprint, alternative technologies for propylene/propane separation are assessed including membrane technologies, extractive distillation, adsorption, and absorption.

However, most of the alternative technologies mentioned are not commercially available due to unstable performance and limitations from chemical and mechanical standpoints. In the case of extractive distillation, there is a problem of high energy use. Moreover, the adsorption technique has low olefin loadings and a complicated regeneration process involving expensive adsorbents [29, 30]. Therefore, there is a critical need to investigate and improve the alternative techniques in the separation of propylene/propane. Out of all the alternative gas separation technologies available, membrane separation processes have gained popularity because they have the potential to be economical and energy-efficient [31] [32]. Combining distillation and membrane separation techniques can result in energy savings ranging from 16.8 to 45.6 TBtu per year [33], which is about saving 38% of the total energy consumption according to the previous literature [34]. Using membrane separation techniques combined with distillation can shrink both the economic and energy burden on propylene/propane separation technologies.

To meet the industrial requirements, researchers explored membrane technology for propylene/propane separations and published several research articles in the field of membrane gas separation as shown in Figure 2.2 [35]. Various kinds of membranes have been studied for propylene/propane separations including facilitated transport (FT) membranes [36], polymer [37, 38], zeolite [39], and carbon molecular sieve (CMS) [40, 41]. However, these membrane materials are not easy to scale up for commercial and industrial use because of their substandard performance in terms of separation factor, durability, and permeability [24, 42]. Recently, metal-organic frameworks (MOFs) have been considered promising membrane materials with high gas separation performance including high thermal and chemical stability.

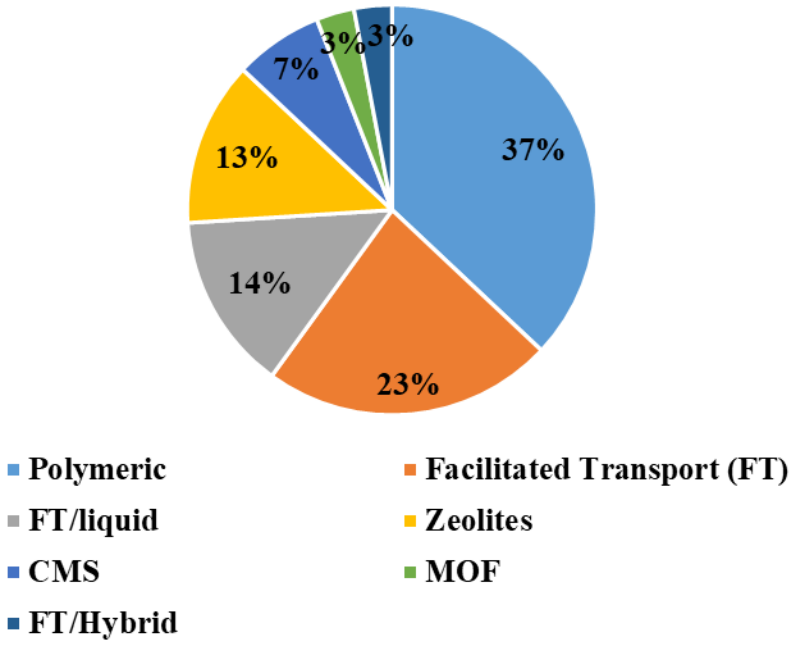

Figure 2.2: Types of membranes used for propylene/propane separation [35].

2.3. Zeolitic imidazole frameworks (ZIFs)

ZIFs are constructed by metal nodes such as zinc and cobalt with imidazole or its substitutes such that there are unlimited combinations theoretically with different topologies. The bonding angle (~145º) of metal-imidazole-metal (mIm) resembles the T-O-T angle found in zeolites giving its name ZIF [13]. Although crystalline structures like ZIFs are studied historically dating back to the 1960s, the recent discovery of the chemical/thermal stability conditions of ZIF membranes has been unleashed, paving the way for more investigation. In addition, stability, tunability, flexibility of the framework, and microporous added value to ZIFs, paving the way to numerous membrane separation applications [43-45]. Among ZIF membranes, ZIF-8 has been a promising candidate in propylene/propane separation where the zinc ions are intertwined with 2-mIm ligands with an aperture size of ~3.4 to 5 Å [46, 47]. However, the flipping motion of the 2-mIm ligand exerting pressure and external introduction of guest molecules results in ZIF-8 not exhibiting a stable sieving cut-off. Li et.al reported that the diffusion rate coefficient of propylene (van-der-Waals diameters: propylene = 4.03 Å, propane = 4.16 Å) is 100 times more than that of propane indicating the potential to separate C_3 molecules using ZIF-8 membranes [48]. Moreover, the molecular sieving property of propylene/propane using ZIF-8 membranes was found by previous computation and experimental research. Koros et.al reported that the effective aperture size of the ZIF-8 is in the range of 4.0 to 4.2 Å which is between the molecular diameters of propylene and propane. The ZIF-8 membranes are considered to be capable of propylene/propane separations however, the microstructural properties and processing methods are needed to be explored to improve the separation efficiency. Therefore, it is important to understand ZIF-8 membrane fabrication processes. Although significant progress has been made on the propylene/propane separation with ZIF-8 membranes grown on porous α-alumina substrates, the preparation of substrate requires rigorous conditions including hydraulic pressure (~10 tons) and sintering temperature (~1100 ˚C) with high energy consumption and low reproducibility [49]. Also, the relatively limited propylene permeances are reported as low as 0.2×10^{-8} mol m^{-2} s^{-1} Pa^{-1} reported when the α-alumina disk was used as a substrate [42, 50]. Another promising choice for membrane support is an

AAO substrate with straight nanochannels and narrow pore size distributions. This has been used for the separation of larger molecules and the support of porous materials [51]. Various MOFs have been successfully fabricated on AAO such as MOF-5 [52], HKUST-1 [53], Sr/Eu(II)-imidazolate [54], and MIL-53 [55]. The thinner AAO substrate having a straight pore channel inside is expected to provide better ZIF-8 crystallization and higher gas permeance. So far, very few studies have been reported about ZIF membranes on AAO for propylene/propane gas separation.

Imidazole ligand deprotonation allows coordination of bidentate sites which are continuously coordinating with metal nodes. This coordination forms a three-dimensional molecular structure that is complex. Multiple variables play a vital role in the yield of ZIF-8 products which requires the correct combination of the variable, where the synthesis of the structure with the intended topology has a small window for the fabrication process [56, 57]. Some of the variables can be solvent, ligand substitution, metal source, synthesis time, and synthesis temperature. The microstructural properties of the ZIF-8 depend on morphology, topology, and composition. Therefore, it is especially important to understand the complex connection between variables and have control over their membrane properties. Finally, the strategies that improve the separation of propylene/propane using ZIF-8 membranes will be discussed in the upcoming sections.

2.4. ZIF-8 membrane synthesis

The fast reaction between metal and ligand precursors is a unique property of ZIF-8 membranes, which provides an opportunity to explore different synthesis methods for improving the separation performance of propylene/propane. Reliable techniques in ZIF-8 membrane fabrication have been developed. Some of the methods developed in ZIF-8 membrane synthesis include in-situ, secondary growth, counter-diffusion, and vapor-phase methods, which are proved to be effective [58-62]. These fabrication methods are efficient because the synthesis procedure involves activating ZIF-8 membranes using mild temperature conditions in liquid or gas phases. Moreover, to ensure substantial separation factor and

propylene permeance, the notable challenge in ZIF-8 membrane synthesis is to reduce the membrane thickness while maintaining the integrity of the crystalline structure.

2.4.1. In-situ growth

In-situ growth is a method used in the fabrication of zeolite membranes that involves precursor solutions to contact with the support surface directly resulting in heterogeneous nucleation and growth of the membrane layer on the support surface. Caro et al. has synthesized ZIF-8 membranes on ceramic supports using in-situ crystallization [63]. The preparation of the ZIF-8 membrane involves the use of methanol as a solvent on titania support aided by microwave solvothermal synthesis, which resulted in crack-free membrane formation. The reason to use methanol is because of its small diameter compared to other solvents and weak interaction with the ZIF-8 framework. In addition, Kwon et al. synthesized ZIF-8 membranes using in-situ crystallization with methanol as a solvent on α-alumina support. A well-intergrown crystal structure resulted in a propylene/propane separation factor of around ~55 [64]. Besides, the use of sodium formate in enhancing the ligand deprotonation was investigated by Shah et al. in ZIF-8 membrane synthesis using organic solutions, which formed uniform crystal growth on α-alumina support [65]. Pan et al. reported that ZIF-8 membrane synthesis using water as a solvent yielded uniform and better growth of crystals on the support surface. Furthermore, the use of water as the solvent can induce better intergrowth of ZIF-8 crystal grains compared to a methanol solvent due to easier deprotonation of the imidazole ligands in water. However, in-situ crystallization methods involve modification of the support surface chemically and require multiple times of synthesis to ensure the integrity of membranes [50, 59, 66, 67]. Therefore, alternative synthesis techniques such as secondary growth have been explored, providing better membrane formation control [7].

2.4.2. Secondary growth

The secondary growth method in ZIF-8 membrane fabrication maintains better quality and control, which involves the decoupling of crystal nucleation and growth. This method involves the seeding of small crystals on the support surface via various synthesis techniques including rubbing, dip-coating, and direct contacting followed by either hydrothermal or solvothermal synthesis for growing continuous membrane films. Previous studies reported that the synthesis of ZIF-8 membranes in aqueous solutions is eco-friendly and economical [68-70]. Moreover, ZIF-8 membrane fabrication using secondary growth methods resulted in a thin membrane (~2 μm thickness) with propylene/propane separation of 45 at room temperature as reported by Pan et al [24]. The methanol exchange step was further introduced by Pan et al. to replace the water molecules inside the ZIF-8 membrane framework which enhanced the separation factor of the propylene/propane from 31 to 89 [71]. Jeong et al. developed a microwave-assisted seeding method followed by secondary growth to improve the interaction between the seed crystals and the support surface. It resulted in the propylene/propane separation factor of ~40 [72]. To generate appropriate ZIF-8 crystal sizes in propylene/propane gas separations, several seeding zinc sources were investigated which induce changes in stability, surface area, and gas separation performance [73]. Kwon et al. reported the effect of zinc salts on the membrane synthesis and separation performance that using $ZnCl_2$ as a zinc source has shown higher separation performance with a separation factor of 38 compared to other zinc sources [49]. The secondary growth synthesis resulted in well-intergrown crystals and high propylene/propane separation performance. However, the synthesis time of ZIF-8 is long with secondary growth, which creates the need to study other synthesis methods.

2.4.3. Counter diffusion

The concept of counter diffusion in membrane synthesis was first developed by Yao et al as shown in Figure 2.3 [74]. The approach includes the use of nylon support which was used to separate zinc and the ligand solution. Once both metal and ligand solutions diffuse through the support, they react chemically

resulting in crystallization on both sides of the support [74]. Later, the efficiency of the counter-diffusion is improved by Jeong et al developing an in-situ synthesis method for ZIF-8 fabrication. Optimizing the synthesis variables including the use of sodium formate and zinc salts, improved the separation performance of the ZIF-8 membrane from 55 to 70 while maintaining propylene permeance [49]. This method was assessed by other research groups that used the modified counter-diffusion approach in propylene/propane separations because it is simple and quick in terms of synthesis procedure and time [75-78]. However, rapid nucleation during synthesis can likely cause defects on the ZIF-8 membrane surface negatively affecting the separation performance of propylene/propane [31].

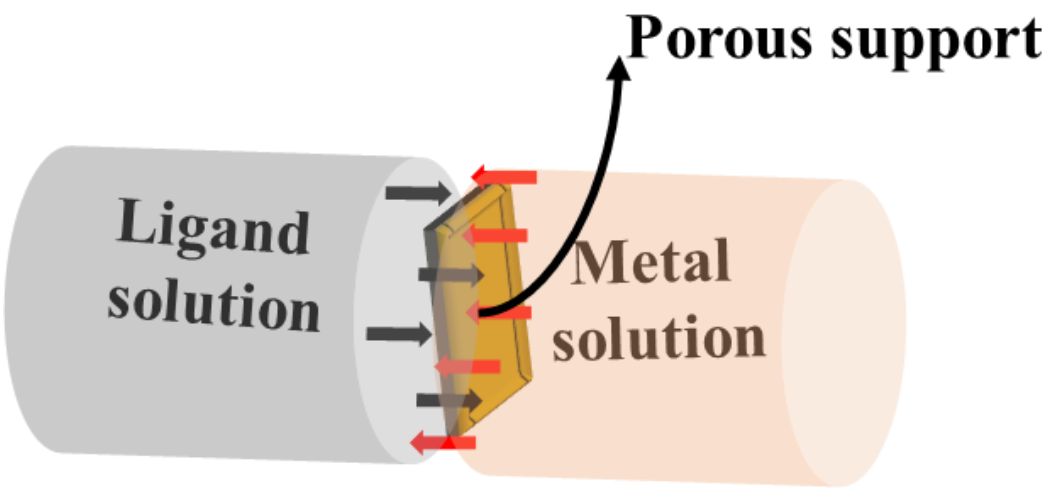

Figure 2.3: Schematic showing counter-diffusion synthesis on the porous support.

2.4.4. Post-synthetic methods

The synthesis methods including in-situ growth, secondary growth, and counter-diffusion have shown substantial separation performance of propylene/propane. However, it is inevitable to have defects on membranes, including inter-crystalline gaps, pinholes, and cracks [31, 72]. To improve the separation performance of ZIF-8 membranes, several research groups have explored post-synthetic treatment

methodologies to reduce the defects on the membrane surface. Recently, Zhang et al. reported that the defects in the ZIF-8 structure are formed in ambient environmental conditions using computational methods by changing chemical and synthesis conditions [79]. The reduction in surface defects can be achieved by post-synthetic modification methods including ligand treatment, metal doping, replacement of building blocks, and polymer layer coating [80, 81]. Lee et al. used post-synthetic ligand treatment operated at 60 - 100°C for 4 h to reduce the surface defects, which resulted in a propylene/propane separation factor enhancement by 6-folds while propylene permeance was reduced by 75% [31]. Li et al. explored coating organic polymer polydimethylsiloxane (PDMS) layer on a pre-synthesized ZIF-8 membrane surface. After PDMS coating, the ZIF-8 membranes enhanced the propylene/propane separation factor from 12 to 67, and there was a drop in propylene permeance from 2.1 to 1.3×10^{-8} mol m^{-2} s^{-1} Pa^{-1} [48]. Although surface defects are healed and the separation performance of the ZIF-8 membranes improved, excessive deposition of the post-synthetic layer might cause a loss in gas permeance [82]. Therefore, both membranes selectivity and gas permeance are needed to be systematically controlled while optimizing the synthesis procedure. To better optimize the ZIF-8 membrane synthesis process, vapor phase methods were also explored which are explained in the following section.

2.4.5. Vapor phase synthesis

Vapor-phase synthesis has been an efficient alternative synthesis method that is suitable for ZIF-8 membrane fabrication as shown in Figure 2.4 [83]. The advantages of this synthesis technique involve a simple membrane fabrication resulting in economical and energy-efficient membrane products. Several research groups have investigated vapor-phase synthesis in ZIF-8 membrane fabrication on porous supports [84]. Based on the previous studies performed by researchers, chemical vapor deposition (CVD) via ALD is a feasible approach to get propylene selective ZIF-8 membranes [85]. Strassen et al. reported that solvent-free synthesis of ZIF-8 membranes on a smooth silicon wafer is possible by converting ZnO films to ZIF-8 by using CVD [86]. Besides, Tanaka et al. investigated ZIF-8 membrane growth using vapor phase

transport methods which use a ZnO nanorod array for ZIF-8 crystal formation [87]. An alternative approach to growing ZIF-8 membranes has been studied by Rief et al., spraying ZnO on support, resulting in the growth of ZIF-8 membranes [88]. Wang et al. reported that using ZnO in the growth of ZIF-8 membranes showed excellent binding strength between supports and membranes [89]. Jeong et al. investigated the vapor-phase defect ripening methods in fabricating ZIF-8 membranes on α-alumina supports, which showed a propylene/propane separation factor of ~120 [90]. Furthermore, Ma et al. fabricated ZIF-8 membranes using vapor-phase methods that the ligand-induced permselective (LIPS) technique aided in converting the impermeable disk into propylene selective membranes. This fabrication process made the vapor-phase treatment substantial for propylene/propane separation applications which have shown a high propylene permeance of 1.67 x 10^{-7} mol m^{-2} s^{-1} $Pa^{-1}$with a separation factor of 74 [84]. Eum et al. used the LIPS process to fabricate ZIF-8 membranes, which resulted in propylene/propane separation of ~75 with propylene permeance of 5.5×10^{-8} mol m^{-2} s^{-1} Pa^{-1} [62]. However, vapor-phase methods are needed to be simplified, since the nucleation process is complex such that the simplification in membrane fabrication will make the synthesis process energy efficient. From the synthesis techniques explained in Chapter 2, the research conducted to improve the propylene/propane separation factor and the novel synthesis techniques developed using ZIF-8 membranes are discussed in Chapters 3, 4, and 5.

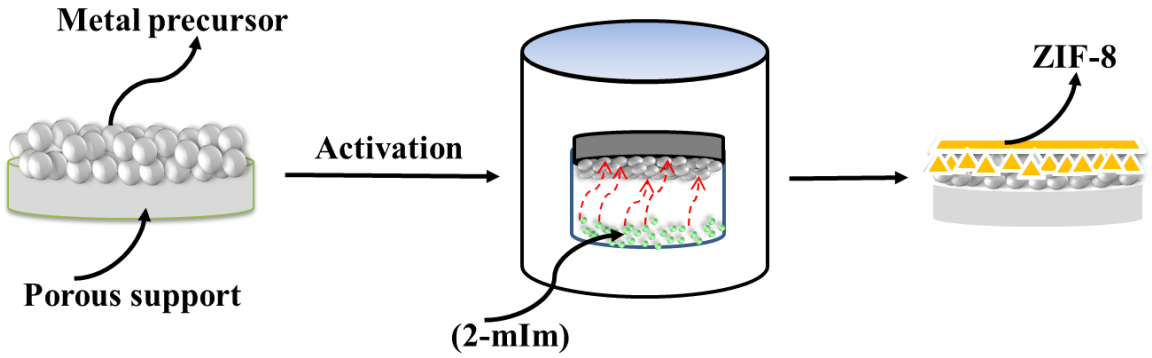

Figure 2.4: Schematic illustration of vapor-phase synthesis.

CHAPTER III

ZIF-8 MEMBRANES SUPPORTED ON SILICALITE-SEEDED SUBSTRATES FOR PROPYLENE/PROPANE SEPARATION

Summary

Secondary growth ZIF-8 membranes were developed using silicalite nano particles as seeding material on porous AAO support. The ZIF-8 membrane performance was investigated by varying synthesis time, seeding type, and zinc source. The silicalite nanoparticles act as anchors to grow the ZIF-8 membrane layer on AAO support. The seed particles are strongly attached to AAO support through hydrogen bonding which aided us to achieve high quality ZIF-8 membrane. The ZIF-8 membranes were tested for propylene/propane separation and characterized using analytical techniques.

3.1. Introduction

Propylene and propane mixture separation is one of the most energy-consuming processes in the industry due to their similar physical properties like melting point, boiling point, and molecular size [37, 91, 92]. The separation is traditionally performed by using low-temperature distillation involving more than 200 stages [93]. Membrane-separation processes have been recognized as an attractive alternative as they have the potential to be energy-efficient, eco-friendly, and cost-effective [31]. Several types of membranes

have been studied such as polymer [37, 38], carbon molecular sieve [40, 41], and zeolite membranes [39]. However, these membranes are not currently suitable for practical applications because of their drawbacks associated with the separation factor, permeability, and/or durability [24, 42]. Therefore, there is a critical need for developing new membranes to enhance the propylene and propane selectivity and propylene flux.

Recently, zeolitic imidazolate frameworks (ZIFs) have been recognized as novel candidates for efficient olefin and paraffin separation. ZIFs are subclass metal-organic frameworks (MOFs), possessing zeolite topologies originating from the metal-ligand-metal bond angle of 145°, which is similar to the Si-O-Si bond angle in zeolites [13]. Among the varieties of ZIFs that exist, ZIF-8, composed of zinc ions interconnected with 2-methylimidazoles, has been the most promising candidate for propylene/propane separation [16, 94, 95]. The effective pore size of ZIF-8 falls in the range of 4.0-4.2 Å, which is larger than the crystallographic diameter of 3.4 Å owing to the flopping motion of the ligands. This allows the membrane to separate propylene (~4.0 Å) from propane (~4.3 Å) based on the size exclusion mechanism[49] [17]. Zhang et al. [17] reported that the diffusivity of propylene was approximately 100 times higher than that of propane by estimating diffusivity in a ZIF-8 crystal. These studies demonstrate the enormous potential of the ZIF-8 membrane to be used for propylene and propane separation based on their diffusivity differences.

Various strategies have been developed to grow ZIF-8 film on porous α-alumina substrates. Pan et al. [68] found that ZIF-8 membranes synthesized in a solution containing water can induce better intergrowth of grains due to easier deprotonation of the imidazole ligands in water than that containing methanol. Kwon et al. [64] prepared thin ZIF-8 membranes through in situ synthesis, which produced well-intergrown ZIF-8 membranes with significantly enhanced microstructure, resulting in propylene/propane selectivity of around 55. Shah et al. [65] investigated the role of sodium formate in the synthesis of ZIF-8 to enhance ligand deprotonation in organic solutions. Pan et al. [71] investigated the effects of the activation

procedure after ZIF-8 membrane synthesis. The optimal activation process included a solvent exchange to remove residual water by using methanol and room temperature drying at a low evaporating rate. Although significant progress was obtained on the propylene/propane separation with ZIF-8 membrane grown on porous α-alumina substrates, the preparation of substrate required rigorous conditions including hydraulic pressing at 10 tons and sintering temperature of ~1100 ^{o}C with high energy consumption and low reproducibility [49]. In addition, the relatively limited propylene permeances of as low as 0.2×10^{-8} mol m^{-2} s^{-1} Pa^{-1} were reported when the α-alumina disk was used as a substrate [42, 50] Another promising choice for membrane support is an anodic aluminum oxide (AAO) substrate with straight nanochannels and narrow pore size distributions. This has been studied for the separation of larger molecules and used for the fabrication of porous materials [51]. Various MOFs have been successfully fabricated on AAO such as MOF-5 [52], HKUST-1 [53], Sr/Eu(II)-imidazolate [54], and MIL-53 [96], etc. There were few studies reported about ZIF membranes on AAO. Babu et al. [97] post-synthetic rapid heat treatment (RHT) at 360 ^{o}C to significantly improve the carbon capture performance of the ZIF-8 membranes on AAO support. Impressive CO_2/CH_4, CO_2/N_2, and H_2/CH_4 selectivities of 30, 30, and 175 were achieved, respectively. He et al. [98] used a novel electrophoretic nuclei assembly for the crystallization of highly intergrown thin films (ENACT) approach for fabricating defect-free and ultrathin ZIF-8 membrane on multiple supports including AAO. High performance of 8.3×10^{-6} mol m^{-2} s^{-1} Pa^{-1} and selectivities of 7.3, 15.5, 16.2, and 2655 were obtained for H_2/CO_2, H_2/N_2, H_2/CH_4, and H_2/C_3H_8, respectively. Hao et al. [99] reported a crystallization using a sustained precursors approach to fabricate well intergrown polycrystalline ZIF-8 having uniform grain size and a thickness of a few nanometers. ZIF-8 membrane grown in 8 min exhibited an impressive H_2/C_3H_8 selectivity of 2433 and C_3H_6/C_3H_8 selectivity of 30.

Since the ZIF-8 particle sizes were demonstrated to induce changes in surface area, stability, and gas adsorption, the species of zinc sources were investigated to generate the appropriate ZIF-8 crystal size for propylene/propane separations [73]. For example, the effects of zinc salts on ZIF-8 membrane synthesis were studied by Kwon et al [49]. When employing $ZnCl_2$ as the zinc source, the synthesized ZIF-8

membrane showed a separation factor of around 38 and propylene permeance of around 2.7×10^{-8} mol m^{-2} s^{-1} Pa^{-1}. However, when the zinc source was changed to zinc nitrate, the ZIF-8 membrane became non-selective for propylene/propane [49].

It should be noted that ZIFs and zeolites have a similar crystallization process, which makes most of the synthesis methods developed for zeolites also applicable to the ZIF membranes [100, 101]. In this study, we fabricated a ZIF-8 membrane on a silicalite-seeded AAO substrate to increase membrane-substrate bonding. The impact of seeding materials, zinc source, and membrane synthesis time were systematically investigated for ZIF-8 membrane separation performance for efficient propylene/propane separation. With the help of characterization techniques and ZIF-8 membrane separation performance tests, optimized membrane synthesis parameters were evaluated.

3.2. Experimental

3.2.1. Synthesis of nanoparticle seeding

ZIF-8 crystals were prepared following a procedure described by Cravillon et al [102]. $Zn(NO_3)_2{\cdot}6H_2O$ (99.5%, Sigma-Aldrich) and 2-methylimidazole (mIm) (99.7%, Sigma-Aldrich) were dissolved in 50 ml methanol (MeOH) (99.5%, Sigma-Aldrich), separately. The molar ratio of Zn: mIm: MeOH was 1:4:1250. Then the mIm solution was added to the $Zn(NO_3)_2$ solution while stirring with a magnetic bar. The liquid mixture was stirred for 30 min and then aged without stirring at 20 ^{o}C for 24 h. The white colloidal particles formed in the solution were collected by centrifugation, followed by washing three times with methanol. The ZIF-8 powder was dried at room temperature overnight, and then re-dispersed into 100 ml methanol while sonicating for 30 min to prepare 0.05 wt.% ZIF-8 seed suspension.

Silicalite seed nanoparticles were prepared by the conventional heating method and the detailed synthesis procedure has been reported in our previous work [103]. To prepare silicalite seed suspension, NaOH (99.99%, Sigma-Aldrich) was dissolved in the mixture solution of H_2O and tetrapropylammonium

hydroxide (TPAOH) solution (1 M, Sigma-Aldrich). SiO_2 (0.2-0.3 μm powder, Sigma-Aldrich) was added to the above solution gradually at 80 ^oC in a water bath to clear the solution with stirring. The molar ratio of each component was maintained as NaOH: H_2O: TPAOH: SiO_2 = 1: 131.5: 2.86: 9.42, respectively. After aging for 4 h, the solution was transferred into a hydrothermal vessel and synthesized at 120 ^oC for 6 h. The synthesized powder was washed in deionized water in a centrifuge, followed by dilution to make 0.05 wt.% silicalite seed suspension.

3.2.2. ZIF-8 Membrane synthesis by secondary growth

AAO disks (diameter: 25 mm, thickness: 100 μm, pore size: 20 nm, porosity: 24%, Whatman) were used as the substrates. For seed layer coating, the AAO disks were immersed into the 0.5 wt.% seed suspensions of ZIF-8 and silicalite, respectively, followed by sonicating 5 min for the seeds to coat homogeneously on the substrate surface. The seeded AAO disks were dried at room temperature overnight. For membrane synthesis, ZIF-8 layers on the AAO seeded substrates were synthesized by the secondary growth method. The metal solution and the ligand solution were prepared separately. Specifically, 0.076 g of zinc chloride (99.99%, Sigma-Aldrich) or 0.165 g of zinc nitrate hexahydrate (98%, Sigma-Aldrich) was dissolved into 20 ml of DI water to prepare a metal solution, and 3.165 g of mIm was dissolved into another 40 ml of DI water to prepare ligand solution. After mixing the metal and the ligand solution, the solution was stirred vigorously for 30 s, the dried AAO substrate was immersed vertically into the mixed solution and held with a Teflon vessel. The membrane synthesis time by secondary growth was varied for 5, 10, and 20 h, respectively, at room temperature. After membrane synthesis, the disk was taken out and immersed in 50 ml of fresh methanol for 12 h, which is the activation process. The activation process removes any guest species like water from the ZIF-8 framework and prepares the evacuated form of the ZIF-8 framework for gas separation experiments. Because water is less acidic than methanol, 2-methylimidazole can be deprotonated in water more easily than methanol. Thus, ZIF-8 membranes washed with methanol were denser and better intergrown [13, 65, 70]. Finally, the membrane was taken out from methanol and dried at

room temperature for another 12 h. The process of the ZIF-8 membrane synthesis on AAO substrate is illustrated in Figure 1.1.

3.2.3. Propylene/propane binary gas separation

All membranes were stored in a desiccator at room temperature before gas permeation measurements. Propylene/propane binary gas permeation measurements were performed at room temperature and atmospheric pressure. The membranes were mounted in a stainless-steel cell with the membrane surface facing the feed side as shown in Figure 3.2. Feed was a mixture of propylene and propane each of 50 cm^3/min and the flow rate was controlled by a mass flow controller (MFC). Argon was used as the sweeping gas at a flow rate of 100 cm^3/min and was supplied to the permeate side. Before recording data for each separation experiment, membrane separation was allowed to stabilize (for concentration to become steady) and it took ~4 h for the system to reach a steady state. The composition of the permeate stream was analyzed by using online gas chromatography (Shimadzu, GC-2014) equipped with a molecular sieve 13X column for the thermal conductivity detector (TCD).

The membrane permeance for gas component i is defined as:

$$P_{m,i} = \frac{Q_i}{A_m \times \Delta P_i} \tag{3.1}$$

where Q_i (mol s^{-1}) is the amount of the permeated gas through the membrane per second; A_m (m^2) is the active membrane area; ΔP_i (Pa) is the trans-membrane partial pressure difference of component i between feed and permeate sides.

The propylene/propane separation factor for the binary mixture is defined as:

$$\alpha_{C_3H_6/C_3H_8} = \frac{(y_{C_3H_6}/y_{C_3H_8})_{permeate}}{(y_{C_3H_6}/y_{C_3H_8})_{feed}} \tag{3.2}$$

where $y_{C_3H_6}$ and $y_{C_3H_8}$ are mole fractions of propylene and propane, respectively

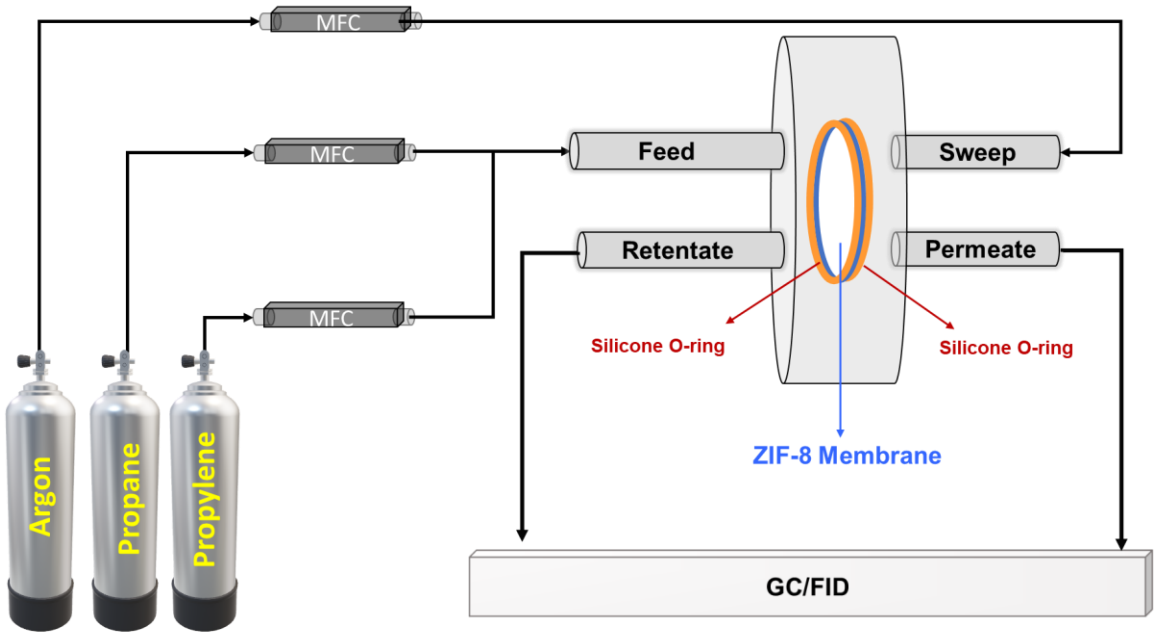

Figure 3.1: Schematic showing the experimental setup for the C_3H_6/C_3H_8 separation.

3.2.4. Characterization

The morphology of the membrane was characterized by Scanning Electron Microscope (SEM) and the elemental composition by Energy Dispersive X-Ray Analysis (EDX), using an FEI Quanta 600 SEM. The crystal structure of the ZIF-8 membrane was characterized by X-ray diffraction (XRD, Bruker AXS D8 Discover diffractometer with General Area Detector Diffraction System, 40 kV, 35mA) with a scan rate of 1.0 degree/min with the two-theta range of 5-40 degrees. The bonding information of samples was measured by X-ray photoelectron spectroscopy (XPS, PHI VersaProbe II Scanning XPS Microprobe with Al Kα line excitation source) and FT-IR characterization using Thermo Nicolet 380 FT-IR with diamond attenuated total reflectance (ATR). Nitrogen absorption and desorption were performed using a Quantachrome Autosorb I. Samples were outgassed at 50 °C overnight under a vacuum. pyGAPS was used

to analyze the resulting isotherms. The surface area and pore volume of the ZIF-8 membrane were measured by N_2 adsorption at 77K based on Brunauer–Emmett–Teller (BET) model.

3.3. Results and Discussion

3.3.1. The effect of nanoparticle seeding

The crystalline structure of the ZIF-8 membrane was compared with XRD patterns from the literature [49, 104]. The XRD patterns of the ZIF-8 membranes grown on ZIF-8 seed layers (Figure 3.3c) were sharper (peak intensity 110 was higher) than those without seed layers (Figure 3.3b), which suggests thicker and denser ZIF-8 layers. This can further be understood by the fact that an extra seeded ZIF-8 layer facilitates the formation of ZIF-8 crystals on AAO substrate in comparison to the ZIF-8 membrane without a seeding layer. In addition, silicalite seeded ZIF-8 membranes (Figure 3.3d) also showed sharper peaks than ZIF-8 membranes directly grown on AAO substrate (Figure 3.3b) indicating thicker and denser ZIF-8 membranes. Figure 3.3d represents the ZIF-8 membrane successfully grown on the silicalite-seeded AAO substrate by matching the typical XRD peaks at the 2θ of 7° and 12° [105].

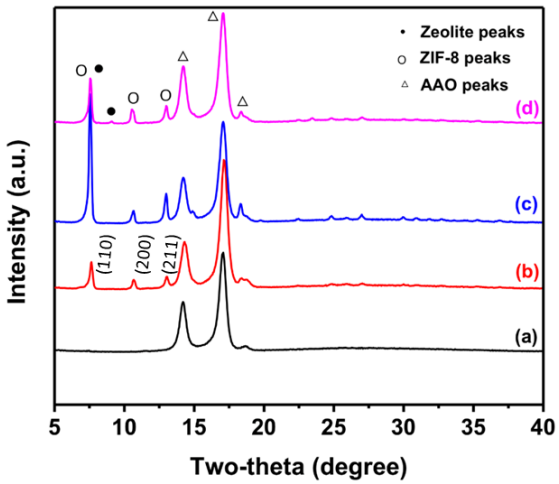

Figure 3.2: XRD patterns of (a) pristine AAO substrate, (b) ZIF-8 membrane without seeding layer, (c) ZIF-8 membrane with ZIF-8 nanocrystals as the seeding layer, and (d) ZIF-8 membrane with silicalite nanocrystals as the seeding layer.

Figure 3.4 shows the SEM images that were used to study the morphology of pristine AAO substrate and ZIF-8 membranes synthesized with and without the seeding process. Uniformly distributed

pore channels can be seen for the AAO substrate (Figure 3.4a). In the ZIF-8 membrane without seeding (Figure 3.4b1), the membrane had more defects in comparison to the ZIF-8 membrane with silicalite and ZIF-8 seeding, which can be explained by the fact that the ZIF-8 layer is not very well grown directly on the AAO substrate. XRD patterns are shown in Figure 3.3 also confirm the relatively insufficient ZIF-8 membrane growth without the seeding process [24]. The lack of active sites on the AAO substrate might be the reason for the poor ZIF-8 structure formation (Figure 3.4b1). However, the introduction of seeding material (ZIF-8 or silicalite) on AAO substrate improved the ZIF-8 membrane morphology (Figure 3.4c and Figure 3.4d). Seeding material helped in avoiding the adverse impact of AAO substrate on ZIF-8 crystal nucleation and improved ZIF-8 membrane morphology. In addition, silicalite seeding nanoparticles attach more firmly to the AAO substrate due to hydrogen bonding and provide a more uniform surface for secondary ZIF-8 membrane layer growth (Figure 3.4d) in comparison to ZIF-8 nanocrystal seeding (Figure 3.4c). Hydrogen bonding takes place by the direct bonding of silicalite crystals with the substrate, which allows for a robust seeded silicalite layer [101, 106, 107]. However, for ZIF-8 nanocrystal as the seeding layer, more disassociated ZIF-8 crystals were attached on the top of the membrane surface, which further resulted in a less intergrown ZIF-8 layer than the layer grown on silicalite seeded AAO substrate. For silicalite seeded AAO substrate, the ZIF-8 layer was smoother, uniformly covered, and more robust.

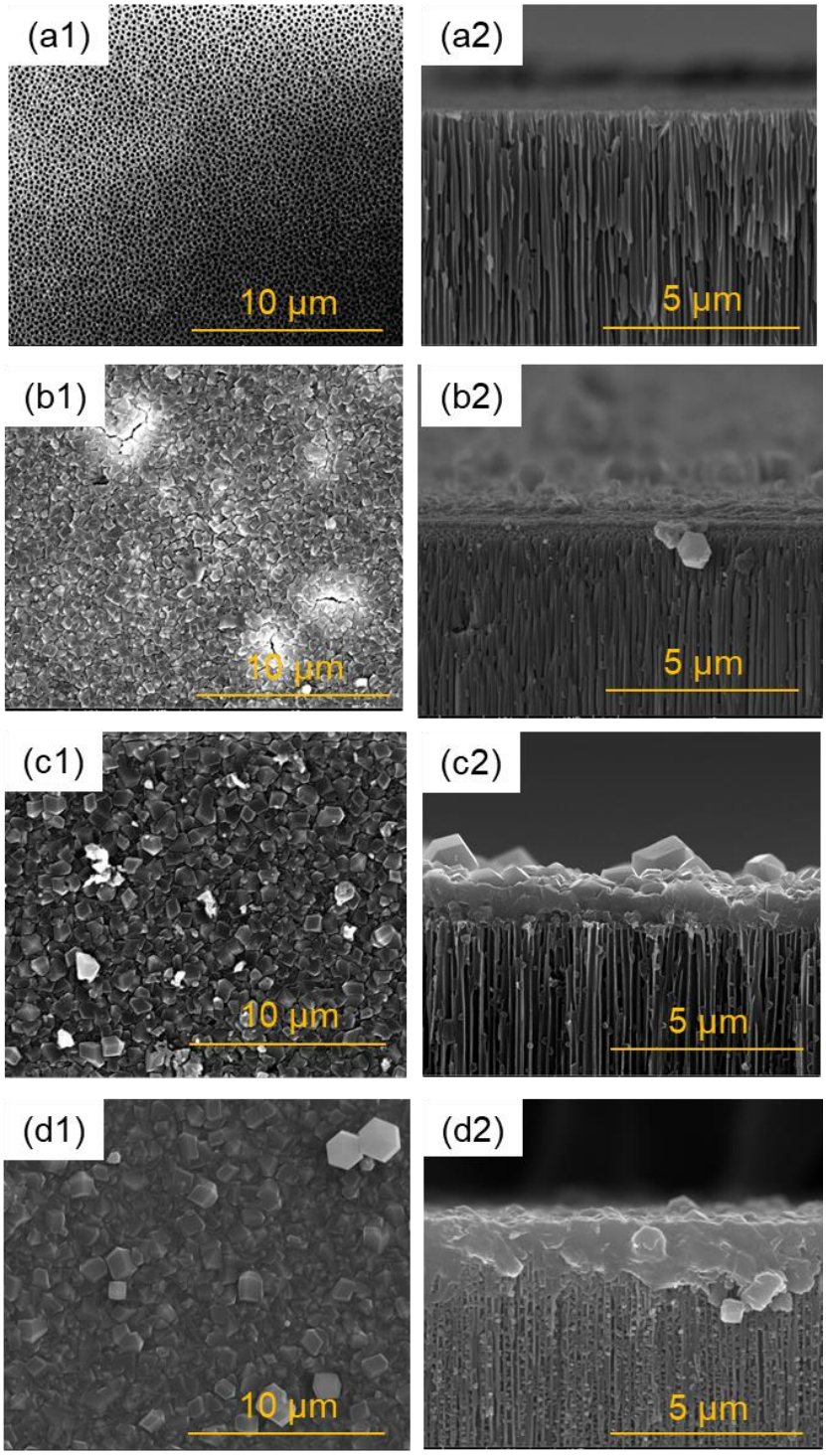

Figure 3.3: Surface SEM images and cross-section SEM images of pristine AAO substrate (a1, a2), ZIF-8 membranes synthesized at 10 h without seeding process (b1, b2), with ZIF-8 nanocrystals as the seeding layer (c1, c2), and with silicalite nanocrystals as the seeding layer (d1, d2), respectively.

Table 3.1 shows the elemental composition on the surface of different membranes obtained from EDX spectroscopy. Silicon concentration was dropped from 26.25 wt.% for silicalite seeded AAO substrate to 0.33 wt.% for silicalite seeded + ZIF-8 membrane. Silicalite seed has silica, which is responsible for silicon concentration. XPS beam can detect elements only up to ~2.5 nm depth, and after ZIF-8 growth, XPS could not detect silica and hence there was a drop in silicon concentration. There was an increase in the concentration of carbon, nitrogen, and zinc after ZIF-8 membrane fabrication. During the secondary synthesis, the use of $ZnCl_2$ and mIm introduced more zinc, nitrogen, and carbon in the membrane framework, and thus there was an increase in the concentration of these elements.

Table 3.1: Elemental composition (wt. %) for silicalite seeded AAO substrate, silicalite seed + ZIF-8 membrane, ZIF-8 seeded AAO substrate, ZIF-8 seed + ZIF-8 membrane, and ZIF-8 in-situ membrane.

On top of the AAO substrate	Silicon	Carbon	Nitrogen	Zinc
Silicalite seed	26.25	25.08	2.28	0.20
Silicalite seed+ ZIF-8 membrane	0.33	63.72	19.35	8.03
ZIF-8 seed	1.13	54.79	24.73	10.91
ZIF-8 seed + ZIF-8 membrane	-	56.55	25.96	11.01
ZIF-8 in-situ membrane	0.04	56.44	26.01	11.54

Figure 3.5 shows the XPS spectra for C 1s, N 1s, and Zn 2p. Particularly, Zn $2p_{3/2}$ and Zn $2p_{1/2}$ showed two intense peaks at 1022 eV and 1045 eV, respectively [49, 71]. Two distinct peaks for Zn imply that most of the Zn are in the tetrahedral coordination. For the ZIF-8 membrane with silicalite seeding, the peak slightly shifted towards higher binding energy for Zn and N atoms, which indicates the decrease in several unsaturated Zn-N bonds and thus reduction of defects in the ZIF-8 framework. The N 1s peak at

398.8 eV can be assigned to the imidazole group in the ZIF-8 framework based on the literature [108-111]. C 1s showed a peak at 286.3 eV, which depicts the carbon linked to N in the methyl imidazole group, and was found to be in good agreement with previously reported literature [109, 112]. The band at 1580 cm^{-1} corresponds to the C=N stretch. In addition, the bands at 1146 cm^{-1} are for =C-H and C-N and 995 cm^{-1} is for the C=C-N, respectively. Moreover, the stretch 3134 cm^{-1} is for the C-H bond [113-115].

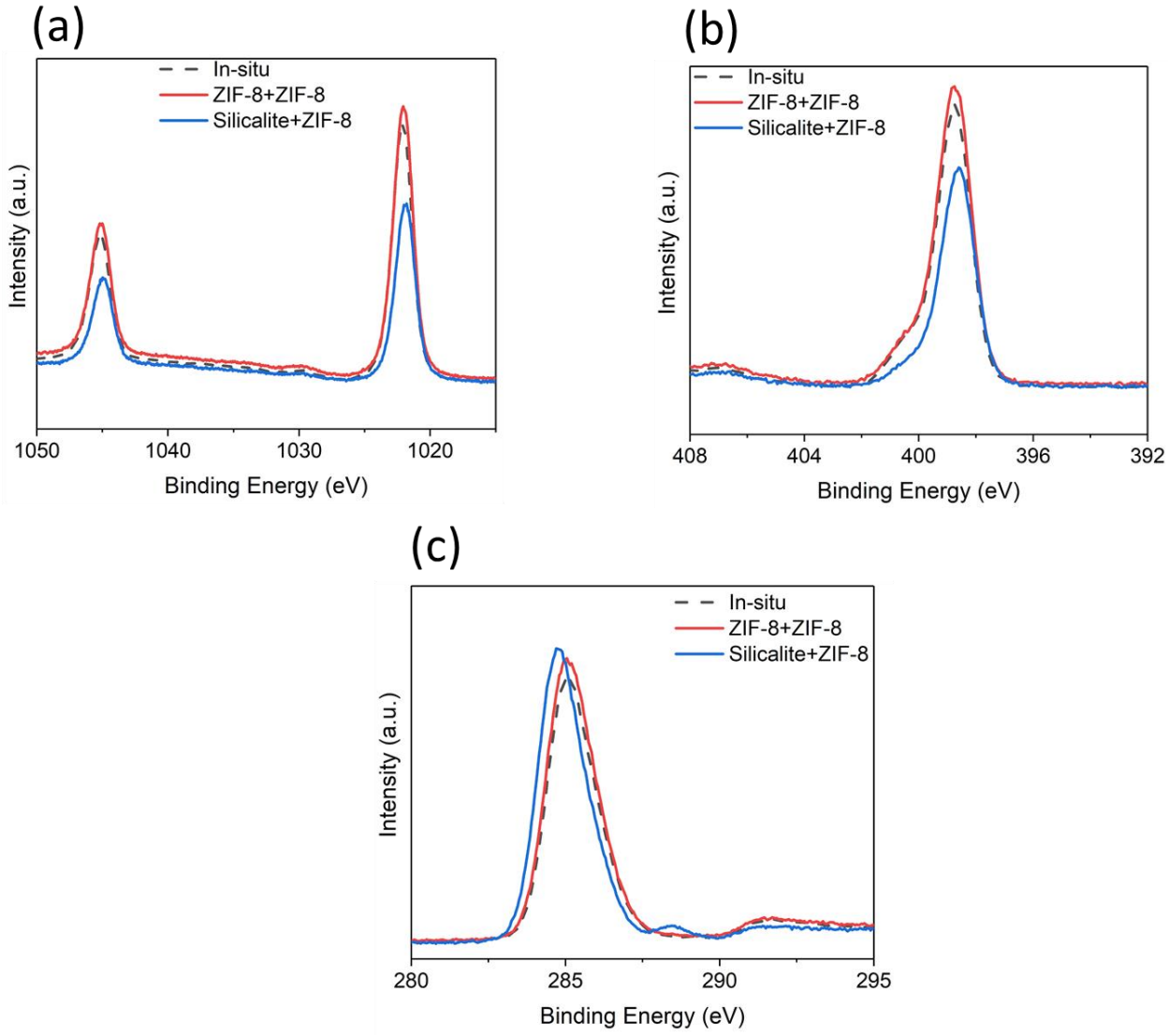

Figure 3.4: XPS spectra for Zn 2p 1s (a), N 1s (b), and C 1s (c) of ZIF-8 membrane for in-situ ZIF-8 membrane, ZIF-8 seeding + ZIF-8 membrane, and silicalite seeding + ZIF-8 membrane.

BET surface area and pore volume for ZIF-8 membrane with silicalite seeding are shown in Table 3.2. Specific surface area for ZIF-8 membranes lies in the range of 1000-1600 m^2/g [116], which indicates the ZIF-8 structure formation [113]. Figure 3.6 shows the N_2 adsorption/desorption isotherm to investigate the N_2 accessible porous characteristic. ZIF-8 membrane with silicalite seeding showed type-1 isotherm,

which is expected for microporous materials (pore size < 2 nm). In addition, there was a sudden increase in N_2 adsorption around a threshold pressure of 0.95 (P/P_0) which was due to the condensation on the external ZIF-8 surface [47, 117-119].

Table 3.2: BET surface area and pore volume of ZIF-8 membrane as measured by N_2 adsorption at 77K.

Membrane	BET surface area (m^2/g)	Pore volume (cm^3/g)
ZIF-8 membrane (this work)	1474	0.71
ZIF-8 membrane [120]	1046	0.51

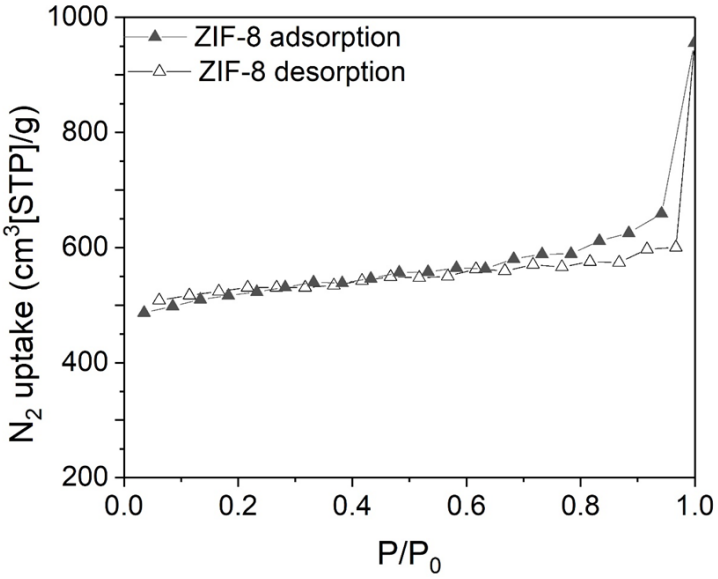

Figure 3.5: N_2 adsorption and desorption isotherms for ZIF-8 membrane.

3.3.2. Effect of Zinc source

The effect of different zinc sources on ZIF-8 membrane growth was investigated. The morphology of ZIF-8 membranes synthesized with zinc nitrate ($ZnNO_3$) and zinc chloride ($ZnCl_2$) as zinc sources, respectively, are shown in Figure 3.7. Under the same synthesis conditions in terms of reagent, molar

amount, and temperature, the ZIF-8 membrane in which $ZnNO_3$ was used as the zinc source showed smaller ZIF-8 crystal size, less intergrown ZIF-8 surface, and thinner ZIF-8 film in comparison to the membrane where $ZnCl_2$ was used as the zinc source. The difference in morphology of ZIF-8 crystals is due to the high reactivity of $ZnNO_3$ in comparison to $ZnCl_2$, which led to the faster reaction during the membrane synthesis and thus generated a smaller crystal size. Schein et al. [73] also reported morphological differences between the ZIF-8 crystals from the two zinc sources. Moreover, when $ZnNO_3$ was used as the Zn source, the ZIF-8 layer forms only on the substrate while $ZnCl_2$ also promotes ZIF-8 film formation inside the AAO substrate. Thus, the ZIF-8 membrane with $ZnCl_2$ enhanced the membrane grain boundary structure. As a result, with $ZnCl_2$ as the zinc source, the appropriate ZIF-8 crystal size for the propylene/propane separations can be synthesized [49, 73]

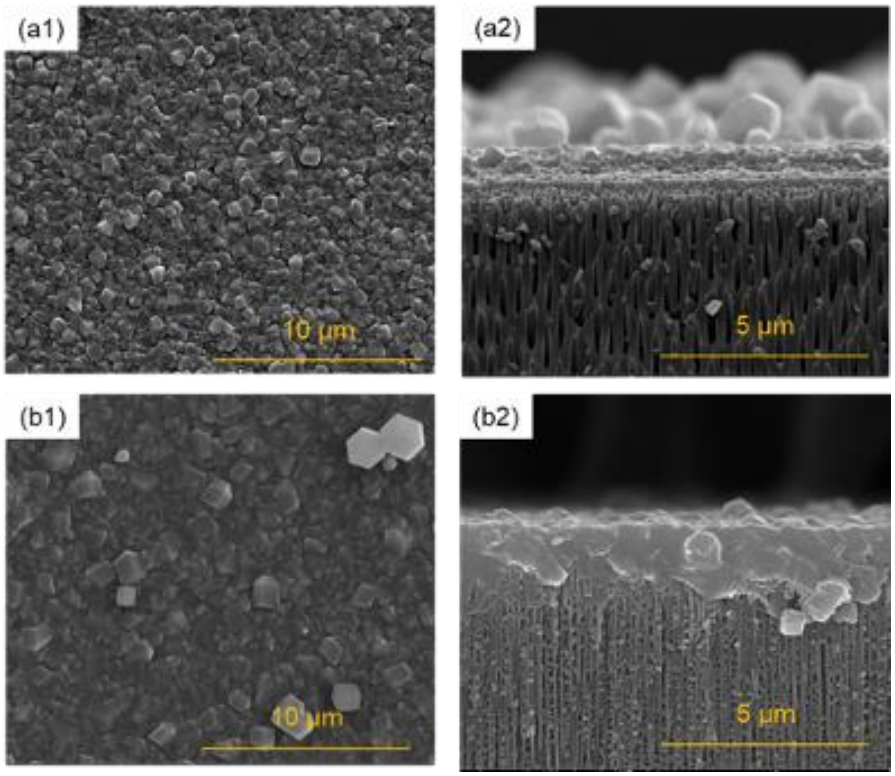

Figure 3.6: Surface SEM images and cross-section SEM images of ZIF-8 membranes synthesized at 10 h (a1, a2) with zinc nitrate and (b1, b2) zinc chloride as the zinc source, respectively, with silicalite nanocrystals as the seeding layer.

3.3.3. Effect of synthesis duration

The morphology of ZIF-8 membranes synthesized with various durations of 5, 10, and 20 h respectively are shown in Figure 3.8. The ZIF-8 crystals started to be formed from a synthesis duration of 5 h, with a limited number of ZIF-8 crystals randomly distributed on top of the silicalite seeded AAO substrate (Figure 3.8a). After 10 h synthesis duration, a ZIF-8 layer was uniformly formed (Figure 3.8b). As shown in Figures 3.8a2 & 8b2, there was a slight change in membrane thickness (650 nm for 5 h and 850 nm for 10 h). For the synthesis duration of 20 h (Figure 3.8c), there was significant growth of ZIF-8 crystals on the surface. The number of accumulated ZIF-8 crystals significantly increased [73], which led to a slight decline in propylene/propane gas selectivity and propylene gas permeance as can be seen in Figure 3.9. For more than 20 h of synthesis time, the membrane got thicker, which led to a further decline in ZIF-8 membrane separation performance. Based on SEM images and separation results as depicted in Figure 3.8b, it was found that for 10 h of synthesis, a well-intergrown continuous ZIF-8 layer was successfully formed with an average membrane thickness of ~850 nm.

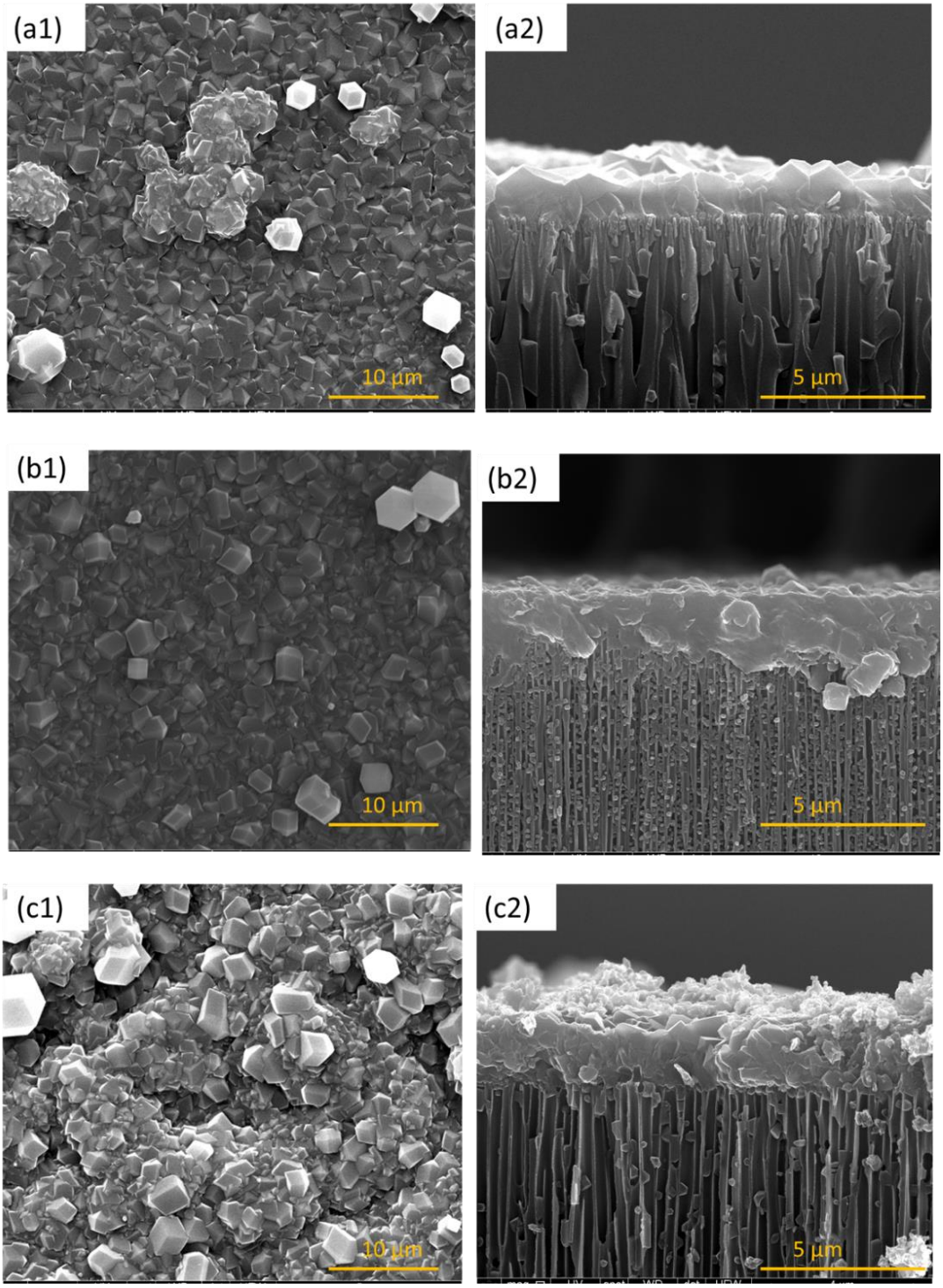

Figure 3.7: (a1, b1, c1) Surface SEM images and (a2, b2, c2) cross-section SEM images of ZIF-8 membranes with silicalite nanocrystals as the seeding layer with the synthesis time of 5, 10, and 20 h, respectively.

3.3.4. ZIF-8 membrane separation performance

The membranes synthesized by various conditions were evaluated for propylene/propane binary gas mixture separation at room temperature for performance evaluation. Table 3.3 presents the results of the propylene/propane mixture gas separation factor and propylene permeance values at room temperature. In Table 3.3, the ZIF-8 membrane synthesized without a seeding process (in situ growth) showed a low propylene/propane separation factor due to defects in the ZIF-8 layer (Figure 3.4b). It was found that different seeding materials had different effects on membrane performances. The ZIF-8 membranes grown on the silicalite seeded AAO substrate exhibited significantly higher performance than membranes using ZIF-8 nanoparticles as seeding material. This can be explained by the strong interactions between silicalite and AAO substrate through hydrogen bonding, which allows for a better grown secondary ZIF-8 layer. The interaction anchored silicalite seeds more firmly onto the AAO substrate, which provided a more stable seeding layer and allowed better reproducibility and control of the membrane quality. In this case, a highly ordered ZIF-8-membrane structure was obtained under such an environment.

Table 3.3: ZIF-8 membrane thickness and propylene/propane binary gas separation results for ZIF-8 membrane synthesized without seeding process, with ZIF-8 nanocrystals as the seeding layer, and with silicalite nanocrystals as the seeding layer for 10 h membrane synthesis time and $ZnCl_2$ as Zn source, respectively.

Seeding layer	$\alpha_{C_3H_6/C_3H_8}$	P_{m,C_3H_6} ($\times 10^{-8}$ mol m^{-2} s^{-1} Pa^{-1})	Thickness (nm)
None	84±0.7	1.86±0.03	380
ZIF-8 nanoparticle	112±0.3	1.27±0.01	720
Silicalite seeding	170±0.5	0.90±0.04	850

The results of propylene/propane binary gas separations by using ZIF-8 membranes with different zinc sources were shown in Table 3.4. ZIF-8 membrane prepared with $ZnNO_3$ as the zinc source showed higher propylene permeance and lower propylene/propane selectivity compared with those prepared with $ZnCl_2$. As shown in Figure 3.7, the ZIF-8 membrane prepared from $ZnNO_3$ was less intergrown and showed a thinner ZIF-8 membrane layer than those with $ZnCl_2$. In addition, the different ZIF-8 crystal sizes affected membrane stability and gas adsorption [49, 73] indicating that the appropriate ZIF-8 crystal size for the propylene/propane separations can be achieved by using $ZnCl_2$. Therefore, $ZnCl_2$ was found to be a promising candidate for improving the membrane synthesis efficiency.

Table 3.4: ZIF-8 membrane thickness and propylene/propane binary gas separation results for ZIF-8 membrane synthesized with zinc nitrate and zinc chloride as the zinc source for 10 h membrane synthesis time, respectively, on silicalite seeded AAO.

Zinc Source	$\alpha_{C_3H_6/C_3H_8}$	P_{m,C_3H_6} ($\times 10^{-8}$ mol m^{-2} s^{-1} Pa^{-1})	Thickness (nm)
$Zn(NO_3)_2$	47±1.1	0.99±0.03	680
$ZnCl_2$	170±0.5	0.90±0.04	850

The ZIF-8 membranes synthesized at various synthesis durations were also assessed for an equimolar propylene/propane mixture and the results are summarized in Figure 3.9. As a comparison, the propylene/propane separation factor significantly increased for synthesis duration of 10 h from 5 h with a slight decline in propylene permeance. However, a further increase in membrane synthesis time decreased propylene permeance and slightly reduced the propylene/propane separation factor. ZIF-8 membrane thickness was 650 nm, 850 nm, and 1630 nm for synthesis times of 5 h, 10 h, and 20 h respectively. In this case, 10 h was found to be the optimized membrane synthesis time for membrane preparation.

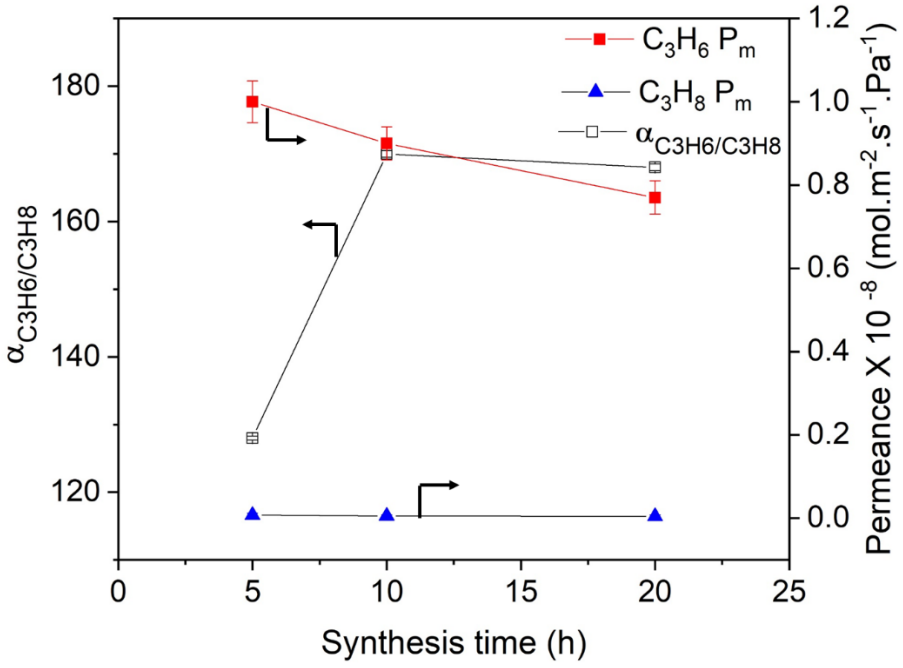

Figure 3.8: Propylene/propane binary gas separation results for ZIF-8 membrane synthesized at 5, 10, and 20 h with silicalite as seeding layer and $ZnCl_2$ as the Zn source, respectively.

3.4. Conclusion

In this work, we demonstrated a novel fabrication method for ZIF-8 membrane growth on the anodic aluminum oxide (AAO) substrate for effective propylene/propane mixture separations based on the size exclusion mechanism. The effects of seeding, zinc salts, and membrane synthesis time on ZIF-8 membrane performance for propylene/propane gas separation were studied. Among in-situ ZIF-8 membrane, silicalite seeding, and ZIF-8 seeding, silicalite seeding exhibited the highest separation performance. Silicalite seeding helped in the proper growth of the ZIF-8 membrane over the AAO substrate. As a precursor, $ZnCl_2$ showed higher separation performance because $ZnNO_3$ as the precursor reacts faster which led to a less intergrown ZIF-8 membrane and a thinner ZIF-8 membrane layer than other zinc sources. ZIF-8 crystal size affected membrane stability and gas adsorption indicating that the appropriate ZIF-8 crystal size for the propylene/propane separations can be achieved by using $ZnCl_2$. The appropriate time

for ZIF-8 membrane fabrication was determined to be 10 h. With the increase in membrane synthesis time from 10 h to 20 h, propylene permeance decreased from 0.9×10^{-8} to 0.7×10^{-8} mol m^{-2} s^{-1} Pa^{-1}. ZIF-8 membranes prepared with silicalite seeding, $ZnCl_2$ precursor, and 10 h synthesis time showed a propylene/propane separation factor of 170 and propylene permeance of 0.9×10^{-8} mol m^{-2} s^{-1} Pa^{-1}

CHAPTER IV

MODIFICATION OF ZIF-8 MEMBRANE BY ATOMIC LAYER DEPOSITION FOR HIGH PROPYLENE/PROPANE SELECTIVITY

Summary

ZnO was coated on the as-synthesized secondary grown ZIF-8 membranes by using atomic layer deposition (ALD). The ZnO ALD coating reduced the density of non-selective defects on the surface of ZIF-8 membrane. Different numbers of ZnO coating cycles were deposited on the membrane surface to investigate the changes in the ZIF-8 membrane microstructure. The resulting ZIF-8 membranes were tested before and after ZnO ALD for propylene/propane separation. The ZnO ALD coated membranes showed enhanced performance compared to the as-synthesized secondary grown ZIF-8 membranes.

4.1. Introduction

Propylene/propane separation is challenging due to their similar physical properties and using conventional distillation methods is energy-intensive [37, 91]. Alternatively, propylene/propane separation using membrane technology is more energy-efficient and cost-effective than conventional techniques [64]. The selection of membranes is vital for achieving lower capital costs when membrane technology is applied [121]. Due to the well-ordered porous structure and the suitable aperture pore size, metal-organic frameworks (MOFs) are well-suited to propylene/propane separation [24, 94, 122]. For example, zeolitic imidazolate framework (ZIF) membranes are a sub-class of MOFs with robust synthesis protocols and

exceptional stability of regular crystalline lattices with confined ultra-micropores [90]. ZIF-8 membranes have been of particular interest due to their appropriate pore size (~0.4 nm) for propylene/propane separation [31]. Diverse types of solvent-based synthesis techniques have been used to synthesize ZIF-8 membranes including in-situ growth, secondary growth, and counter diffusion methods [64, 70, 76]. Both in-situ and counter diffusion methods are favorable to high nucleation and rapid synthesis of ZIF-8 membranes. However, the rapid nucleation likely causes defects on the ZIF-8 membrane surface, significantly affecting ZIF-8 performance in propylene/propane separation [31]. Among these methods, particularly the secondary growth method, produces a strong attachment of seed crystals to porous supports, acting as anchors to achieve a well-intergrown membrane [72].

However, defects in the membrane are inevitable, including inter-crystalline gaps, pinholes, and cracks, when secondary growth methods are used to fabricate high-quality ZIF-8 membranes [31, 90]. For example, Zhang et al. computationally investigated structural stability and defect formation in ZIF-8 structure by varying chemicals and synthesis conditions. They found that defects can form at ambient environmental conditions based on the solvents used in the process [79]. These defects generate the viscous flow of gases across the membrane, diminishing the separation performance of ZIF-8 membranes. To alleviate defects and improve the gas separation performance, post-synthetic modification methods such as ligand treatment, doping with metals, building block replacement, and additional polymer layer coating have been used [80, 81]. For example, Kwon et al. investigated the post-synthetic hydrothermal ligand treatment to minimize the defect sites in ZIF-67 membranes. After ligand treatment, the propylene/propane separation factor increased from 85 to 220, while propylene permeance dropped from 4.6 to 3.7×10^{-8} mol $m^{-2}\,s^{-1}\,Pa^{-1}$ [123]. Lee et al. found that defect formation depends on kinetic variables such as the synthesis protocol, temperature, and chemical composition. They used post-synthetic ligand treatment at 60 – 100 ˚C for 4 h to reduce the surface defects. Reduction in defects resulted in a 6-fold propylene/propane separation factor enhancement concomitant with the reduction of the propylene permeance by ~75% [31]. Li et al. explored defects healing by applying organic polymer polydimethylsiloxane (PDMS) layer on a pre-

synthesized ZIF-8 membrane surface. After PDMS coating, the propylene/propane separation factor improved from 12 to 67 and propylene permeance dropped from 2.1 to 1.3×10^{-8} mol m^{-2} s^{-1} Pa^{-1} [48].

Although the post-synthetic methods increased the ZIF-8 membrane separation factor by removing surface defects, excessive deposition can cause an unacceptable loss in gas permeance [82]. The takeaway is that post-synthetic treatment methods can be used to maximize the selectivity but at the expense of compromising the gas permeance through the membrane. Therefore, both membrane gas permeance and selectivity need to be systematically monitored and controlled when performing post-synthetic treatments. Several post-synthetic treatment studies have been conducted to address the defects problem, where highly controlled deposition of a secondary layer by atomic layer deposition (ALD) is a promising approach. ALD, a vapor phase deposition technique, is a sequential, self-limiting gas-phase deposition method for growing atomic-scale thin films of oxides, metals, polymers, and many other materials in a layer-by-layer fashion. ALD has emerged as an exciting new route for producing membranes with nanoscale control of the pore size, which is extremely attractive from the standpoint of membrane design [124-128]. Hence, ALD allows one to precisely engineer the pore size to a specific molecular species, particularly small molecules (shifting of the cut-off pore size) [129]. Atomic layer deposition has already been successfully used to tune the pore size of membranes for a variety of gas-phase separation processes [24, 130-132].

In this work, we synthesized a ZIF-8 membrane and deposited ZnO on the membrane surface by ALD. The process involves silicalite seeding and secondary growth for ZIF-8 membrane synthesis, followed by membrane surface modification by ZnO deposition using ALD. The ZnO layer is expected to minimize membrane defects and improve propylene/propane separation while minimizing the loss of propylene permeance. The gas permeance and separation factor of the propylene/propane binary mixture were measured for the ZIF-8 membranes before and after ZnO ALD. To investigate microstructural changes, the membranes were characterized using X-ray diffraction (XRD), X-ray photoelectron

spectroscopy (XPS), Fourier transform infrared (FT-IR) spectroscopy, and scanning electron microscopy (SEM).

4.2. Experimental section

4.2.1. Silicalite nanoparticle seeding

Silicalite nanoparticles were prepared by the detailed synthesis procedure that has been previously reported [103]. The molar composition of each component for preparing silicalite seed suspension is NaOH: H_2O: TPAOH: SiO_2=1.00: 131.50: 2.86: 9.42, respectively. The procedure followed for seed synthesis includes NaOH (99.99%, Sigma-Aldrich) being dissolved in the mixture containing H_2O and tetra-propyl-ammonium hydroxide (TPAOH, 1 M, Sigma–Aldrich). Afterward, fumed SiO_2 (0.2-0.3 μm powder, Sigma-Aldrich) was added to the above solution in a water bath having a temperature of 80 °C and stirred to dissolve properly. The obtained clear solution was left for 4 h and transferred to an autoclave jacketed vessel for hydrothermal synthesis with a duration of 6 h at 120 °C. The synthesized powder (seed suspension) was washed with deionized water (DI water) and then centrifuged at 4000 rpm for 30 min. Finally, the silicalite seed suspension was diluted to 0.05 wt.% for dip coating a seed layer.

4.2.2. ZIF-8 membrane synthesis via secondary growth

For membrane fabrication, an anodic aluminum oxide (AAO) support disk (diameter: 25 mm, thickness: 60 μm, pore size: 20 nm, porosity: 24%, Whatman) was used as a support. AAO disks were immersed into the seed suspension solution, then were sonicated for 5 min to distribute the seeds uniformly to coat the support surface. The seeded AAO support was dried overnight at room temperature. After drying, ZIF-8 layers were synthesized on the silicalite seeded AAO support via the secondary growth method. For ZIF-8 membranes, metal and ligand solutions were prepared separately. Specifically, 0.076 g of zinc chloride (99.99%, Sigma-Aldrich) was dissolved into 20 mL of DI water, and 3.165 g of methyl imidazolate (mIm) (99.7%, Sigma-Aldrich) was dissolved into 40 mL of DI water to prepare metal and ligand solution,

respectively. Subsequently, both the metal and the ligand solutions were vigorously stirred for 30 sec. For the secondary growth, the dried seeded AAO support was immersed vertically into the synthesis (metal + ligand) solution and held for 10 h in a Teflon vessel at room temperature. The synthesized membrane was taken from the Teflon vessel and immersed in 50 mL of methanol, (99.5%, Sigma-Aldrich). The membrane was removed from the methanol and dried for 12 h at room temperature. The detailed ZIF-8 membrane synthesis on the AAO support procedure steps is illustrated in Figure 1.1. The ZIF-8 membrane synthesis procedure has been previously reported in detail [133].

4.2.3. ZnO atomic layer deposition

To reduce defects in the membrane surface, a thin layer of ZnO was coated on the ZIF-8 membrane via the ALD process. ZnO film formation occurred by the mechanism [128] shown in equation 4.1**.**

$$Zn(C_2H_5)_2 + H_2O\ (g) \rightarrow ZnO + 2C_2H_6\ (g) \qquad (4.1)$$

The ZnO deposition procedure was conducted using the ALD unit (OkYay Tech, Turkey). During the ZnO deposition process, the ALD chamber temperature was maintained at 70°C with a baseline pressure of ~200 milliTorr. To achieve the homogeneous coating, ZIF-8 membranes were initially stabilized inside the chamber for 30 min before the deposition. During the ALD process, $Zn(C_2H_5)_2$ (>95%, Strem Chemicals Inc.) is introduced into the ALD unit at a pressure of 700 mTorr and held for 100 ms, and then vacuum is applied to remove the unreacted $Zn(C_2H_5)_2$. Ultrahigh pure N_2 is used at a flow rate of 10 sccm for 20 s, controlled by a mass flow controller, followed by a vacuum to evacuate N_2. After that, water vapor is introduced into the cell to a pressure of 800 mTorr and held for 60 ms, vacuumed, and purged using ultrahigh pure N_2. This entire process constitutes one ALD cycle. In the process, two and four cycles of ZnO were deposited using ALD with a film thickness of ~0.8 Å per cycle. The deposition of ZnO on ZIF-8 membranes is illustrated in Figure 1.2.

4.2.4. Propylene/propane binary gas separation experiment

All membranes were stored in a desiccator at room temperature before gas permeation measurements. Propylene/propane binary gas permeation measurements were performed at room temperature and atmospheric pressure. The membrane was mounted in a stainless-steel cell with the membrane surface facing toward the feed side, as shown in Figure 3.1. The flow rate (100 cm^3/min) of an equimolar propylene/propane mixture was controlled with mass flow controllers (MFC), where the gases were mixed before feeding into the membrane separator. Argon was used as a sweeping gas at a flow rate of 100 cm^3/min on the permeate side. Before collecting the data for each set of conditions, the membrane separation was allowed to stabilize for ~4 h at room temperature to get steady-state data points. The permeate gas composition was analyzed using online gas chromatography (Shimadzu, GC-2014) equipped with a molecular sieve 13X column for the thermal conductivity detector (TCD). The membrane permeance and separation efficiency measurement details are described in section 3.2.3.

4.2.5. Characterization

The surface and cross-section morphology of the membranes were characterized using a scanning electron microscope (SEM) and the elemental composition was identified by Energy Dispersive X-Ray (EDX) analysis, using an FEI Quanta 600 SEM. The crystal structure of the ZIF-8 membrane was characterized by X-ray diffraction (XRD, Bruker AXS D8 Discover diffractometer with General Area Detector Diffraction System, 40 kV, 35mA) with a scan rate of 1.0-degree min^{-1} and the two-theta range of 5-40 degrees. The chemical structure of the samples was measured by X-ray photoelectron spectroscopy (XPS, PHI Versa Probe II Scanning XPS Microprobe with Al Kα line excitation source) and by Fourier-transform infrared (FT-IR) analysis using Thermo Nicolet 380 FT-IR with Diamond attenuated total reflectance (ATR). Nitrogen absorption and desorption were performed using a Quantachrome Autosorb I. Samples were outgassed at 50 °C overnight under a vacuum. pyGAPS was used to analyze the resulting

isotherms. The surface area and pore volume of the ZIF-8 membranes were measured by N_2 adsorption at 77 K based on the Brunauer–Emmett–Teller (BET) model.

4.3. Results and Discussion

4.3.1. Membrane characterization

AAO supports have a uniform, vertically aligned pore channels, as shown in Figure 4.2 (a, b). After seed layer coating, silicalite nanoparticles were homogeneously coated on the support surface [133]. After secondary growth, the ZIF-8 membranes were uniformly grown on the AAO support, as shown in Figure 4.2c. The cross-section SEM images of the interface between AAO support and ZIF-8 membrane show that tightly packed grain boundaries are formed due to intergrowth between them. The membrane thickness was ~850 nm when synthesized for 10 h at room temperature and atmospheric pressure, which is thinner than previously reported secondary grown ZIF-8 membranes [70, 72]. While the secondary grown ZIF-8 membrane on AAO support has a well inter-grown, homogeneous, and compact structure, they can have defects that are nonselective to molecules. Moreover, the formation of defects is typically caused by changes in temperature and chemical composition. For example, during rapid crystal growth, which creates defects on the membrane surface due to the kinetic trapping of defective structures [31]. Additionally, surface defects are the solvation effect and salt formation on the ZIF-8 framework during synthesis [79]. Ultimately, defects, regardless of how and why they form, affect the membrane's pore structure due to the lack of proper inter-linkage in the structural framework, which compromises propylene/propane gas separation [31, 79].

To minimize the density of nonselective membrane defects, ZnO was deposited on the ZIF-8 membrane surface using the ALD technique. As shown in Figure 4.2c, the secondary grown ZIF-8 membrane exhibits a typical intergrown ZIF-8 crystal morphology. Two ALD cycles of ZnO produced a continuous ZnO layer on top of the ZIF-8 membrane (Figure 4.2e). The ZIF-8 membranes after four cycles of ZnO ALD had an amorphous morphology, indicating that precipitation of ZnO has occurred Figure 4.2

(e, g) shows that the membrane surface was uniformly covered by the ZnO layer during 2-4 cycles of the ALD process. Figure 4.2 (f, h) showed the cross-sectional view of the ZIF-8 membranes treated with ZnO ALD. The effect of ZnO ALD treatment on the thickness of the ZIF-8 membranes was negligible while the membrane surface was uniformly covered by the ZnO layer. ZnO ALD ZIF-8 membranes showed negligible thickness change (around ~850 nm) compared to secondary grown ZIF-8 membranes, indicating the ALD treatment generates an extremely thin ZnO layer.

We anticipate that ZnO ALD on ZIF-8 membranes will minimize the defect density. However, excessive deposition of ZnO at the ZIF-8 pore mouth could clog the pores and cause a severe decrease in permeance [134]. Therefore, to avoid excessive deposition, we calibrated the effect of pore closure as a function of ALD cycles through the propylene/propane separation measurement.

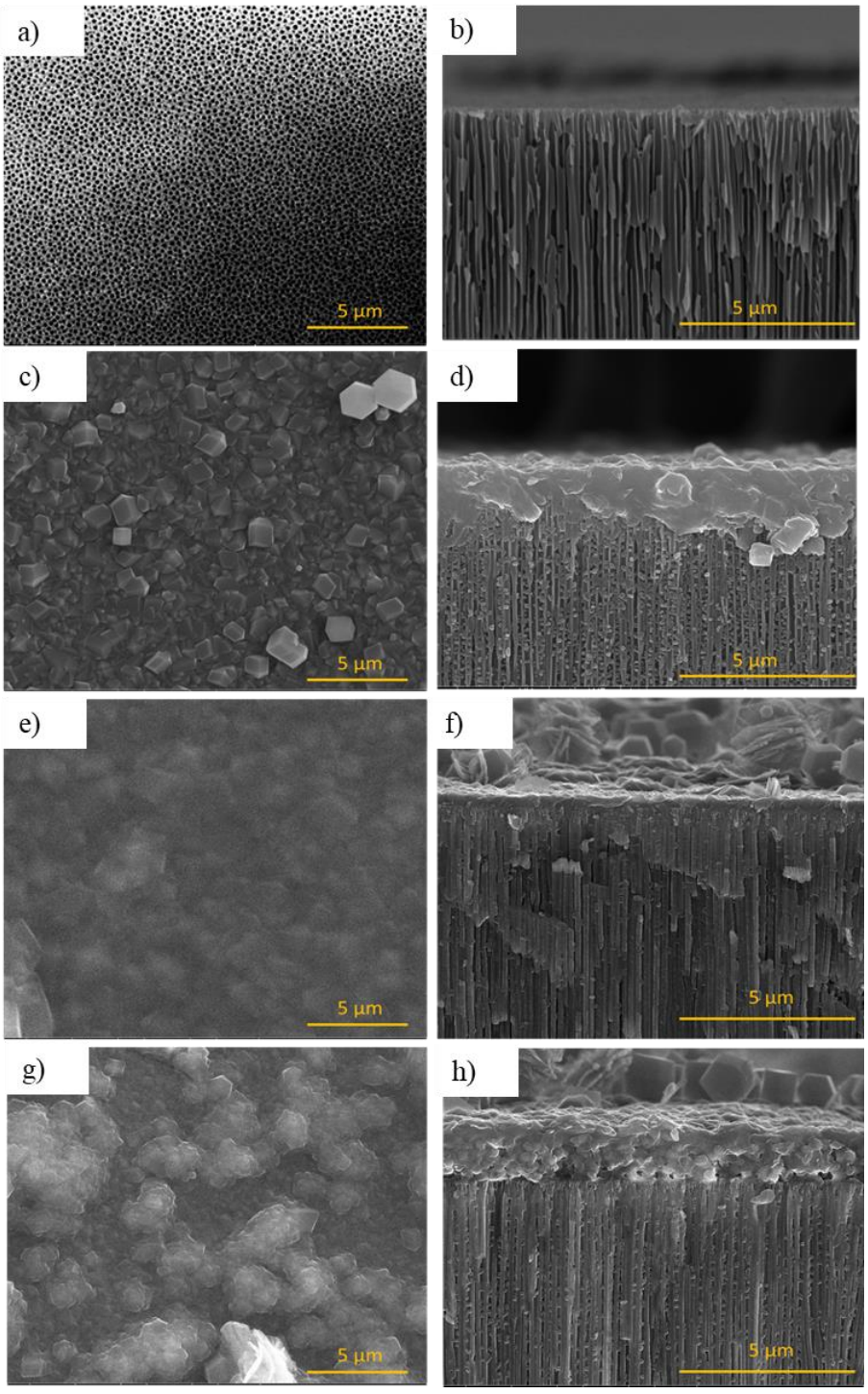

Figure 4.1: SEM images of (a, b) AAO, (c, d) ZIF-8 membrane, (e, f), ZIF-8 membrane after two cycles of ZnO ALD, (g, h) ZIF-8 membrane after four cycles of ZnO ALD.

For understanding the compositional changes in the membranes, EDX elemental mapping was performed on the surface of the AAO supports, ZIF-8 membranes, and ZnO ALD ZIF-8 membranes (2 cycles) as shown in Figure 4.3. The nanocomposite membranes synthesized at room temperature resulted in the ZIF-8 membrane formation, confirmed by EDX analysis. Elemental mapping of Al and Zn as a function of ALD cycles by EDX is displayed in Figures 4.3 (a-c). Upon examination, the ZnO is uniformly distributed across the membrane surface, and the ZnO coverage increases with the number of cycles, as expected.

The results of the EDX analysis of the AAO support, ZIF-8/AAO support, and ZnO/ZIF-8/AAO support are summarized in Table 4.1. As expected, the AAO support has an abundance of aluminum compared to other elements, including carbon, nitrogen, and zinc. The carbon and nitrogen content increased with the application of the ZIF-8 membrane, while the aluminum content decreased since the EDX probed depth is ~1 um. Zn content increased from 0.098 wt.% (AAO support) to 2.42 wt.% (ZIF-8 membrane). The Zn content increases after ZnO ALD to 3.49 wt.% or a 44% relative increase.

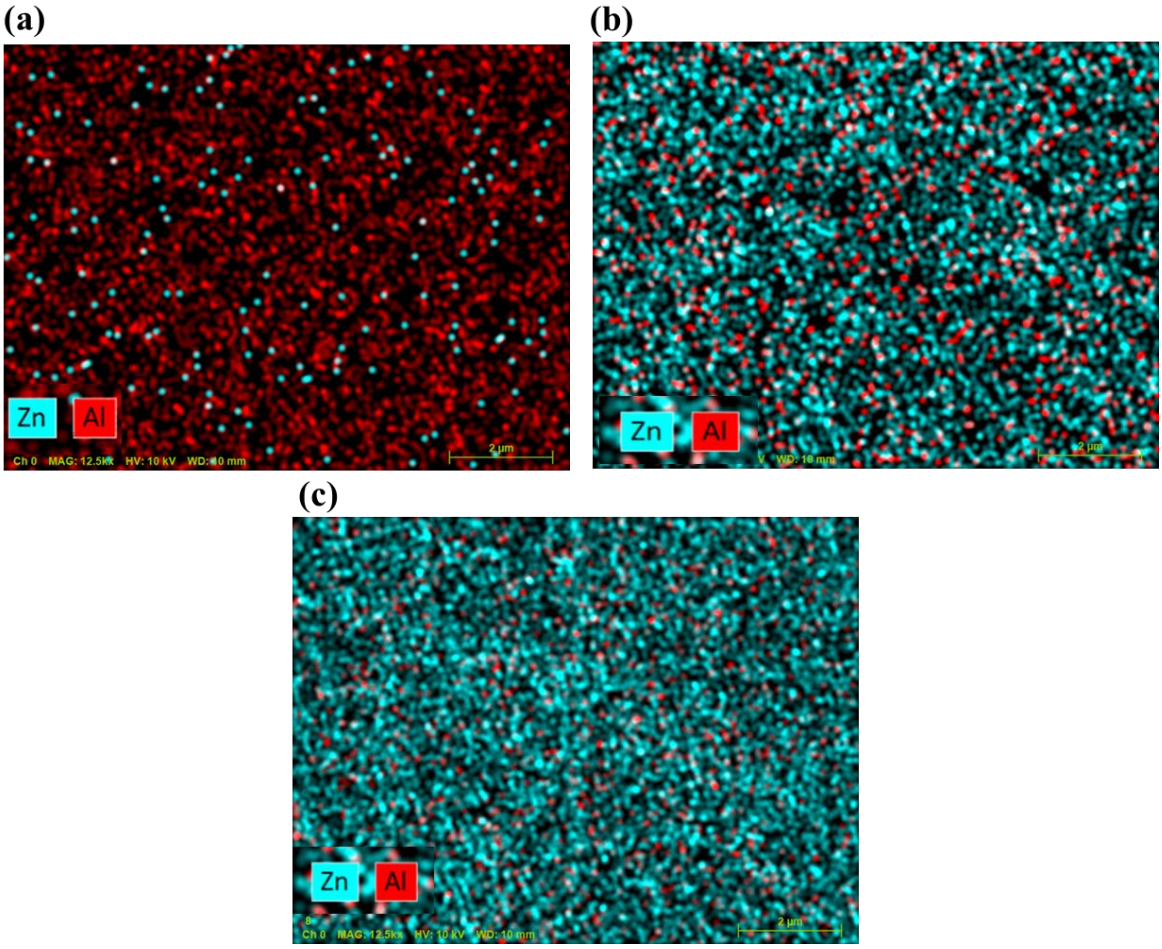

Figure 4.2: EDX elemental mapping on the surface of (a) AAO support, (b) ZIF-8 membrane, and (c) ZnO ALD ZIF-8 membrane (2 cycles).

Table 4.1: The elemental composition analysis data of AAO, ZIF-8, and ZnO ALD ZIF-8 (2 cycles).

Sample	Carbon (%)	Nitrogen (%)	Zinc (%)	Aluminum (%)
AAO support	23.32	12.22	0.098	64.36
ZIF-8 membrane	53.54	43.82	2.42	0.20
ZnO ALD ZIF-8 membrane	53.23	43.52	3.49	0.15

The crystal pattern of the secondary grown ZIF-8 membranes was characterized by X-ray diffraction (XRD), as presented in Figure 4.4. The XRD analysis indicated the formation of ZIF-8 membranes. ZIF-8 and ZnO ALD ZIF-8 membrane peaks were observed at 2θ of 7, and 11°, consistent with crystallographic information previously reported [133]. Before and after ZnO ALD, the XRD patterns were similar, indicative of membrane structural integrity.

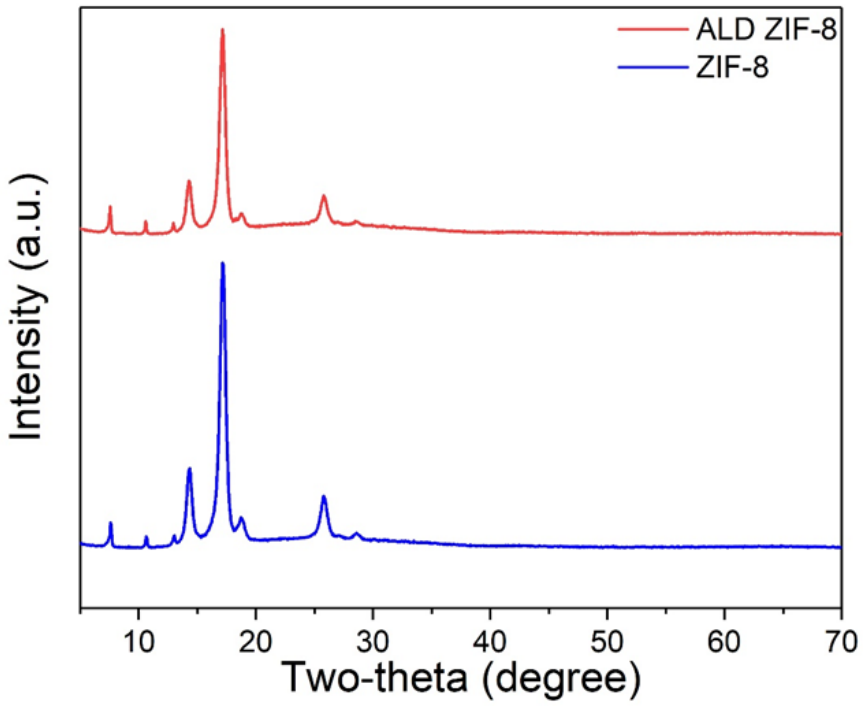

Figure 4.3: XRD patterns of ZIF-8 membrane and ZnO ALD ZIF-8 membrane (2 cycles).

The X-ray photoelectron spectroscopy (XPS) analysis in Figure 4.5 shows Zn 2p spectra with two distinct peaks at 1022 and 1045 eV, which is characteristic of the Zn $2p_{3/2}$ and Zn $2p_{1/2}$ in ZIF-8, respectively. The Zn 2p core levels shift slightly to higher binding energy (BE) upon coating with ZnO, which is to be expected for the higher oxidation state of ZnO relative to ZIF-8 [135]. The Zn 2p spectral intensity also increases, as expected, and is consistent with Table 4.1. Moreover, Zn $2p_{3/2}$ has a lower BE, and Zn $2p_{1/2}$ is assigned to a higher BE. The shift of the Zn 2p without significant broadening suggests that

the spectrum is a convolution of the Zn in ZnO and ZIF-8. Therefore, one can conclude that there is a decrease in several number unsaturated Zn-N bonds in the ZIF-8 membranes and thus a reduction of defects due to Zn deposition [79, 82, 136, 137].

Similarly, after ZnO ALD, N1s peak (398 eV) shifted to higher BE. The peak shifts also support the enhancement in Zn-N BE, which further indicates the defects are healed and a more robust ZIF-8 membrane with fewer defects is achieved [31, 82]. Furthermore, the peak intensities and BE of the C 1s peak (at 285 eV) from the imidazole group indicate that the defects are healed, consistent with the literature [108, 109]. XPS results, along with the data represented in Table 4.1 show no significant increase in the carbon atomic percentage after ALD. We conclude that ZnO ALD ZIF-8 membranes have fewer unsaturated Zn atoms and fewer defects.

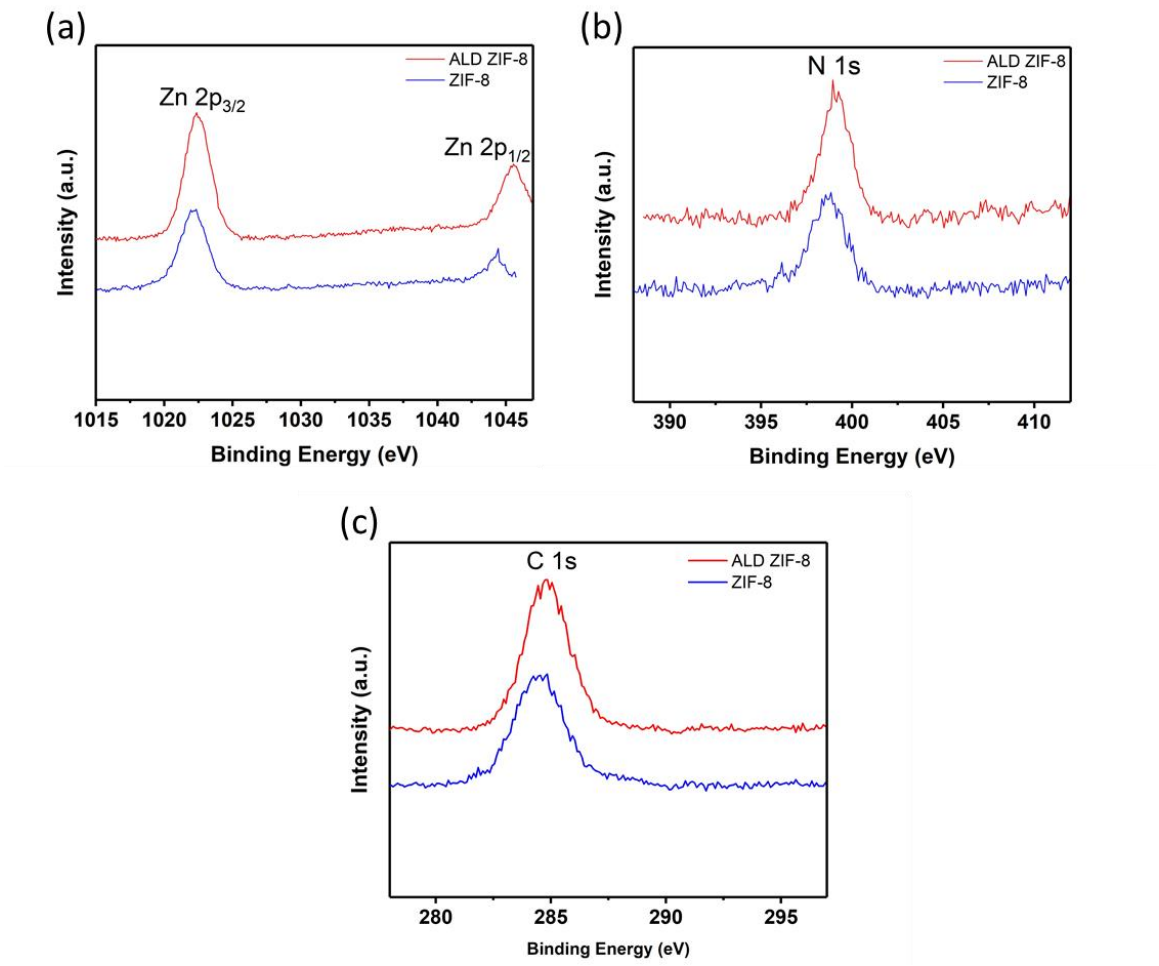

Figure 4.4: XPS spectra of ZIF-8 membrane and ZnO ALD ZIF-8 membrane (2 cycles): (a) Zn 2p, (b) N 1s, and (c) C 1s.

The FT-IR spectra in Figure 4.6 were acquired for the two samples to observe structural changes in the ZnO ALD ZIF-8 membrane. The band at 995 cm^{-1} is the C=C-N stretching mode, at 1146 cm^{-1} is the =C–H and C–N stretching modes, at 1580 cm^{-1} is the C=N stretching mode, and at 3134 cm^{-1} is for C–H bond stretching mode, respectively [115]. After ZnO ALD treatment, the FT-IR peak intensities increase significantly. It was found that ZIF-8 membranes displayed less absorbance than ZnO ALD ZIF-8 membranes, indicating that ZIF-8 membranes have a higher density of defects relative to ZnO ALD ZIF-8 membranes. Furthermore, the increase in the intensity of the FT-IR peaks is consistent with XPS results

and indicative of an increase in the robustness in grain boundary structure and reduction in defects of the ZnO ALD ZIF-8 membranes [113, 115].

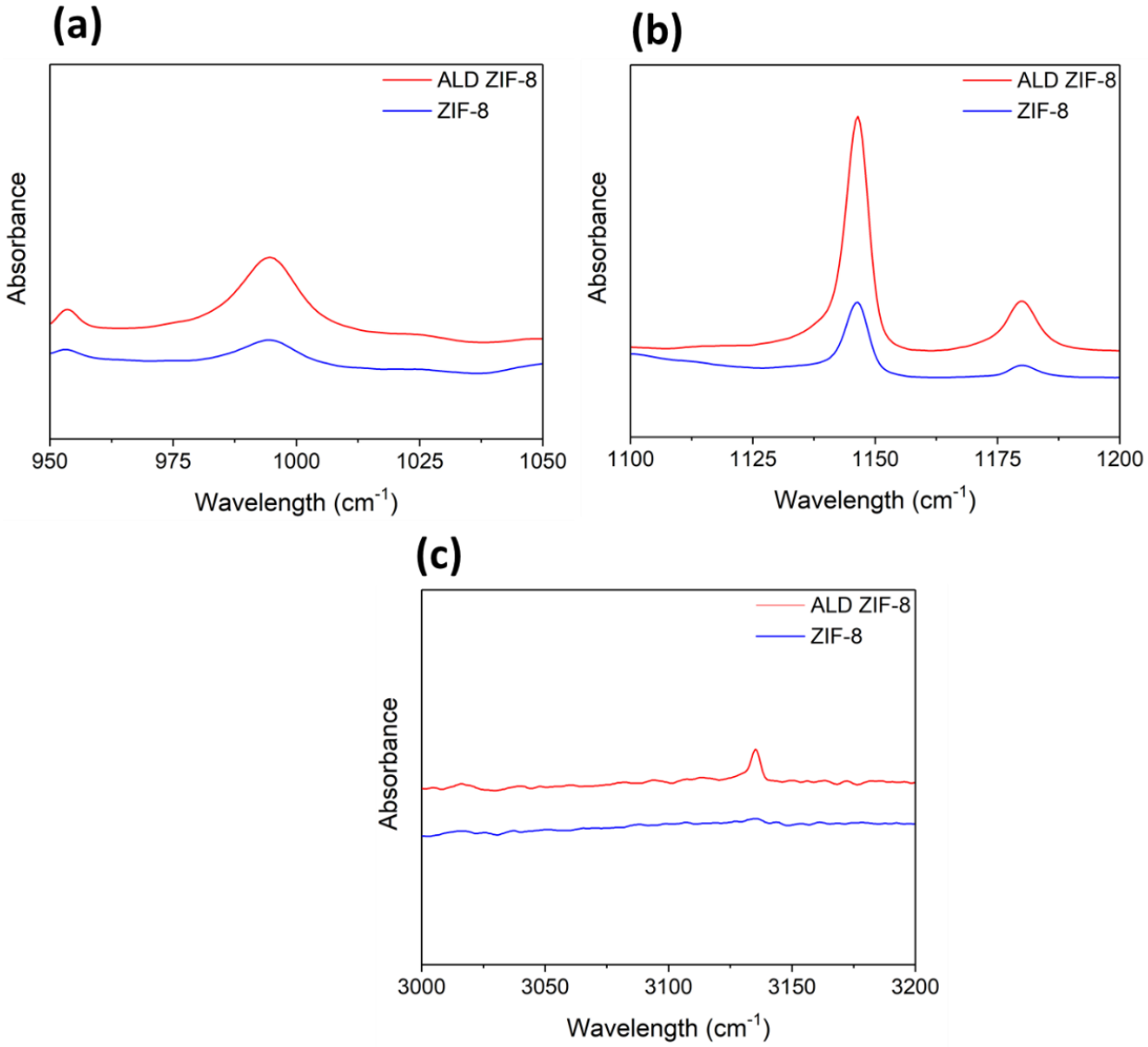

Figure 4.5: FT-IR spectra of ZIF-8 membrane and ZnO ALD ZIF-8 membrane (2 cycles): (a) Zn 2p, (b) N 1s, and (c) C 1s.

N_2 adsorption and desorption tests were performed on the ZIF-8 and ZnO ALD ZIF-8 membranes, where the type-1 isotherm is indicative of the microporous structure (pore size <2 nm) of the membranes [114]. Desorption hysteresis was visible for $P/P_0 > 0.8$ for the ZIF-8 and ZnO ALD ZIF-8 membranes, indicating the presence of micropores and mesopores [116]. Typically, ZIF-8 has a specific surface area ranging from 1000 to 1600 $m^2 g^{-1}$ [138] and depends on the concentration of the unreacted residues [139]. The BET analysis summarized in Table 4.2 for both types of samples indicates that there are negligible changes in the surface area and pore volume of the membrane with the addition of the ZnO coating. This indicates that ZnO is on the external surface and/or pore entrance of ZIFs, thereby reducing the density of surface defects.

Table 4.2: BET surface area and pore volume of ZIF-8 and ZnO ALD ZIF-8 (2 cycles) as measured by N_2 adsorption at 77 K.

Description	BET surface area ($m^2 g^{-1}$)	Pore volume ($cm^3 g^{-1}$)
ZIF-8 membrane (this work)	1474	0.71
ZnO ALD ZIF-8 membrane (this work)	1424	0.70
ZIF-8 membrane [113, 140]	1046	0.51

4.3.2. Membrane separation

The performance of the ZIF-8 membranes and the ZnO ALD treated ZIF-8 membranes for propylene/propane binary gas mixture separation at room temperature is displayed in Figure 4.7. The as-prepared ZIF-8 membranes were assessed, then coated with ZnO by ALD, and then retested. For the as-prepared ZIF-8 membranes, the separation factor was 141. After coating two cycles of ZnO ALD, the separation factor improved to 264. The significant enhancement in propylene/propane gas separation is

attributed to the healing of surface defects of the membranes. Membrane defects, intercrystalline gaps, and grain boundaries in the membranes can generate viscous flow through them, which will strongly affect the diffusion rate. Minimizing defects reduces viscous flow through these non-selective paths. The conclusion is that ALD processing is an excellent approach for fine-tuning the membranes by way of reducing the density of surface defects.

Membranes with four ZnO ALD cycles were also prepared as part of the membrane optimization process. Four ALD cycles reduced the propylene/propane separation factor from 264 to 238 (Figure 4.7). This is attributed to clogging the membrane pores. Therefore, 2 cycles of ZnO ALD aided in minimizing surface defects, but 4 cycles had the added effect of blocking the membrane pores. The propylene permeance decreased from 0.9×10^{-8} to 0.6×10^{-8} mol m^{-2} s^{-1} Pa^{-1} when increasing the ZnO ALD cycles from 2 to 4 (Figure 4.7). The decrease in the propylene permeance is a combination of a reduction in pore size and clogging of pores. These results demonstrate that to avoid excessive deposition, ALD processing post-processing of ZIF-8 membranes needs to be calibrated to ensure optimal propylene/propane separation.

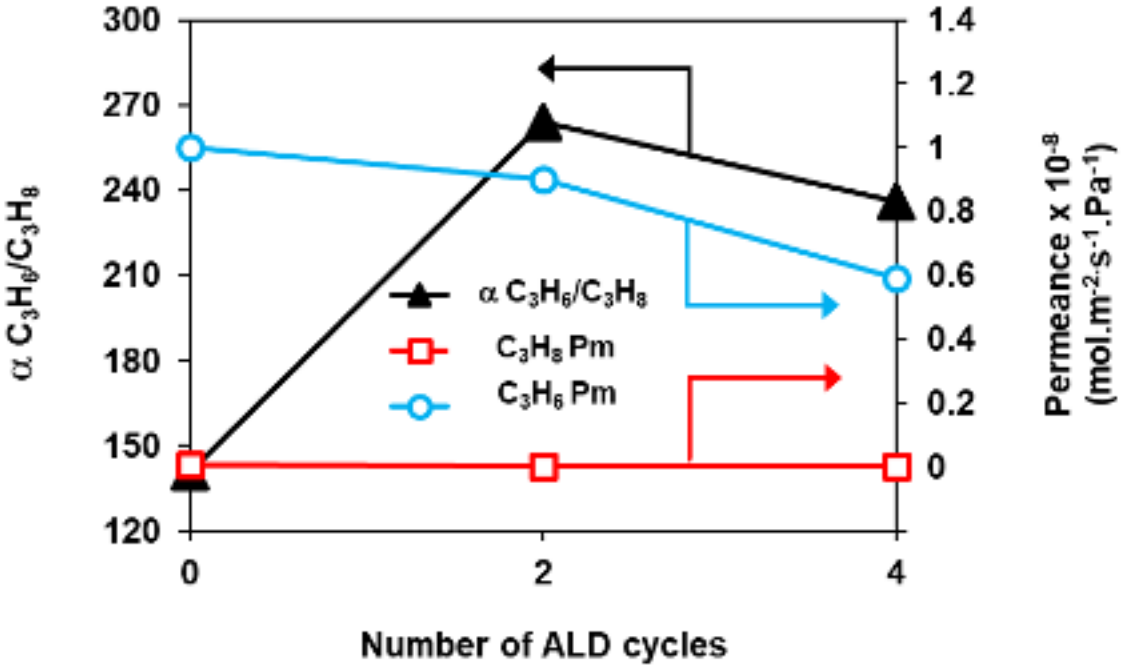

Figure 4.6: Effect of the number of ZnO ALD cycles on propylene/propane separation performance of the ZIF-8 membranes.

The results of the propylene/propane separation factor vs. permeance of this study are being plotted with ZIF-8 data from the literature [24, 48, 64, 71, 72, 119, 141-149] in Figure 4.8. Our as-prepared ZIF-8 membranes (~850 nm thick) exhibited a separation factor of 141 with the propylene permeance of ~1.0×10^{-8} mol m^{-2} s^{-1} Pa^{-1}, where the separation factor is slightly higher than the average value from the literature scattered around 75. The ZnO ALD treated ZIF-8 membranes of this study improved the separation factor by 87% relative to the as-prepared ZIF-8 membrane with only a 10% drop in permeance. Note that the ZnO ALD treated membrane (2 cycles) outperformed the average propylene/propane separation factor of ~75 of the previously reported results in Figure 4.8 by ~350%.

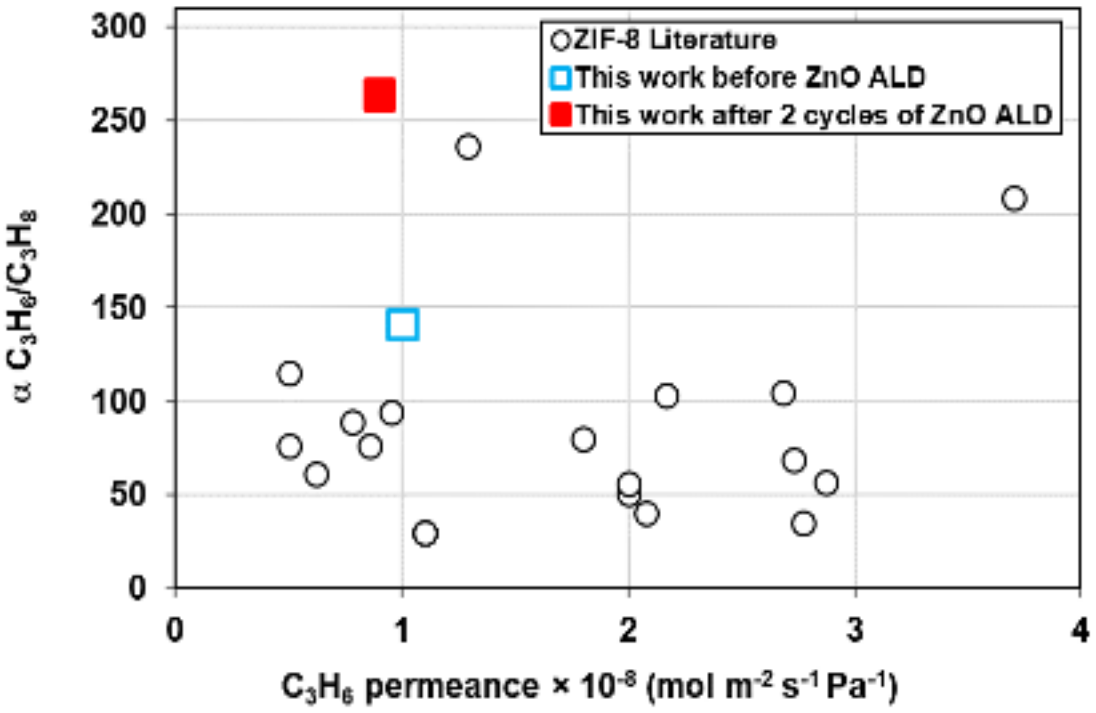

Figure 4.7: Propylene/propane separation performance comparison with literature data.

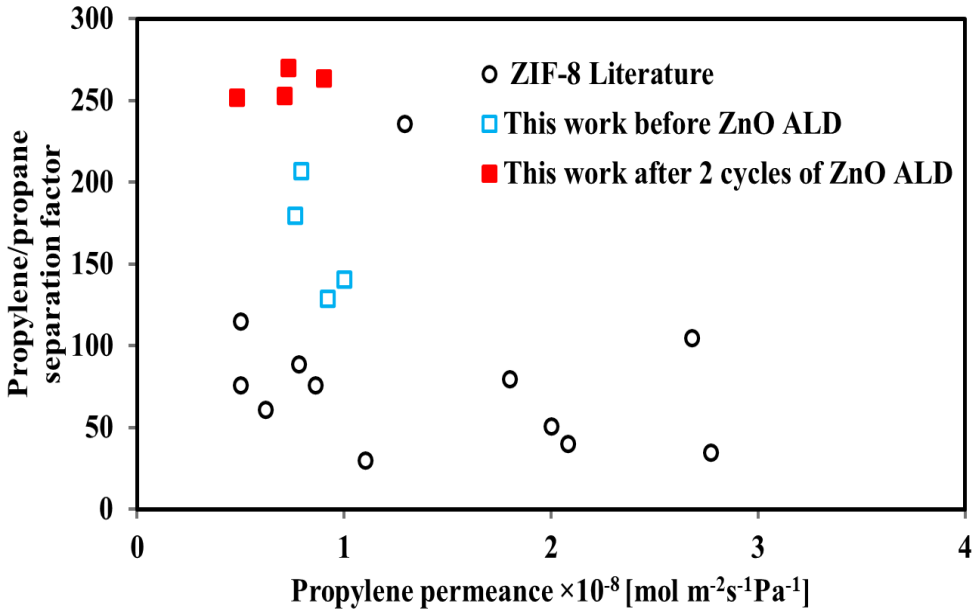

Figure 4.8: Propylene/propane binary gas separation performance comparison with literature data.

4.4. Conclusion

ZIF-8 membranes fabricated using the secondary growth method exhibited impressive separation performance for propylene/propane binary gas mixture. Moreover, we identified a unique strategy of ZnO ALD on ZIF-8 membranes to enhance membrane performance, specifically, the propylene/propane separation factor. The deposition of a ZnO layer on the surface of the ZIF-8 membranes by atomic layer deposition reduced the density of non-selective defects, which significantly improved the ZIF-8 membrane performance. The optimal number of two ZnO ALD cycles improved the propylene/propane separation factor from 141 to 264 (87%) at the expense of only a ~10% decrease in propylene permeance. This study demonstrated that the ALD postprocessing of ZIF-8 is ideal for minimizing the density of defects and for reducing viscous flow through non-selective paths.

CHAPTER V

HIGH-FLUX ZIF-8 MEMBRANES ON ZnO-COATED SUPPORTS FOR ENHANCED PROPYLENE PERMEANCE AND SELECTIVITY

Summary

The vapor phase synthesis technique was utilized to produce ultra-thin ZIF-8 membrane on ZnO deposited AAO support. The method involves the ZnO coating on AAO surface and subsequent conversion to the ZIF-8 layer using vapor-phase treatment of 2-mIm. This process enables solvent-free synthesis, which reduces the number of chemicals in the fabrication and results in ultrathin (~350 nm) propylene selective ZIF-8 membranes. The vapor phase synthesized ZIF-8 membranes show enhanced propylene permeance.

5.1. Introduction

Propylene is a highly demanding compound in chemical and polymer industries and is widely used to manufacture various petrochemical products [150]. Due to high demand in the growing market conditions, industrially produced propylene has been a shortage [21]. According to Energy Information Administration (EIA) standards, petrochemical industries produced ~94 million tons of propylene via traditional distillation in 2015 and are expected to reach ~132 million tons by 2025 [151]. Based on increasing market demand, propylene production in high volumes creates high energy requirements in the

industry. For propylene/propane separation, conventional technologies such as cryogenic distillation require low temperature and high pressure, increasing the cost and energy demand. There is a need for energy-efficient separation technologies to reduce the energy demand and make the separation process more sustainable. For example, researchers attempted to separate the propylene/propane mixture using energy-efficient techniques such as absorption, adsorption, and membrane processes [35]. Due to its low energy consumption and small footprint, membrane technology gained more attention and is a great alternative for cost-effective propylene/propane separation [37].

Recent research indicates that metal-organic framework (MOF) membranes efficiently separate gases via molecular sieving or selective adsorption mechanisms [152]. MOFs have tunable surface chemistry properties, including adjustable pore size, high porosity with a large surface area, and thermal and chemical stabilities [94]. Zeolitic imidazole framework (ZIF) is a subclass of MOF, mainly studied and tested for propylene/propane separation [16]. One reason for using ZIF-8 membranes for propylene/propane is the ZIF-8 pore size locating between the molecular sizes of propylene and propane [142]. Besides, the slight difference in molecular sizes enables the diffusion of propylene (0.40 nm) through ZIF-8 pores, which is approximately 125 times higher than propane (0.42 nm) [82]. The flexible structure of ZIF-8 and high propylene/propane selectivity inspired researchers to investigate various fabrication methods. The frequently used fabrication methods for ZIF-8 membranes are mostly solvent-based ones, such as in-situ, secondary growth, and the counter diffusion method [153]. However, the solvent-based techniques typically used in membrane fabrication have drawbacks. Due to heterogeneous nucleation, the problems include generating hazardous wastes, forming defects, and increasing thickness, negatively affecting the crystal growth and separation performance [64, 86, 154]. To overcome these challenges a more efficient way of ZIF-8 synthesis is critically needed.

One of the alternative methods is the vapor-phase synthesis method which was reported for generating ZIF-8 membranes [155]. Due to a simple synthesis process, the vapor-phase synthesis has shown a possibility to be a low-cost and eco-friendly fabrication. For example, chemical vapor deposition (CVD)

using atomic layer deposition (ALD) has been used to synthesize ZIF-8 membranes [85]. Stassen et al. have investigated a solvent-free synthesis of ZIF films on smooth silicon wafers by converting pre-deposited ZnO films to ZIF-8 via the CVD process [86]. Tanaka et al. examined the growth of ZIF-8 on porous substrates using the vapor-phase transport method, which includes converting ZnO nanorod array film to a ZIF-8 layer [87]. Rief et al. reported another approach to growing ZIF-8, which includes spraying ZnO on porous support followed by subsequent growth of the ZIF-8 layer by a vapor-solid reaction [156]. Wang et al. reported that the growth of ZIF-8 using ZnO has an excellent binding strength between porous support and membrane, which makes it superior in mechanical and thermal stabilities [89].

Kwon et al. developed a thinner ZIF-8 membrane around 300 - 400 nm using the vapor-phase method and the fabricated membranes showed a propylene/propane separation factor of ~120 with propylene permeance of 1.25×10^{-8} mol m^{-2} s^{-1} Pa^{-1} [90]. Ma et al. reported a solvent-free synthesis process of ZIF-8 membranes using a vapor-phase method. The ligand-induced permselective (LIPS) technique converted an impermeable ZnO-coated layer on an alumina disk to a propylene-selective ZIF-8 membrane layer. The ZIF-8 membranes showed high propylene permeance of 1.67×10^{-7} mol m^{-2} s^{-1} Pa^{-1} with a propylene/propane separation factor of 74 [84]. Using the LIPS procedure, Eum et al. fabricated a ZIF-8 membrane with a high propylene/propane separation factor of ~75 and propylene permeance of 5.5×10^{-8} mol m^{-2} s^{-1} Pa^{-1} [62].

Although achieving propylene selective ZIF-8 membrane fabrication is possible, an efficient synthesis process needs to further improve propylene permeance. In this study, a vapor-phase synthesis method was systemically investigated to convert a ZnO ALD layer to a thin high-flux ZIF-8 layer supported on anodic aluminum oxide (AAO) substrate. The commercially available AAO support was used to deposit a thin layer of ZnO via ALD, which was subsequently converted into a ZIF-8 layer by 2- methyl imidazole (2-mIm) vapor treatment. The vapor-phase treatment to synthesize a high propylene permeable ZIF-8 membrane was found to be solvent-free, seed-free, and reliable and the further membranes were characterized using SEM, EDX, XRD, and FT-IR, respectively.

5.2. Experimental

The strategy developed in this work for obtaining an AAO/ZIF-8 nanocomposite membrane confined in the pores of AAO support involves two key steps: i) deposition of a ZnO thin layer on the surface of the grain (pore walls) walls of the porous support by using ALD; ii) growth of ZIF-8 material in the pores of (ALD-ZnO) disk synthesized by vapor-phase treatment. In further sections, ZIF-8 membrane characteristics are described and discussed hereafter their structure, morphology, and gas mixture separation performance. Synthesis of ZIF-8 membranes prepared through a vapor-phase synthesis was provided below in a detailed procedure.

5.2.1. Atomic layer deposition of ZnO

ZnO was deposited at the external AAO surface and inside AAO pores using an ALD system (OkYay Tech, Turkey). The growth of ZnO is chemically represented based on the reaction described below [157].

$$Zn(C_2H_5)_2 + H_2O\ (g) \rightarrow ZnO + 2C_2H_6\ (g) \qquad (5.1)$$

The AAO support was placed horizontally inside the ALD deposition chamber at 70 ºC with a baseline pressure of ~200 millitorrs. The supports were first stabilized inside the chamber for 30 min before the deposition to achieve the homogeneous coating. Diethylzinc ($Zn(C_2H_5)_2$) and deionized (DI) water (Strem Chemicals Inc., >95%) were introduced into the ALD chamber as precursors for the deposition of ZnO. A typical ALD cycle consists of 100 ms exposure to diethylzinc followed by 15 s vacuum purge of N_2, and 60 ms exposure to water vapor followed by 15 s vacuum purge of N_2 as shown in Figure 5.1.

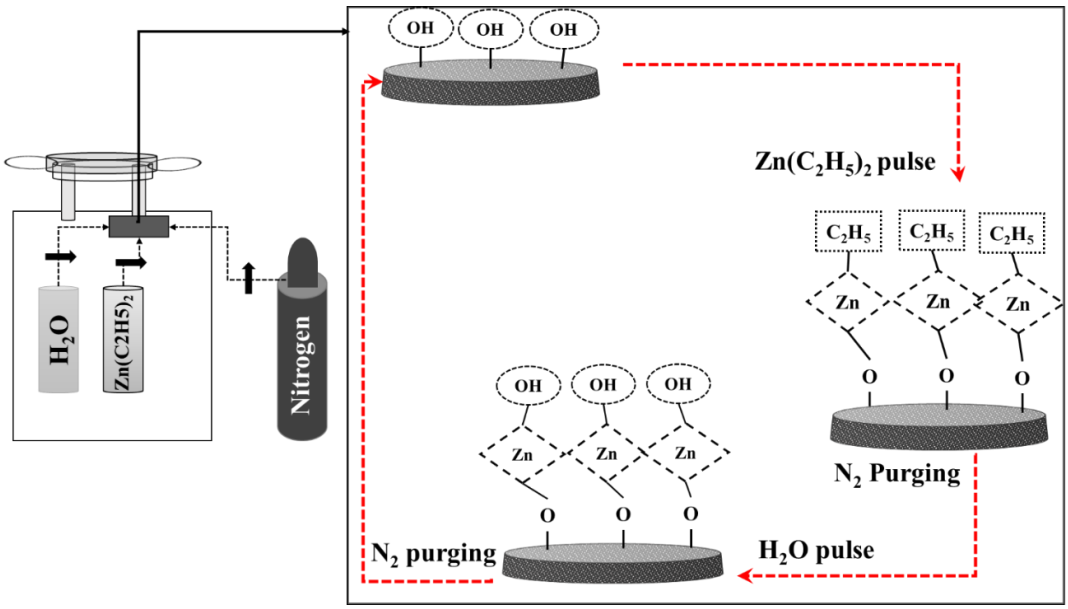

Figure 5.1: Schematic showing the ALD process of ZnO coating on an AAO support.

5.2.2. 2-mIm Vapor-phase treatment

The conversion of a ZnO layer to ZIF-8 was performed by using the vapor-phase treatment. The number of deposition cycles was varied (60-90 ZnO ALD cycles) to change the amount of ZnO deposited on the support to tune the ZIF-8 membrane thickness. The side on which ZnO is deposited was exposed to 0.2 g of 2-methylimidazole (2-mIm) in the Teflon vessel and then sealed in a stainless-steel autoclave reactor. As shown in Figure 1.3, the reactor was heated at 85- 125 ºC in an oven for 20- 28 h during the conversion of ZnO to the ZIF-8 layer.

5.2.3. Gas permeation measurements

The gas separation efficiency of the synthesized ZIF-8 membranes was assessed by conducting experiments on propylene/propane separation under atmospheric conditions. The membranes were installed in a stainless-steel cell with the synthesized membrane surface facing toward the feed side as shown in Figure 3.1. The propylene/propane equimolar mixture was introduced to the feed side with a flow rate of 100 $cm^3\,min^{-1}$ and the flow rates were regulated by mass flow controllers (MFC). The sweeping gas argon

was supplied to the permeate side at a flow rate of 100 cm^3 min^{-1}. For the steady-state permeation measurements, the membranes were assessed for 4 h and then the stable data points were collected. The compositions of permeate were analyzed using online gas chromatography (Shimadzu, GC-2014 equipped with molecular sieve 13X column). The membrane permeance and separation efficiency measurement details are explained in section 3.2.3.

5.2.4. Characterization

Surface and cross-section micrographs (SEM) were taken with a quanta 600 field emission scanning electron microscopy (SEM) operating at 20 kV acceleration voltage and a lens distance of 10 mm. Energy-dispersive X-ray spectroscopy (EDS) mapping and programmed imaging analysis were performed using Quanta 600 SEM. The X-ray diffraction (XRD) reflections were measured using Bruker AXS D8 Discover diffractometer with General Area Detector Diffraction System, 40 kV, 35 mA with a sampling frequency of 1.0 degree/min and a scan range of 5- 45 degrees. The Infrared spectra measurements were collected using a Thermo Nicolet 380 FT-IR coupled with Diamond attenuated total reflectance [ATR].

5.3. Results and Discussion

5.3.1. ZIF-8 membrane characterization

As shown in Figure 5.4 (a1, a2) AAO supports were used because of the uniform pore-size distribution and compact cylindrical channels with low tortuosity [158]. To synthesize the ZIF-8 membrane, ZnO as a metal precursor was coated on an AAO support then it was converted to a ZIF-8 layer [159]. Based on the good conformity control via ALD, a ZnO layer was uniformly deposited on the AAO support surface. Figure 5.4b1 shows the morphology of the ZnO layer on the surface of AAO after depositing 70 cycles of ZnO ALD. Figure 5.4b2 shows that the ZnO crystals have seamlessly grown on the AAO support, indicating a strong adhesion on the support surface. The strong bonding of hydroxyl groups of AAO support with ZnO results in homogeneous polyhedral crystals, ranging between 15 to 20 nm. Lee et al. reported that

the ZnO layer coated on the alumina support surface via the dip-coating process generated strong adhesion between ZnO and the support surface [160]. Drobek et al. reported that ALD provides a significant advantage over other methods in depositing ZnO with great control of coating thickness on porous supports [85]. This bonding between ZnO coating and the AAO support surface shows the uniform distribution of the Zn layer, which is an essential step before fabricating thin ZIF-8 membranes.

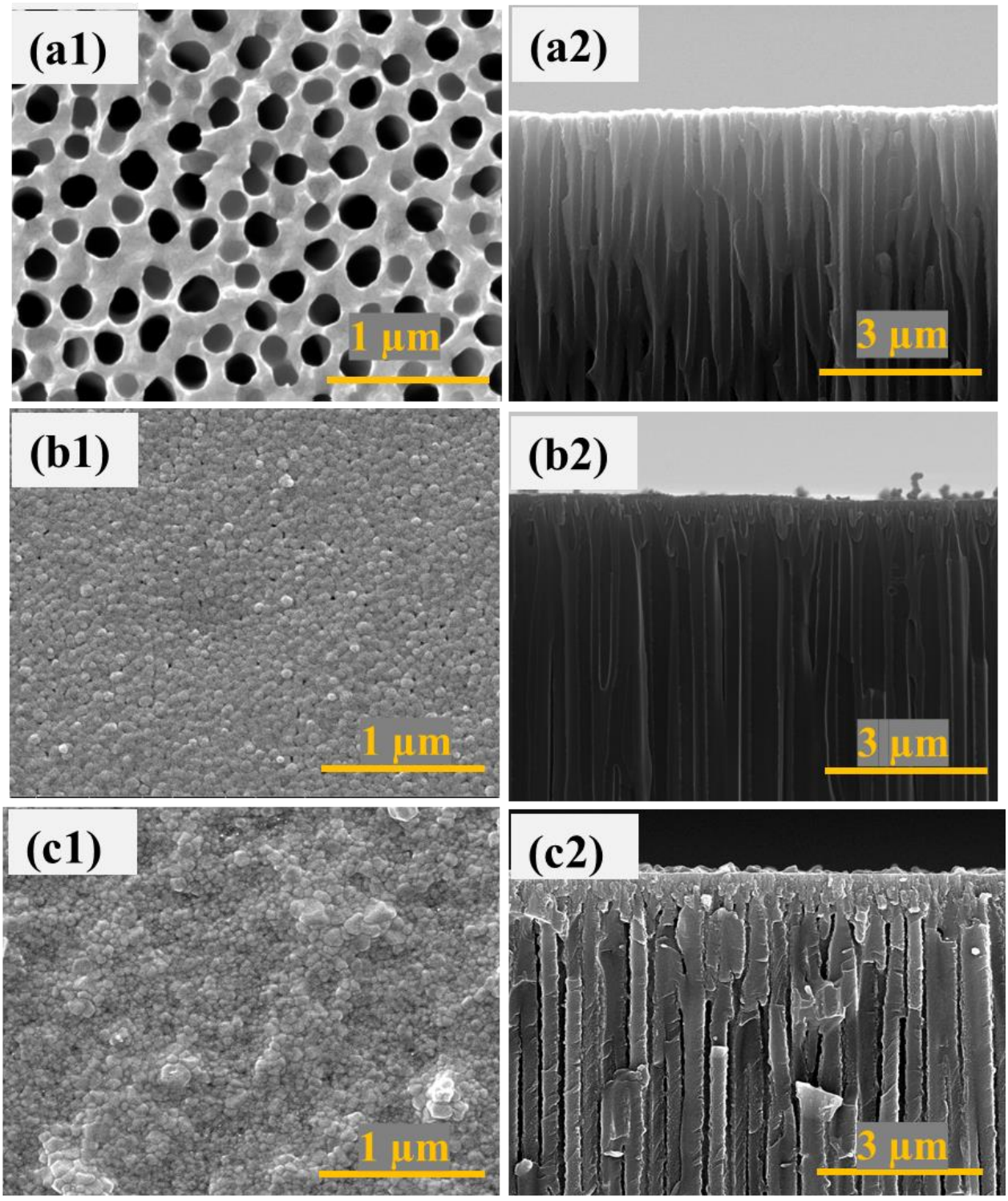

Figure 5.2: SEM surface and cross-section micrographs of AAO support (a1, a2), 70 cycled ZnO ALD layer (b1, b2), and ZIF-8 membrane synthesized at 100 ºC for 24 h (c1, c2).

From the top and cross-section SEM images, as shown in Figure 0.4 (b1, b2) the ZnO layer was uniformly deposited over the entire surface and tightly packed on the porous AAO support, acting as an intermediate support layer in ZIF-8 membrane growth. The addition of ZnO to the AAO support surface resulted in a thin uniform seed crystal layer with a thickness of ~85 nm. In Figure 5.4c1, the change in surface morphology is shown after the ZnO layer was treated with ligand 2-mIm using the vapor-phase treatment method. Tanaka et al. reported that the vapor treatment method using a ligand dramatically changed ZnO nanoscale morphology [87]. The SEM images showed that after the vapor treatment the ZIF-8 growth resulted in amorphous particles with rarely defined faces and edges. After the vapor treatment, the change in morphology was observed and a well-intergrown interconnected crystal with a homogeneous compact structure was obtained.

The partial conversion of ZnO to ZIF-8 by the vapor treatment generated a thin layer due to lower homogeneous nucleation than the solvent-based synthesis methods [86]. The layer of the excessive ZnO, which has not been fully converted to ZIF-8, provides an oxide bridging material between the AAO support surface and the membrane, acting as a diffusion barrier for gas permeation [25]. The ZIF-8 layers formed on the ZnO surface provide a selective permeation of propylene across the membrane. The cross-section views show the homogenous and conformal crystal layer due to the intergrowth between the support surface and the ZIF-8 layer. The thickness is narrowed to ~350 nm, due to a solid-vapor conversion, which is confined to the AAO support surface. In addition, this thin layer formation is probably due to the low mobility of the ZnO metal precursor during the solvent-free synthesis [86].

The chemical composition of the membranes was characterized using EDX. The ZIF-8 membrane synthesized at 100 ºC resulted in the ternary ZIF-8/ZnO/AAO material composition. As shown in Figure 5.5 and Table 5.1, in the pristine AAO support, a significant portion of the materials includes aluminum and oxygen. The EDX mapping results show aluminum and oxygen's dominance, uniformly distributed in the support [161, 162]. On the surface of the AAO support, ZnO was deposited using ALD. The consequent outcome includes deposition of Zn and ZnO, showing the homogenous and uniform covering of the material

over the surface [85, 163]. The Zn source was mobilized by diffusion and deposited over the AAO support surface so that most of the material is present on top of the support. For the ZnO layer, the surface and cross-sectional EDX images confirm the uniform distribution of Zn both on the surface and inside the AAO pore channels. After the ligand vapor treatment, ZnO was converted to ZIF-8, as indicated by the percentage increase in C, N, and consequent decrease in Zn concentration.

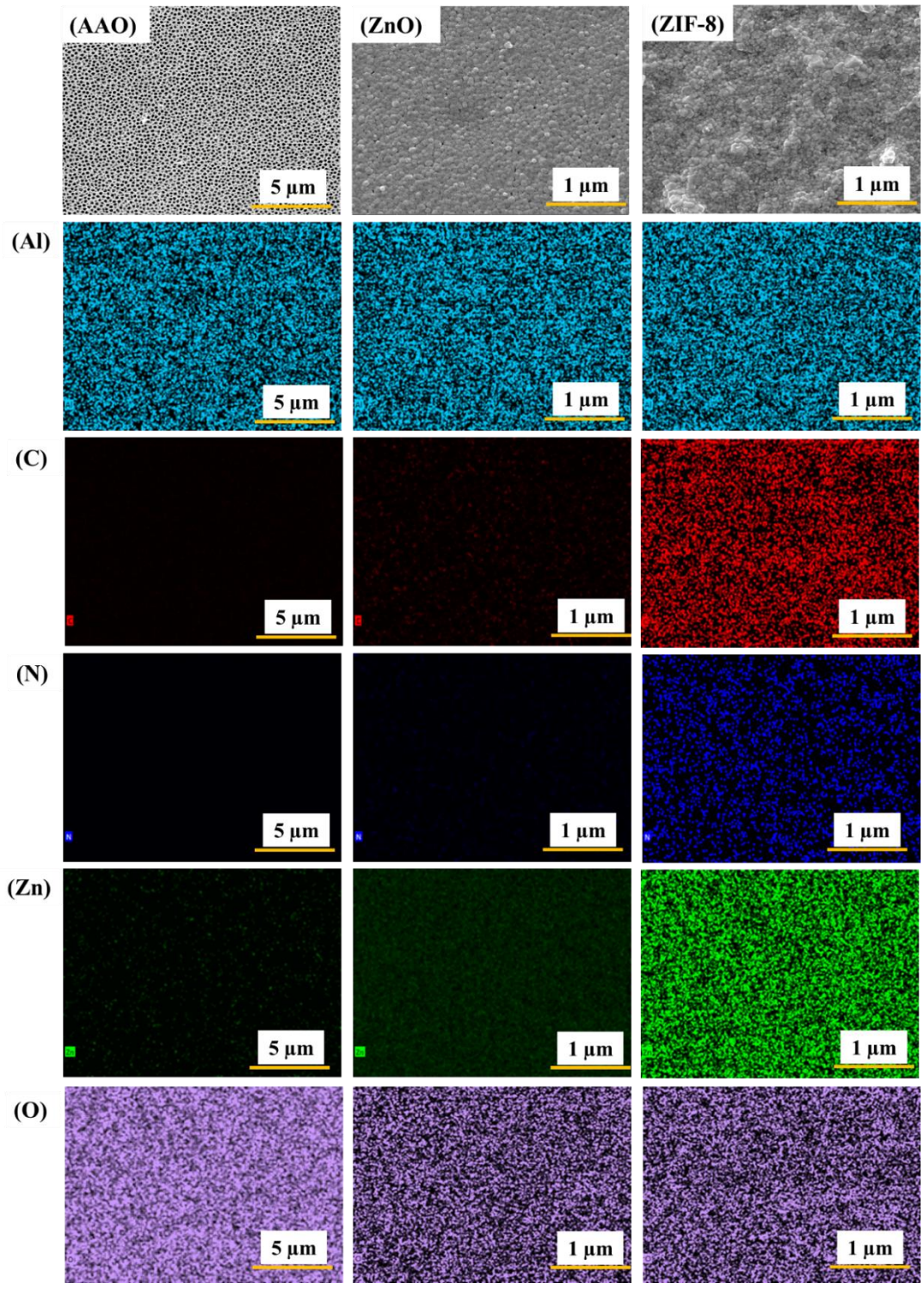

Figure 5.3: Surface SEM images and corresponding EDX elemental mapping of pristine AAO support, 70 ZnO ALD layer, and ZIF-8 membrane vapor treated at 100 ºC for 24 h.

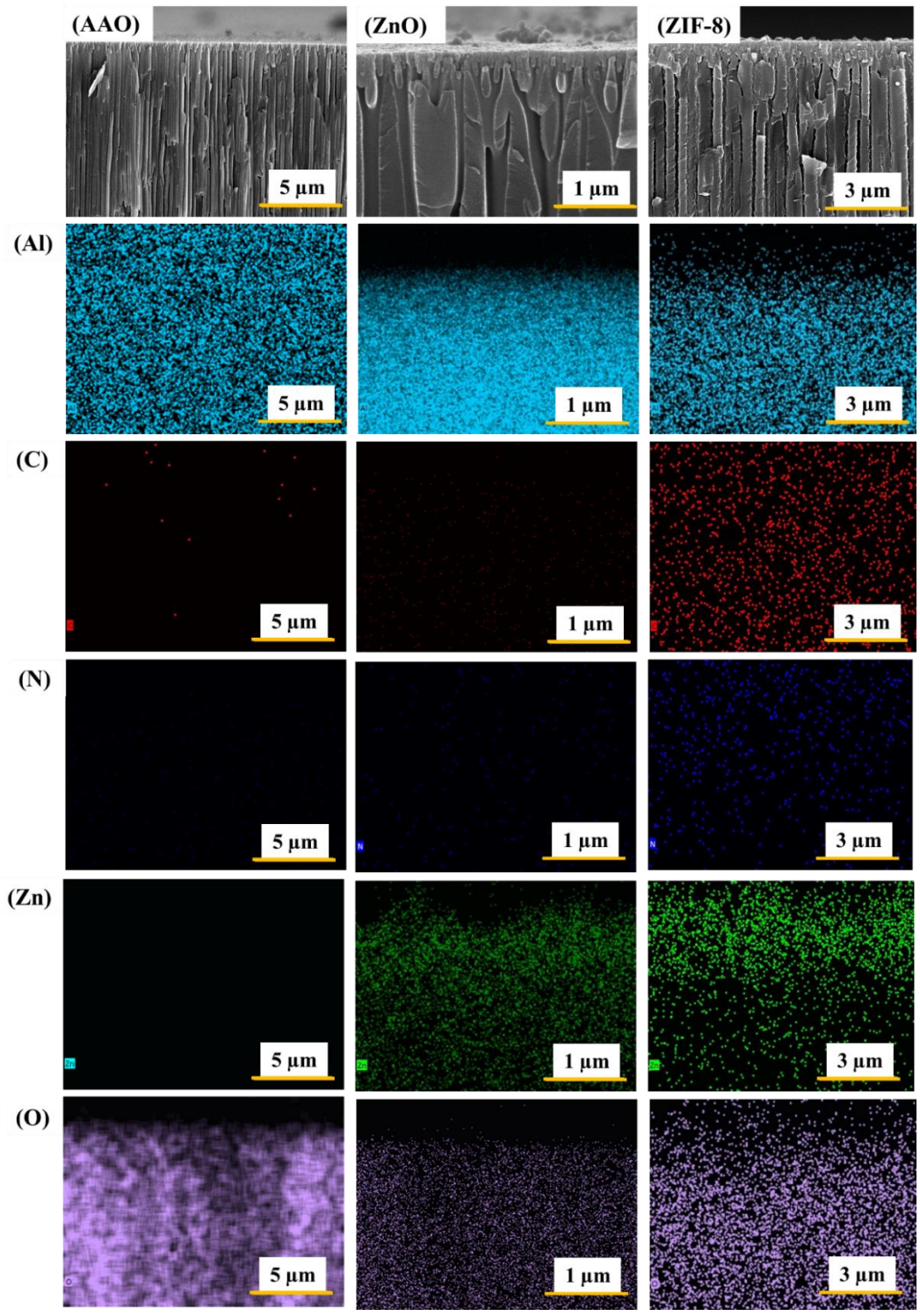

Figure 5.4: Cross-sectional SEM images and corresponding EDX elemental mapping of pristine AAO support, 70 ZnO ALD layer, and ZIF-8 membrane vapor treated at 100 ºC for 24 h.

The decrease in Zn concentration indicates the successful conversion of ZnO to ZIF-8 by the ligand vapor treatment. However, the low density of the ZIF-8 layer was formed upon exposure to 2-mIm subsequently and the unconverted ZnO was likely present in the interface between AAO and ZIF-8 [84]. According to SEM and EDX results, all the ALD-deposited ZnO is not transformed to ZIF-8. The elemental composition of the ZIF-8 membrane was validated with the AAO support and ZnO layer in Table 5.1. Also, the color models (Figure 5.6) composed of the Al, Zn, C, N, and O elemental maps show the composition of the merged elements from support to the membrane surface and cross-section.

Table 5.1: Elemental composition of pristine AAO support, 70 ALD ZnO layer, and ZIF-8 membrane.

Element	AAO (%)	ZnO (%)	ZIF-8 (%)	Secondary grown ZIF-8 [133]
Carbon	12.10	14.84	28.48	56.55
Nitrogen	1.39	1.10	7.84	25.96
Oxygen	60.85	51.56	36.98	-
Aluminum	25.49	26.98	23.36	-
Zinc	0.18	5.53	3.34	11.01

X-ray diffraction is used to assess the crystalline structure of the ZIF-8 membrane compared to the ZnO ALD layer and pristine AAO support. As shown in Figure 5.7, typical diffraction patterns observed at 2θ of 14°, 17°, and 23° represents the Al and Al_2O_3 crystalline phase as well as amorphous alumina compound [133, 164]. Similarly, the diffraction peak for the ZnO deposited layer showed a small broad peak with low intensity at 2θ of ~31.8° which indicates the amorphous nature of the ZnO layer [85, 87]. The formation of crystalline ZIF-8 at 100 ºC was found at 2θ of 7.3°, 10.4°, 12.7°, and 18°, however, the

intensity of peaks was not significantly large due to the presence of residual ZnO that was left unconverted, and because of the formation of a thinner ZIF-8 layer. Stassen et al. reported that the partial conversion of ZnO is possible at a temperature close to 100 °C, which corresponds to our results [86]. The diffraction patterns of the synthesized ZIF-8 membranes are consistent with the literature [84, 85, 160].

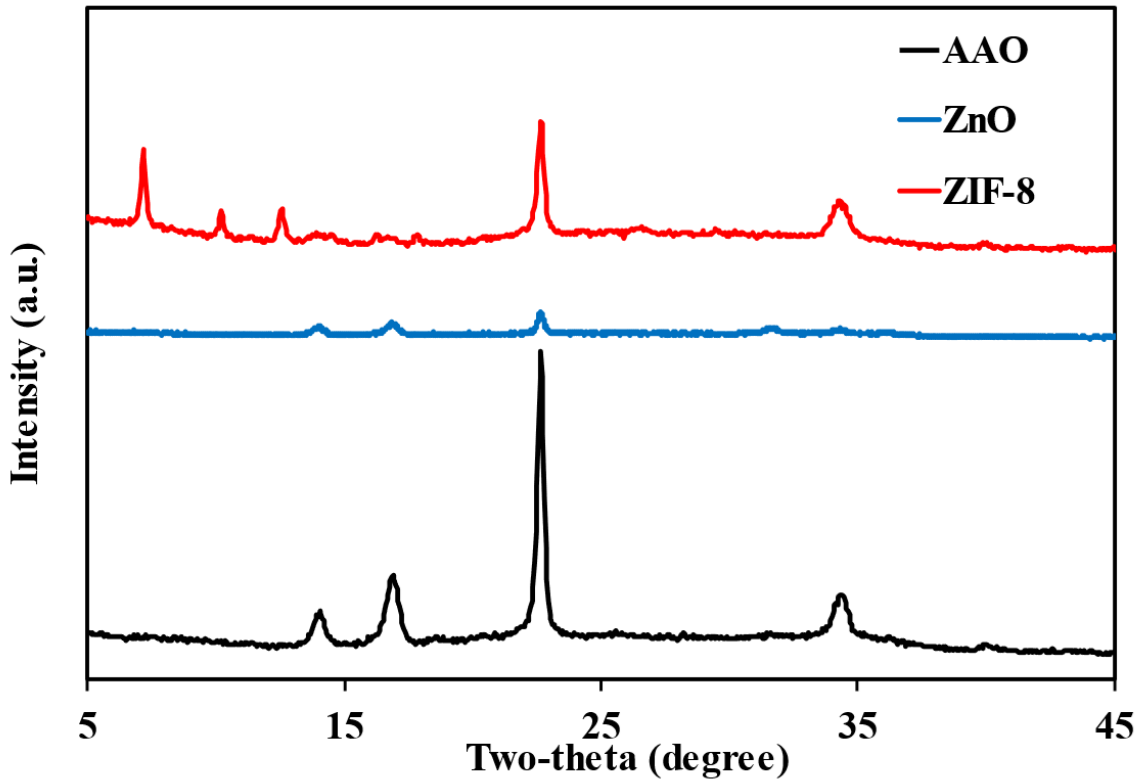

Figure 5.5: XRD patterns of pristine AAO support, 70 ALD ZnO layer, and ZIF-8 membrane.

In the FT-IR spectra, both strong and weak peaks were observed at 1036 cm^{-1}, 1477 cm^{-1}, 1570 cm^{-1}, and 2344 cm^{-1}. The weak vibrational peak was observed at 2344 cm^{-1} due to the C-O bond, and symmetric, asymmetric peaks were observed between 1470 and 1570 cm^{-1} due to the presence of carboxyl ions. The strong vibrations were found at 1000 - 1036 cm^{-1} because of the Al-O bond complex vibration. These peaks were all consistent with the FT-IR spectra of the nanoporous AAO [161, 165, 166].

The FT-IR spectra on the ZIF-8 layer show linker deprotonated 2-mIm, which is incorporated into the framework of ZIF-8. Therefore, only the ZnO layer's top surface was converted to ZIF-8 membrane after the vapor-phase treatment technique. After vapor treatment, this residual ZnO layer acts as efficient intermediate support between the support surface and the ZIF-8 membrane, confirmed by the EDX analysis. The peaks for ZIF-8 show the vibration of 2-mIm units and are described based on the bond origins. The band ranged from 1300 to 1500 cm^{-1}, and 1584 cm^{-1} correspond to the stretching of the entire aromatic ring C=N stretching bond vibrations respectively [167]. Similarly, the absorption bands between 3135 and 2929 cm^{-1} ascribed to the 2-mIm C-H in both aromatic, aliphatic functional groups stretching, respectively. The spectra pattern of the ZIF-8 membranes satisfactorily agreed with the literature [168-170].

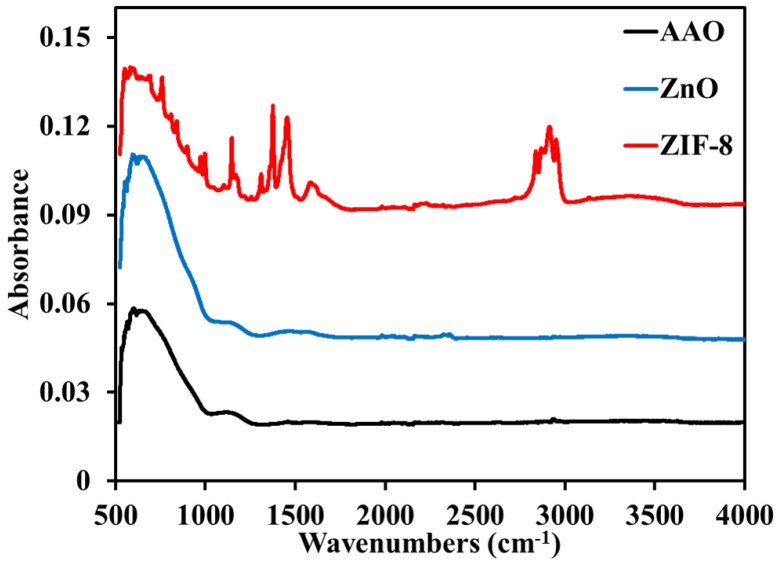

Figure 5.6: FT-IR spectra patterns of pristine AAO support, 70 ZnO ALD cycled layer, and ZIF-8 membrane.

5.3.2. Effect of ZnO ALD cycles

The effect of ZnO ALD cycles was examined with varying ALD cycles (60 to 90) on an AAO support while maintaining the vapor treatment condition under constant reaction time (24 h) and

temperature (100 ºC). The ZIF-8 crystal morphologies and sizes were changed relying upon the number of ZnO ALD cycles, as shown in surface and cross-sectional SEM images in Figure 5.9. According to the ZnO ALD cycles of 60, 70, and 90, the thickness of the ZIF-8 membrane was found to be 260, 420, and 850 nm, respectively. For the 70 ALD cycled membrane, a well-intergrown uniform crystal growth was observed throughout the support surface and showed a separation factor of ~46 with propylene permeance of 1.4×10^{-7} mol m^{-2} s^{-1} Pa^{-1}. The 60 ALD cycled membranes had ~260 nm thickness and showed high permeance with a low separation factor due to insufficient crystal growth and incomplete interconnection between ZIF-8 crystals. The 90 ALD cycled membranes showed significantly increased crystal growth (850 nm thickness), and crystals were excessively accumulated on the support surface. The 90 ALD cycled membranes showed a separation factor of ~ 24 with propylene permeance of 1.7×10^{-8} mol m^{-2} s^{-1} Pa^{-1}. Therefore, the 70 ALD cycled membranes were selected for further experiments.

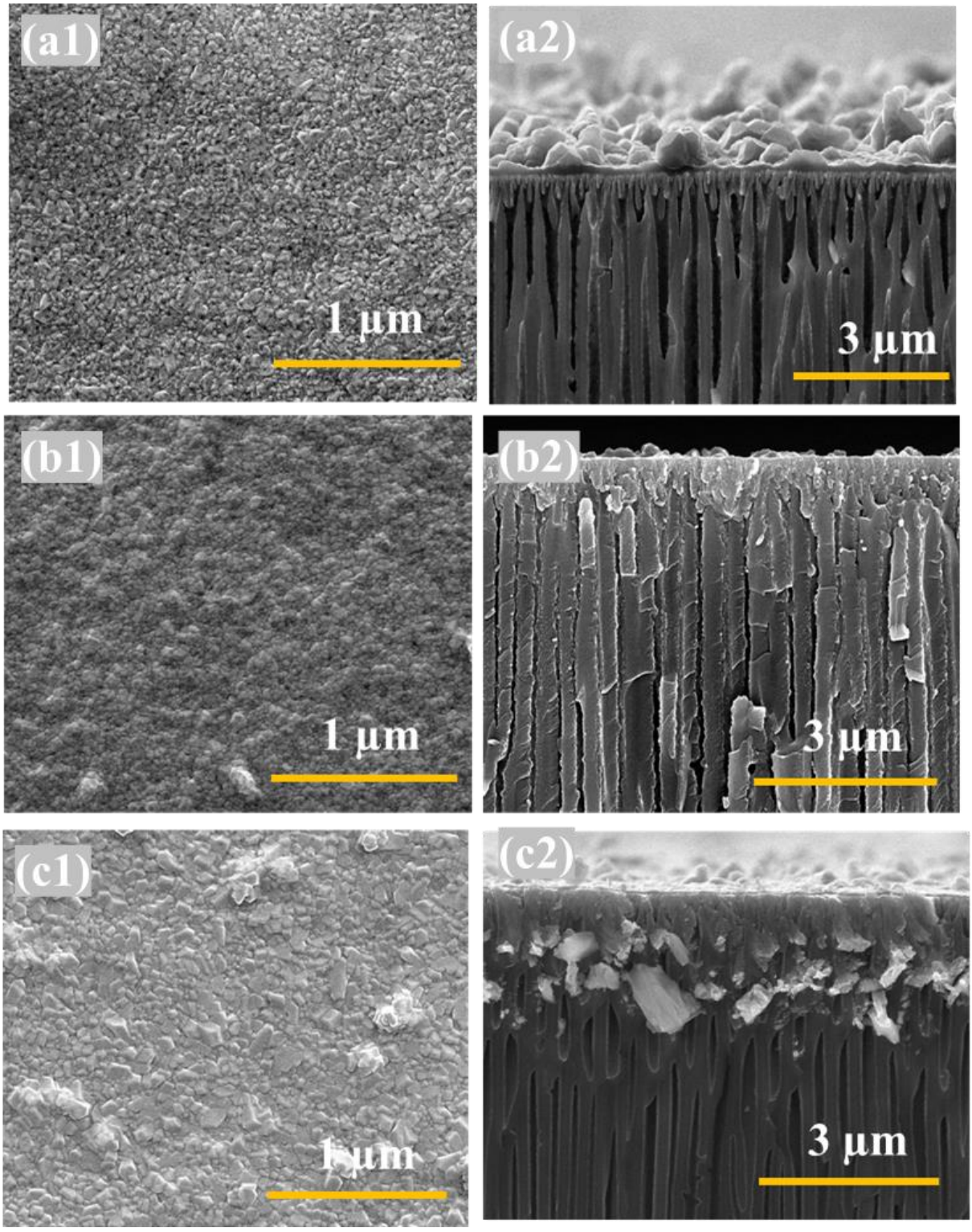

Figure 5.7: Surface and cross-sectional SEM images of ZIF-8 membranes synthesized at 100 ^{o}C for 24 h on 60 ALD (a1, a2), 70 ALD (b1, b2), and 90 ALD cycled supports (c1, c2), respectively.

5.3.3. Effect of vapor treatment time

The optimum vapor treatment (synthesis) time to have a uniform ZIF-8 crystal growth was explored utilizing the 70 ZnO ALD cycled AAO support. According to the vapor treatment time of 20, 24, and 28 h, the membrane film thickness was found to be 300, 420, and 490 nm, respectively. The surface and cross-sectional crystal morphology of the membranes are shown in Figure 5.10. The vapor treatment of 24 h delivered a consistent interlinked crystal growth all over the support surface. The vapor treatment time of 20 h had a partial growth with the absence of interconnection, and the vapor treatment time of 28 h caused large overgrown ZIF-8 crystals on the surface [133]. As indicated by the obtained results, the membranes treated for 24 h had good propylene permeance of 2.9×10^{-7} mol m^{-2} s^{-1} Pa^{-1} with a separation factor of ~37, which is higher than the membranes treated for 20 and 28 h.

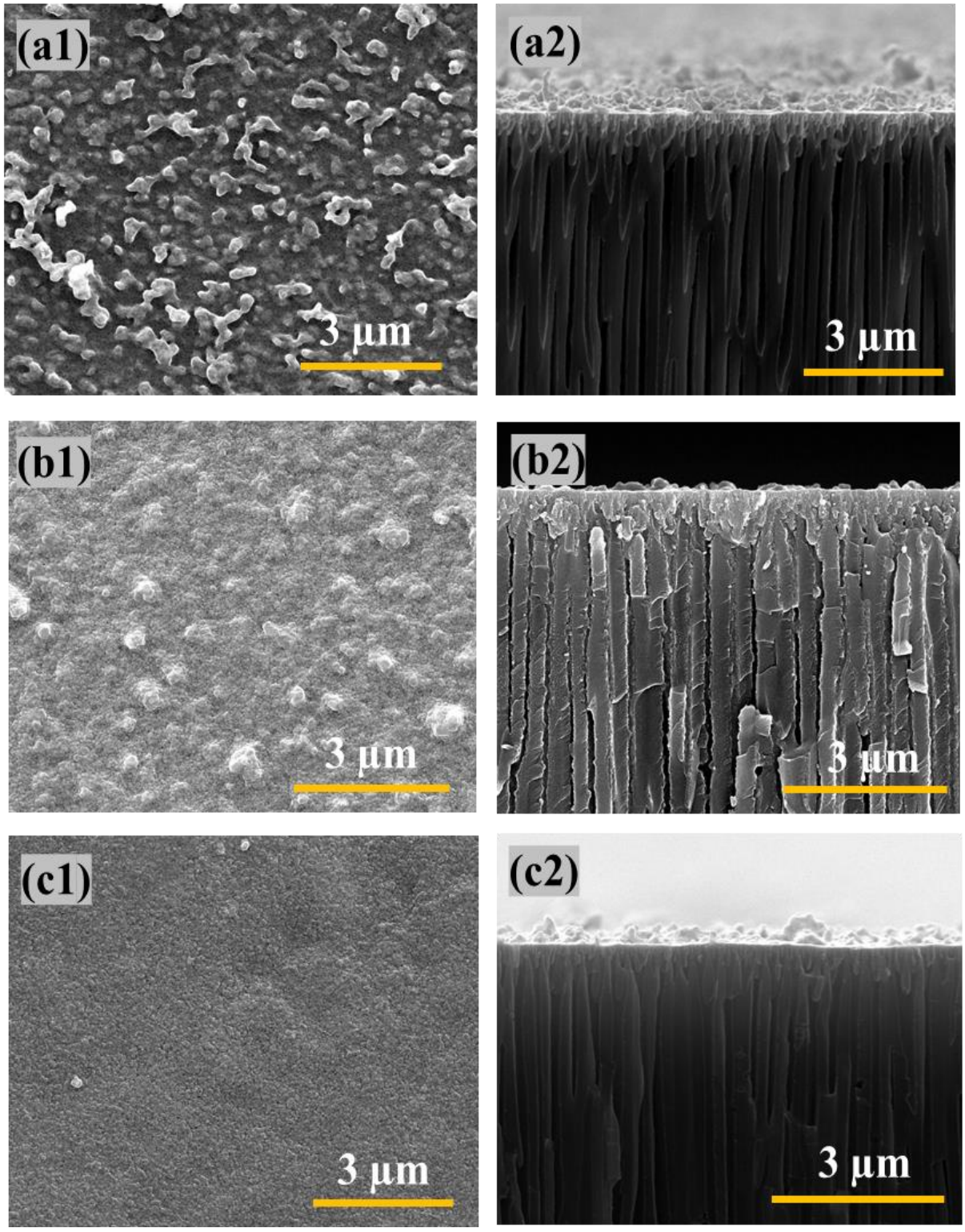

Figure 5.8: Surface (a1, b1, c1) and cross-sectional (a2, b2, c2) SEM images of the membranes synthesized by the vapor treatment time for 20, 24, and 28 h, respectively (on 70 ALD cycled support).

5.3.4. Effect of vapor treatment temperature

The vapor treatment temperature to grow the ZIF-8 membranes on 70 ALD cycled supports was investigated with a constant synthesis time of 24 h. According to the temperature of 85, 100, and 125 ºC, the membrane thickness was found to be 270, 420, and 700 nm, respectively, as shown in Figure 5.11. The surface thickness increased with increasing the vapor treatment temperature. The ZIF-8 growth was found even at a low temperature of 85 ºC. However, a random crystal growth with a slow nucleation rate resulted in incomplete membrane growth. An optimum temperature for ZIF-8 formation was found to be 100 ºC with well-interlinked crystals caused by a homogenous growth. Meanwhile, 85 ºC had inadequate ZIF-8 growth, and 125 ºC had a large crystal-covered support surface. We came to the conclusion that temperature enhances the nucleation rate and leads to an increase in the crystal size and thickness [86]. The membrane obtained by the vapor treatment temperature of 100 ºC showed a separation factor of ~ 43 with propylene permeance of 2.59×10^{-7} mol m^{-2} s^{-1} Pa^{-1}.

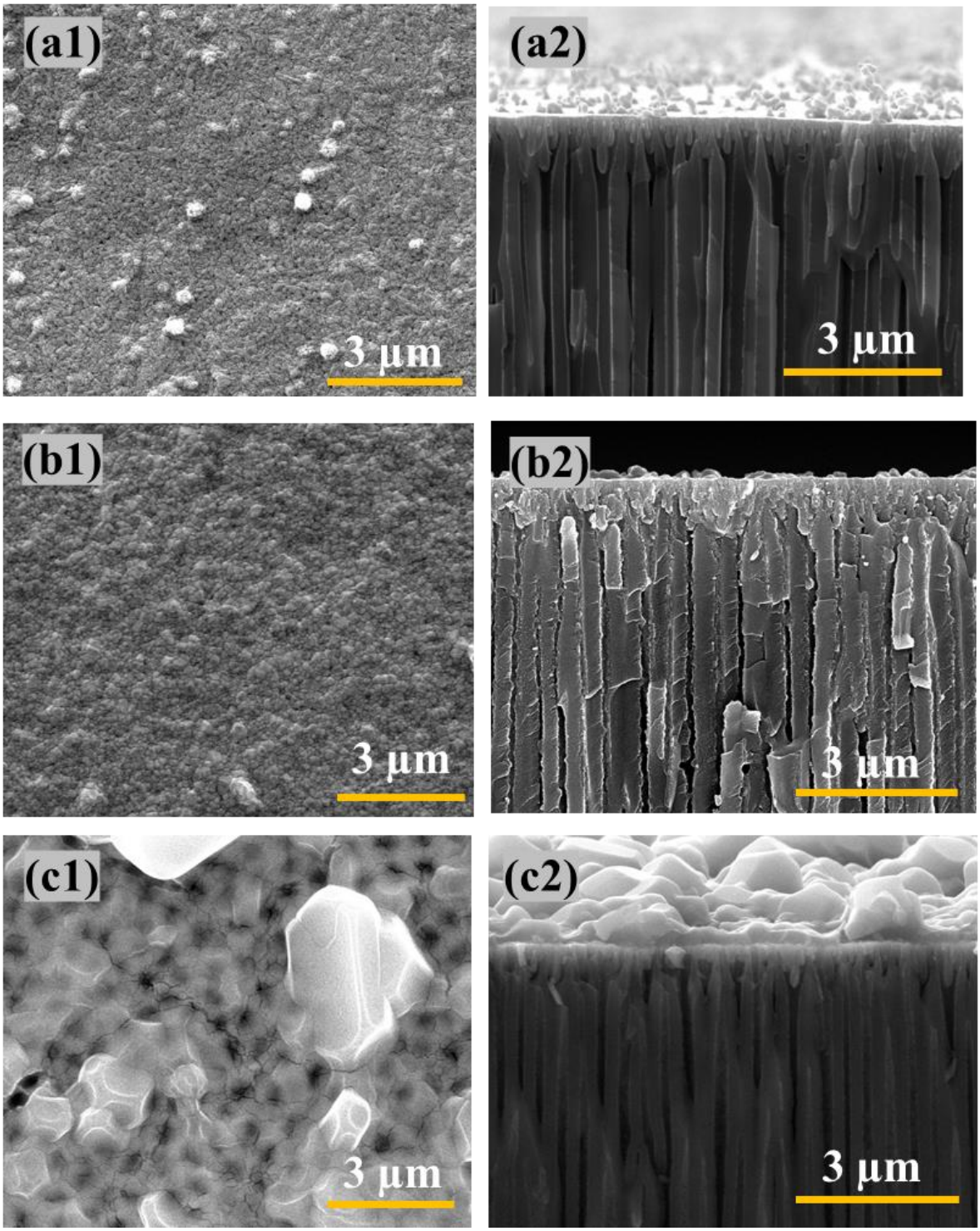

Figure 5.9: Surface (a1, b1, c1) and cross-sectional (a2, b2, c2) SEM images of the ZIF-8 membranes synthesized by the vapor treatment temperature for 24 h of 85 ºC, 100 ºC, and 125 ºC, respectively (on 70 ALD cycled support).

5.3.5. Gas permeation measurements of-ZIF-8 membranes

The ZIF-8 membranes were evaluated for the separation of propylene/propane equimolar mixture at room temperature and atmospheric pressure. The commercially available AAO support with pore size 20 nm has propylene permeance of 10^{-6} mol m^{-2} s^{-1} Pa^{-1} and is not propylene selective. Depositing ZnO on the AAO support using 70 ALD cycles did not result in notable changes in propylene permeance and propylene/propane separation factor. Deposition of ZnO partially blocked gas passage with an increasing number of ALD cycles from 60 to 90 [161]. These permeable and non-selective ZnO-coated AAO supports were exposed to 2-mIm vapor. After the vapor treatment, it was found that the thin ZIF-8 layer was formed (~400 nm), and the membranes became propylene selective while keeping propylene permeance high [84]. The synthesized membranes showed high propylene permeance of 3.6×10^{-7} mol m^{-2} s^{-1} Pa^{-1} with a propylene/propane separation factor of ~58. In this work, the permeable ZnO layer was successfully converted to a propylene selective ZIF-8 membrane, while providing high propylene permeance. Reduction in membrane thickness corresponded to high propylene permeance and enhanced propylene selectivity was attributed to the increased compactness between the crystals. Using ALD under low-temperature operation followed by the vapor treatment allowed slow crystal growth, resulting in a high-flux propylene selective ZIF-8 membrane. As shown in Figure 5.12, propylene/propane separation results were compared with the previous literature [24, 42, 49, 50, 64, 71, 72, 76, 77, 82, 84, 90, 141-145, 149, 171-176]. The membrane from this work showed higher permeance of 3.6×10^{-7} mol m^{-2} s^{-1} Pa^{-1} with a separation factor of ~58.

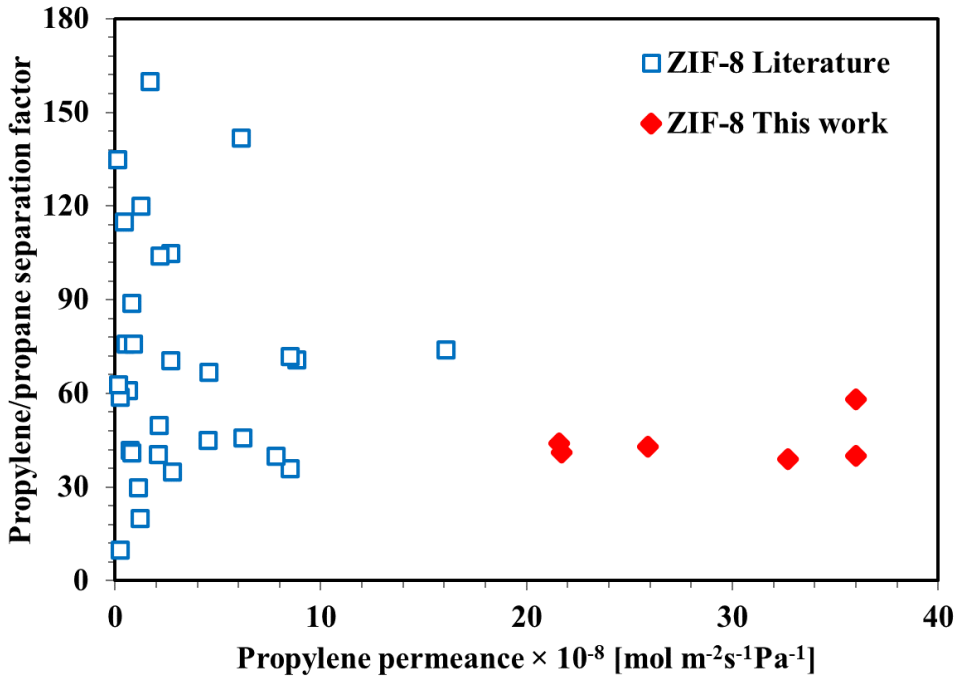

Figure 5.10: Propylene/propane separation performances of ZIF-8 membranes from the literature [24, 42, 49, 50, 64, 71, 72, 76, 77, 82, 84, 90, 141-145, 149, 171-176].

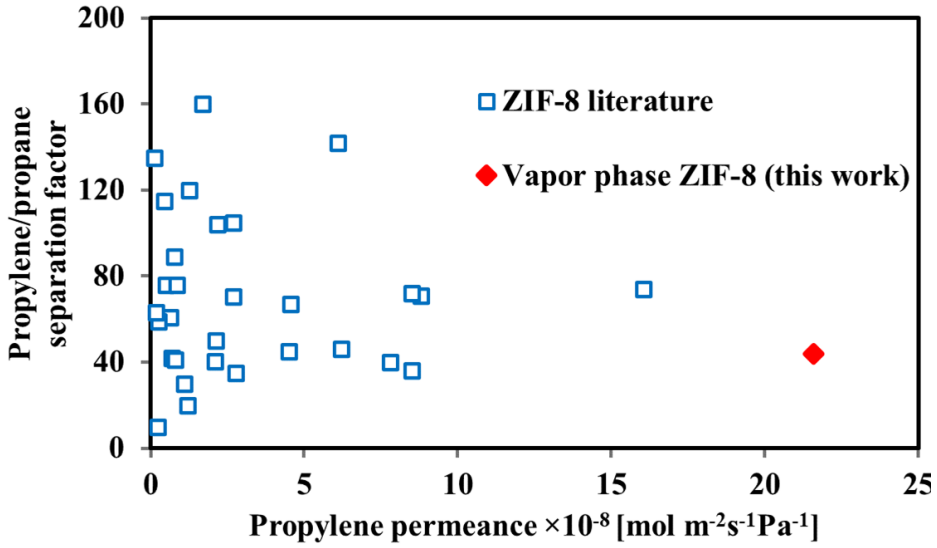

Figure 5.11: Propylene/propane separation average performance of ZIF-8 membranes comparison with literature [24, 42, 49, 50, 64, 71, 72, 76, 77, 82, 84, 90, 141-145, 149, 171-176].

5.4. Conclusion

In this work, the vapor-phase treatment was demonstrated for converting ZnO to ZIF-8 films on AAO support. The effects of ZnO ALD cycles, vapor treatment time, and temperature were investigated on ZIF-8 membrane performance for propylene/propane separation. The 70 ZnO ALD cycled support was activated with 2-mIm at 100 ºC for 24 h and the ZnO layer was converted to ZIF-8. Deposition of ZnO followed by the vapor activation treatment with 2-mIm at low temperature allowed slow crystal growth, which resulted in a high-flux propylene selective ZIF-8 membrane. The solvent-free vapor treatment process helped in producing a thin ZIF-8 membrane with a thickness of ~ 400 nm. The ZIF-8 membranes showed high propylene permeance of 3.6×10^{-7} mol m^{-2} s^{-1} Pa^{-1} with a propylene/propane separation factor of 58. The demonstrated conversion of thin ZnO films into highly crystalline porous ZIF-8 layer can be utilized in the development of new materials for gas separations. The ALD using various metal oxides have great potential for integrating MOF thin films and nanostructures into membranes.

CHAPTER VI

SUMMARY AND FUTURE WORK

6.1. ZIF-8 Membranes for propylene/propane separation

This work aims to develop and evaluate ZIF-8 membranes in producing potential commercial membrane products for the separation of propylene/propane. This work aims to develop and evaluate ZIF-8 membranes in producing potential commercial membrane products for the separation of propylene/propane. In this dissertation, three synthesis methods including silicalite-seeded secondary growth, ZnO ALD treatment, and vapor-phase methods were developed and assessed successfully. All the above-mentioned synthesis techniques resulted in the successful growth of ZIF-8 membranes while efficiently separating the propylene/propane mixture. The first technique was a novel silicalite nanoparticles seeded via dip-coating method on commercially available AAO support. The key step in silicalite nanoparticle seeding enabled strong bonding between silicalite seed particles and AAO support surface via hydrogen bonding. The subsequent secondary growth of this ZIF-8 layer led to a well-intergrown membrane layer from silicalite crystal, resulting in a reduction of synthesis time typically from days to ~10 h which is a significant improvement in synthesis efficacy. The resultant ZIF-8 membranes showed an average propylene/propane separation factor of ~170 with propylene permeance of 0.9×10^{-8} mol m^{-2} s^{-1} Pa^{-1}.

The second technique involved using ZnO-ALD treatment to heal non-selective defects on the membrane surface to improve the propylene/propane separation performance. The key step in improving the ZIF-8 membrane performance is based on using the ZnO-ALD treatment which treated surface defects. It was found that two ZnO-ALD cycles on the surface of ZIF-8 membranes significantly improved the propylene/propane separation factor from 141 to 264. This post-synthetic ZnO-ALD treatment process is highly versatile from an engineering standpoint and the ZnO deposition process is rapid compared to other post-synthetic treatment methods. The second technique is a strategy to move forward by providing alternative ways to enhance stability in the practical applications of numerous MOF polycrystalline membranes for prospective gas separation applications.

The third technique involved vapor phase methods where a low quantity of chemicals is used in the synthesis process when compared to other solvent-based methods. The third technique involved vapor phase methods where a low quantity of chemicals is used in the synthesis process when compared to other solvent-based methods. This new technique produced ultra-thin (400 nm) ZIF-8 membranes which showed high propylene permeance of 3.6×10^{-7} mol m^{-2} s^{-1} Pa^{-1} with a separation factor of ~58. The vapor phase synthesized ZIF-8 membranes were assessed the reproducibility and these membranes resulted in propylene permeance of $\sim10^{-7}$ mol m^{-2} s^{-1} Pa^{-1} with an average propylene/propane separation factor of ~42. The vapor phase synthesized ZIF-8 membranes were assessed for reproducibility and these membranes resulted in propylene permeance of $\sim10^{-7}$ mol m^{-2} s^{-1} Pa^{-1} with an average propylene/propane separation factor of ~42. This novel ALD technique demonstrates the conversion of ZnO to ultra-thin ZIF-8 membranes, which suggests immense potential in integrating MOF thin films and nanostructures into gas separation membrane applications.

6.2. Future work

To overcome the barriers of the commercial applications, improving the membrane fabrication process potentially reduces the synthesis cost and increases the membrane performance for the commercial gas separations. However, the framework flexibility of ZIF-8 membranes paves the way to investigate several synthesis methods to enhance the propylene/propane separation applications. It has been found that ZIF-8 membranes are limited in terms of propylene selectivity, but this dissertation shows the potential of synthesis techniques that can enhance the selectivity of propylene/propane while producing high-quality ultra-thin ZIF-8 membranes. This proves that these ZIF-8 membrane fabrication methods can be further explored to improve the propylene/propane separation performance.

The reported ZIF-8 membranes which were fabricated using synthesis techniques as explained in Chapters 3, 4, and 5, show potential in propylene/propane separations on a lab-scale (atmospheric pressure and room temperature). However, upscaling these techniques for commercial or industrial applications requires ideal operating conditions such as high pressure and temperatures. In addition to operating conditions, there might be impurities in feed mixtures of propylene/propane, which is a general challenge in chemical industrial operations. Therefore, further modifications of these ZIF-8 membranes might be required for commercial upscaling which is especially important for practical applications.

As reported in Chapter 4, coating additional ZnO on the secondary grown ZIF-8 membrane displayed a dramatic improvement in propylene/propane separation factor, which is made possible by minimizing the density of non-selective defects. This shows that ZIF-8 fabrication combined with ZnO, or any other metals can potentially improve the separation performance of C_3 mixtures. Also, the coordination chemistry of ZIF-8 can be modified by using post-synthetic treatment methods, which can further improve the membrane separation performance. ZnO-ALD treatment can be further investigated in detail to understand the intrinsic properties of enhanced ZIF-8 membranes compared to traditionally synthesized ZIF-8 membrane

REFERENCES

1. Worrell, E., et al., Energy use and energy intensity of the US chemical industry (No. LBNL–44314). Lawrence Berkeley National Laboratory, CA, 2000.
2. Xu, H., U. Lee, and M. Wang, Life-cycle energy use and greenhouse gas emissions of palm fatty acid distillate derived renewable diesel. Renewable and Sustainable Energy Reviews, 2020. **134**: p. 110144.
3. Gadalla, M., et al., Estimation and reduction of CO2 emissions from crude oil distillation units. Energy, 2006. **31**(13): p. 2398-2408.
4. Pamula, A.S.P., D.J. Lampert, and H.K. Atiyeh, Well-to-wake analysis of switchgrass to jet fuel via a novel co-fermentation of sugars and CO2. Science of The Total Environment, 2021. **782**: p. 146770.
5. Velasco, J.A.C., M. Tawarmalani, and R. Agrawal, Systematic analysis reveals thermal separations are not necessarily most energy intensive. Joule, 2021. **5**(2): p. 330-343.
6. Hou, J., et al., Olefin/paraffin separation through membranes: from mechanisms to critical materials. Journal of Materials Chemistry A, 2019. **7**(41): p. 23489-23511.
7. Ma, X. and D. Liu, Zeolitic imidazolate framework membranes for light olefin/paraffin separation. Crystals, 2019. **9**(1): p. 14.
8. Zhang, G., et al., Giant discoveries of oil and gas fields in global deepwaters in the past 40 years and the prospect of exploration. Journal of Natural Gas Geoscience, 2019. **4**(1): p. 1-28.
9. Dewprashad, B. and E. Eisenbraun, Fundamentals of epoxy formulation. Journal of chemical education, 1994. **71**(4): p. 290.

10. Liu, J., Y. Xiao, and T.-S. Chung, Flexible thermally treated 3D PIM-CD molecular sieve membranes exceeding the upper bound line for propylene/propane separation. Journal of Materials Chemistry A, 2017. **5**(9): p. 4583-4595.

11. Chen, X.Y., A. Xiao, and D. Rodrigue, Polymer-based Membranes for Propylene/Propane Separation. Separation & Purification Reviews, 2021: p. 1-13.

12. Campos, A.C.C., et al., A perspective of solutions for membrane instabilities in olefin/paraffin separations: a review. Industrial & Engineering Chemistry Research, 2018. **57**(31): p. 10071-10085.

13. Park, K.S., et al., Exceptional chemical and thermal stability of zeolitic imidazolate frameworks. Proceedings of the National Academy of Sciences, 2006. **103**(27): p. 10186-10191.

14. Lai, Z., Development of ZIF-8 membranes: Opportunities and challenges for commercial applications. Current opinion in chemical engineering, 2018. **20**: p. 78-85.

15. Banerjee, R., et al., High-throughput synthesis of zeolitic imidazolate frameworks and application to CO2 capture. Science, 2008. **319**(5865): p. 939-943.

16. Li, K., et al., Zeolitic imidazolate frameworks for kinetic separation of propane and propene. Journal of the American Chemical Society, 2009. **131**(30): p. 10368-10369.

17. Zhang, C., et al., Unexpected molecular sieving properties of zeolitic imidazolate framework-8. The journal of physical chemistry letters, 2012. **3**(16): p. 2130-2134.

18. Park, Y.-K., et al., Catalytic cracking of lower-valued hydrocarbons for producing light olefins. Catalysis surveys from Asia, 2010. **14**(2): p. 75-84.

19. Syah, R., et al., The Economic Evaluation of Methanol and Propylene Production from Natural Gas at Petrochemical Industries in Iran. Sustainability, 2021. **13**(17): p. 9990.

20. Degnan Jr, T.F., C.M. Smith, and C.R. Venkat, Alkylation of aromatics with ethylene and propylene: recent developments in commercial processes. Applied catalysis A: general, 2001. **221**(1-2): p. 283-294.

21. Akah, A. and M. Al-Ghrami, Maximizing propylene production via FCC technology. Applied Petrochemical Research, 2015. **5**(4): p. 377-392.
22. https://www.statista.com/statistics/1099349/global-polypropylene-demand/.
23. https://www.nexanteca.com/reports/evolving-propylene-sources-solution-supply-shortages.
24. Pan, Y., et al., Effective separation of propylene/propane binary mixtures by ZIF-8 membranes. Journal of Membrane Science, 2012. **390**: p. 93-98.
25. Ravanchi, M.T., T. Kaghazchi, and A. Kargari, Facilitated transport separation of propylene–propane: experimental and modeling study. Chemical Engineering and Processing: Process Intensification, 2010. **49**(3): p. 235-244.
26. Wade, N.M., Distillation plant development and cost update. Desalination, 2001. **136**(1-3): p. 3-12.
27. Kiss, A.A., Distillation technology–still young and full of breakthrough opportunities. Journal of Chemical Technology & Biotechnology, 2014. **89**(4): p. 479-498.
28. Eom, Y., et al., CO 2 Absorption Characteristics of Physical Solvent at High Pressure. Transactions of the Korean hydrogen and new energy society, 2013. **24**(4): p. 334-339.
29. Parshetti, G.K., S. Chowdhury, and R. Balasubramanian, Biomass derived low-cost microporous adsorbents for efficient CO2 capture. Fuel, 2015. **148**: p. 246-254.
30. Zhou, W., et al., Electrochemical regeneration of carbon-based adsorbents: a review of regeneration mechanisms, reactors, and future prospects. Chemical Engineering Journal Advances, 2021. **5**: p. 100083.
31. Lee, M.J., H.T. Kwon, and H.-K. Jeong, Defect-dependent stability of highly propylene-selective zeolitic-imidazolate framework ZIF-8 membranes. Journal of Membrane Science, 2017. **529**: p. 105-113.
32. Zhou, S., et al., Paralyzed membrane: Current-driven synthesis of a metal-organic framework with sharpened propene/propane separation. Science advances, 2018. **4**(10): p. eaau1393.

33. Merkel, T.C., et al., Separation of Olefin/Paraffin Mixtures with Carrier Facilitated Membrane Final Report, E. United States. Department Of Energy. Office Of Energy and E. Renewable, Editors. 2007, Membrane Technology and Research, Inc., Menlo Park, CA.

34. Majumdar, S., Novel Membranes for Olefin/Paraffin Separation Final Report. 2016, Compact Membrane Systems, Inc., Newport, DE (United States).

35. Miranda, D.M.V.d., et al., A bibliometric survey of Paraffin/Olefin separation using membranes. Membranes, 2019. **9**(12): p. 157.

36. Kang, Y., K. Cha, and S. Kang, The facilitated olefin transporting composite membrane comprising nanosized silver metal and ionic liquid. 2007, KR 10-2006-0037430, May 3.

37. Burns, R.L. and W.J. Koros, Defining the challenges for C3H6/C3H8 separation using polymeric membranes. Journal of Membrane Science, 2003. **211**(2): p. 299-309.

38. Staudt-Bickel, C. and W.J. Koros, Olefin/paraffin gas separations with 6FDA-based polyimide membranes. Journal of Membrane Science, 2000. **170**(2): p. 205-214.

39. Giannakopoulos, I.G. and V. Nikolakis, Separation of propylene/propane mixtures using faujasite-type zeolite membranes. Industrial & engineering chemistry research, 2005. **44**(1): p. 226-230.

40. Ma, X., et al., Propylene/propane mixture separation characteristics and stability of carbon molecular sieve membranes. Industrial & Engineering Chemistry Research, 2015. **54**(40): p. 9824-9831.

41. Hayashi, J.-i., et al., Separation of ethane/ethylene and propane/propylene systems with a carbonized BPDA− pp ‘ODA polyimide membrane. Industrial & engineering chemistry research, 1996. **35**(11): p. 4176-4181.

42. Hara, N., et al., Diffusive separation of propylene/propane with ZIF-8 membranes. Journal of Membrane Science, 2014. **450**: p. 215-223.

43. Andres-Garcia, E., et al., Cation influence in adsorptive propane/propylene separation in ZIF-8 (SOD) topology. Chemical Engineering Journal, 2019. **371**: p. 848-856.

44. Wu, X., et al., Force field for ZIF-8 flexible frameworks: atomistic simulation of adsorption, diffusion of pure gases as CH 4, H 2, CO 2 and N 2. RSC Advances, 2014. **4**(32): p. 16503-16511.

45. Huang, L., et al., Porous and flexible membrane derived from ZIF-8-decorated hyphae for outstanding adsorption of Pb2+ ion. Journal of Colloid and Interface Science, 2020. **565**: p. 465-473.

46. Krokidas, P., et al., Molecular simulation studies of the diffusion of methane, ethane, propane, and propylene in ZIF-8. The Journal of Physical Chemistry C, 2015. **119**(48): p. 27028-27037.

47. Fairen-Jimenez, D., et al., Opening the gate: framework flexibility in ZIF-8 explored by experiments and simulations. Journal of the American Chemical Society, 2011. **133**(23): p. 8900-8902.

48. Li, J., et al., Synthesis of tubular ZIF-8 membranes for propylene/propane separation under high-pressure. Journal of Membrane Science, 2020. **595**: p. 117503.

49. Kwon, H.T. and H.-K. Jeong, Improving propylene/propane separation performance of Zeolitic-Imidazolate framework ZIF-8 Membranes. Chemical Engineering Science, 2015. **124**: p. 20-26.

50. Tanaka, S., et al., Grain size control of ZIF-8 membranes by seeding-free aqueous synthesis and their performances in propylene/propane separation. Journal of Membrane Science, 2017. **544**: p. 306-311.

51. He, M., et al., A fast in situ seeding route to the growth of a zeolitic imidazolate framework-8/AAO composite membrane at room temperature. RSC Advances, 2014. **4**(15): p. 7634-7639.

52. Yoo, Y. and H.-K. Jeong, Rapid fabrication of metal organic framework thin films using microwave-induced thermal deposition. Chemical communications, 2008(21): p. 2441-2443.

53. Maksoud, M., et al., Efficient growth of sub-micrometric MOF crystals inside the channels of AAO membranes. Journal of Materials Chemistry A, 2013. **1**(11): p. 3688-3693.

54. Meyer, L.V., et al., In situ growth of luminescent MOF thin films of Sr/Eu (II)-imidazolate on functionalized nanostructured alumina. CrystEngComm, 2013. **15**(45): p. 9382-9386.

55. Yim, C., et al., CO 2-selective nanoporous metal-organic framework microcantilevers. Scientific reports, 2015. **5**(1): p. 1-8.

56. Zhang, S., et al., Zeolite-Like Metal Organic Framework (ZMOF) with a rho Topology for a CO2 Cycloaddition to Epoxides. ACS Sustainable Chemistry & Engineering, 2020. **8**(18): p. 7078-7086.

57. Dai, H., et al., Recent advances on ZIF-8 composites for adsorption and photocatalytic wastewater pollutant removal: Fabrication, applications and perspective. Coordination Chemistry Reviews, 2021. **441**: p. 213985.

58. Hayashi, M., et al., ZIF-8 Membrane Permselectivity Modification by Manganese (II) Acetylacetonate Vapor Treatment. Angewandte Chemie International Edition, 2021. **60**(17): p. 9316-9320.

59. Huang, A., W. Dou, and J.r. Caro, Steam-stable zeolitic imidazolate framework ZIF-90 membrane with hydrogen selectivity through covalent functionalization. Journal of the American Chemical Society, 2010. **132**(44): p. 15562-15564.

60. Kim, J. and M.R. Othman, Research trend on ZIF-8 membranes for propylene separation. Membrane Journal, 2019. **29**(2): p. 67-79.

61. Akti, F., Effect of kaolin on aluminum loading success in synthesis of Al-SBA-15 catalysts: Activity test in ethanol dehydration reaction. Microporous and Mesoporous Materials, 2020. **294**: p. 109894.

62. Eum, K., et al., ZIF-8 Membrane Separation Performance Tuning by Vapor Phase Ligand Treatment. Angewandte Chemie, 2019. **131**(46): p. 16542-16546.

63. Bux, H., et al., Zeolitic imidazolate framework membrane with molecular sieving properties by microwave-assisted solvothermal synthesis. Journal of the American Chemical Society, 2009. **131**(44): p. 16000-16001.

64. Kwon, H.T. and H.-K. Jeong, In situ synthesis of thin zeolitic–imidazolate framework ZIF-8 membranes exhibiting exceptionally high propylene/propane separation. Journal of the American Chemical Society, 2013. **135**(29): p. 10763-10768.

65. Shah, M., et al., One step in situ synthesis of supported zeolitic imidazolate framework ZIF-8 membranes: Role of sodium formate. Microporous and mesoporous materials, 2013. **165**: p. 63-69.

66. Huang, A., et al., Molecular-sieve membrane with hydrogen permselectivity: ZIF-22 in LTA topology prepared with 3-aminopropyltriethoxysilane as covalent linker. Angewandte Chemie, 2010. **122**(29): p. 5078-5081.

67. Liu, Q., et al., Bio-inspired polydopamine: a versatile and powerful platform for covalent synthesis of molecular sieve membranes. Journal of the American Chemical Society, 2013. **135**(47): p. 17679-17682.

68. Pan, Y., et al., Rapid synthesis of zeolitic imidazolate framework-8 (ZIF-8) nanocrystals in an aqueous system. Chemical Communications, 2011. **47**(7): p. 2071-2073.

69. Pan, Y., et al., Tuning the crystal morphology and size of zeolitic imidazolate framework-8 in aqueous solution by surfactants. CrystEngComm, 2011. **13**(23): p. 6937-6940.

70. Pan, Y. and Z. Lai, Sharp separation of C2/C3 hydrocarbon mixtures by zeolitic imidazolate framework-8 (ZIF-8) membranes synthesized in aqueous solutions. Chemical Communications, 2011. **47**(37): p. 10275-10277.

71. Pan, Y., et al., Improved ZIF-8 membrane: effect of activation procedure and determination of diffusivities of light hydrocarbons. Journal of Membrane Science, 2015. **493**: p. 88-96.

72. Kwon, H.T. and H.-K. Jeong, Highly propylene-selective supported zeolite-imidazolate framework (ZIF-8) membranes synthesized by rapid microwave-assisted seeding and secondary growth. Chemical Communications, 2013. **49**(37): p. 3854-3856.

73. Schejn, A., et al., Controlling ZIF-8 nano-and microcrystal formation and reactivity through zinc salt variations. CrystEngComm, 2014. **16**(21): p. 4493-4500.

74. Yao, J., et al., Contra-diffusion synthesis of ZIF-8 films on a polymer substrate. Chemical Communications, 2011. **47**(9): p. 2559-2561.

75. Jang, E., et al., Formation of ZIF-8 membranes inside porous supports for improving both their H2/CO2 separation performance and thermal/mechanical stability. Journal of Membrane Science, 2017. **540**: p. 430-439.

76. Hara, N., et al., Effect of temperature on synthesis of ZIF-8 membranes for propylene/propane separation by counter diffusion method. Journal of the Japan Petroleum Institute, 2015. **58**(4): p. 237-244.

77. Hara, N., et al., Thickness reduction of the zeolitic imidazolate framework-8 membrane by controlling the reaction rate during the membrane preparation. Journal of Chemical Engineering of Japan, 2014. **47**(10): p. 770-776.

78. Dang, Y.T., et al., Microwave-assisted synthesis of nano Hf-and Zr-based metal-organic frameworks for enhancement of curcumin adsorption. Microporous and Mesoporous Materials, 2020. **298**: p. 110064.

79. Zhang, C., et al., Computational characterization of defects in metal–organic frameworks: Spontaneous and water-induced point defects in ZIF-8. The journal of physical chemistry letters, 2016. **7**(3): p. 459-464.

80. Sutrisna, P.D., et al., A mini-review and recent outlooks on the synthesis and applications of zeolite imidazolate framework-8 (ZIF-8) membranes on polymeric substrate. Journal of Chemical Technology & Biotechnology, 2020. **95**(11): p. 2767-2774.

81. Deria, P., et al., Beyond post-synthesis modification: evolution of metal–organic frameworks via building block replacement. Chemical Society Reviews, 2014. **43**(16): p. 5896-5912.

82. Wei, R., et al., Aqueously cathodic deposition of ZIF-8 membranes for superior propylene/propane separation. Advanced Functional Materials, 2020. **30**(7): p. 1907089.

83. Li, Z., et al., The OncoPPi network of cancer-focused protein–protein interactions to inform biological insights and therapeutic strategies. Nature communications, 2017. **8**(1): p. 1-14.

84. Ma, X., et al., Zeolitic imidazolate framework membranes made by ligand-induced permselectivation. Science, 2018. **361**(6406): p. 1008-1011.

85. Drobek, M., et al., An innovative approach for the preparation of confined ZIF-8 membranes by conversion of ZnO ALD layers. Journal of Membrane Science, 2015. **475**: p. 39-46.

86. Stassen, I., et al., Chemical vapour deposition of zeolitic imidazolate framework thin films. Nature materials, 2016. **15**(3): p. 304-310.

87. Tanaka, S., et al., Vapor-phase synthesis of ZIF-8 MOF thick film by conversion of ZnO nanorod array. Langmuir, 2018. **34**(24): p. 7028-7033.

88. Ascrizzi, R., et al., Geographical patterns of in vivo spontaneously emitted volatile organic compounds in Salvia species. Microchemical Journal, 2017. **133**: p. 13-21.

89. Wang, Y., et al., Preparation of ZIF-8 membranes on porous ZnO hollow fibers by a facile ZnO-induced method. Industrial & Engineering Chemistry Research, 2020. **59**(35): p. 15576-15585.

90. Kwon, H.T., et al., Defect-induced ripening of zeolitic-imidazolate framework ZIF-8 and its implication to vapor-phase membrane synthesis. Chemical Communications, 2016. **52**(78): p. 11669-11672.

91. Baker, R.W., Future directions of membrane gas separation technology. Industrial & engineering chemistry research, 2002. **41**(6): p. 1393-1411.

92. Eldridge, R.B., Olefin/paraffin separation technology: a review. Industrial & engineering chemistry research, 1993. **32**(10): p. 2208-2212.

93. Mauhar, S.M., B. Barjaktarovic, and M. Sovilj, Optimization of propylene-propane distillation process. Chem. Pap, 2004. **58**(6): p. 386-390.

94. Melgar, V.M.A., J. Kim, and M.R. Othman, Zeolitic imidazolate framework membranes for gas separation: A review of synthesis methods and gas separation performance. Journal of Industrial and Engineering Chemistry, 2015. **28**: p. 1-15.

95. Pimentel, B.R., et al., Zeolitic imidazolate frameworks: next-generation materials for energy-efficient gas separations. ChemSusChem, 2014. **7**(12): p. 3202-3240.

96. Yim, C., et al., CO2-selective nanoporous metal-organic framework microcantilevers. Scientific reports, 2015. **5**(1): p. 1-8.

97. Babu, D.J., et al., Restricting lattice flexibility in polycrystalline metal–organic framework membranes for carbon capture. Advanced Materials, 2019. **31**(28): p. 1900855.

98. He, G., et al., Electrophoretic nuclei assembly for crystallization of high-performance membranes on unmodified supports. Advanced Functional Materials, 2018. **28**(20): p. 1707427.

99. Hao, J., et al., Synthesis of high-performance polycrystalline metal–organic framework membranes at room temperature in a few minutes. Journal of Materials Chemistry A, 2020. **8**(16): p. 7633-7640.

100. Caro, J., Are MOF membranes better in gas separation than those made of zeolites? Current Opinion in Chemical Engineering, 2011. **1**(1): p. 77-83.

101. Li, L., et al., Infiltration of precursors into a porous alumina support for ZIF-8 membrane synthesis. Microporous and mesoporous materials, 2013. **168**: p. 15-18.

102. Cravillon, J., et al., Controlling zeolitic imidazolate framework nano-and microcrystal formation: insight into crystal growth by time-resolved in situ static light scattering. Chemistry of Materials, 2011. **23**(8): p. 2130-2141.

103. Kim, S.-J., et al., Ion exchange of zeolite membranes by a vacuum ‘flow-through’technique. Microporous and Mesoporous Materials, 2015. **203**: p. 170-177.

104. Ray, S.S. and M. Okamoto, Polymer/layered silicate nanocomposites: a review from preparation to processing. Progress in polymer science, 2003. **28**(11): p. 1539-1641.

105. Nishihama, S., Y. Tsutsumi, and K. Yoshizuka, Separation of tetramethyl ammonium hydroxide using an MFI-type zeolite-coated membrane. Separation and Purification Technology, 2013. **120**: p. 129-133.

106. Rangnekar, N., et al., Zeolite membranes–a review and comparison with MOFs. Chemical Society Reviews, 2015. **44**(20): p. 7128-7154.

107. Jentys, A., et al., Adsorption of water on ZSM 5 zeolites. The Journal of Physical Chemistry, 1989. **93**(12): p. 4837-4843.

108. Liédana, N., et al., CAF@ ZIF-8: one-step encapsulation of caffeine in MOF. ACS applied materials & interfaces, 2012. **4**(9): p. 5016-5021.

109. Xue, G., Q. Dai, and S. Jiang, Chemical reactions of imidazole with metallic silver studied by the use of SERS and XPS techniques. Journal of the American Chemical Society, 1988. **110**(8): p. 2393-2395.

110. Tian, F., D.F. Taber, and A.V. Teplyakov, –NH–Termination of the Si (111) Surface by Wet Chemistry. Journal of the American Chemical Society, 2011. **133**(51): p. 20769-20777.

111. Matloob, M.H. and M.W. Roberts, Electron spectroscopic study of nitrogen species adsorbed on copper. Journal of the Chemical Society, Faraday Transactions 1: Physical Chemistry in Condensed Phases, 1977. **73**: p. 1393-1405.

112. Dedryvère, R., et al., Characterization of lithium alkyl carbonates by X-ray photoelectron spectroscopy: experimental and theoretical study. The Journal of Physical Chemistry B, 2005. **109**(33): p. 15868-15875.

113. Cacho-Bailo, F., et al., ZIF-8 continuous membrane on porous polysulfone for hydrogen separation. Journal of Membrane Science, 2014. **464**: p. 119-126.

114. Ordonez, M.J.C., et al., Molecular sieving realized with ZIF-8/Matrimid® mixed-matrix membranes. Journal of Membrane Science, 2010. **361**(1-2): p. 28-37.

115. Cheng, P. and Y.H. Hu, H2O-functionalized zeolitic Zn (2-methylimidazole) 2 framework (ZIF-8) for H2 storage. The Journal of Physical Chemistry C, 2014. **118**(38): p. 21866-21872.

116. Duke, M.C., et al., Structural effects on SAPO-34 and ZIF-8 materials exposed to seawater solutions, and their potential as desalination membranes. Desalination, 2016. **377**: p. 128-137.

117. Park, S. and H.-K. Jeong, In-situ linker doping as an effective means to tune zeolitic-imidazolate framework-8 (ZIF-8) fillers in mixed-matrix membranes for propylene/propane separation. Journal of Membrane Science, 2020. **596**: p. 117689.

118. Krokidas, P., et al., On the efficient separation of gas mixtures with the mixed-linker zeolitic-imidazolate framework-7-8. ACS applied materials & interfaces, 2018. **10**(46): p. 39631-39644.

119. Song, E., et al., Improved propylene/propane separation performance under high temperature and pressures on in-situ ligand-doped ZIF-8 membranes. Journal of Membrane Science, 2021. **617**: p. 118655.

120. Cacho-Bailo, F., et al., ZIF-8 continuous membrane on porous polysulfone for hydrogen separation. J. Membr. Sci., 2014. **464**: p. 119-126.

121. Baker, R., Membrane technology in the chemical industry: future directions. Membrane Technology: in the Chemical Industry, 2001: p. 268-295.

122. Millward, A.R. and O.M. Yaghi, Metal− organic frameworks with exceptionally high capacity for storage of carbon dioxide at room temperature. Journal of the American Chemical Society, 2005. **127**(51): p. 17998-17999.

123. Kwon, H.T., et al., Heteroepitaxially grown zeolitic imidazolate framework membranes with unprecedented propylene/propane separation performances. Journal of the American Chemical Society, 2015. **137**(38): p. 12304-12311.

124. George, S.M., Atomic layer deposition: an overview. Chemical reviews, 2010. **110**(1): p. 111-131.

125. Weber, M., et al., Atomic layer deposition for membranes: basics, challenges, and opportunities. Chemistry of Materials, 2018. **30**(21): p. 7368-7390.

126. Palmstrom, A.F., P.K. Santra, and S.F. Bent, Atomic layer deposition in nanostructured photovoltaics: tuning optical, electronic and surface properties. Nanoscale, 2015. **7**(29): p. 12266-12283.

127. Ponraj, J.S., G. Attolini, and M. Bosi, Review on atomic layer deposition and applications of oxide thin films. Critical reviews in solid state and materials sciences, 2013. **38**(3): p. 203-233.

128. Tynell, T. and M. Karppinen, Atomic layer deposition of ZnO: a review. Semiconductor Science and Technology, 2014. **29**(4): p. 043001.

129. Weber, M., et al., Atomic layer deposition (ALD) on inorganic or polymeric membranes. Journal of Applied Physics, 2019. **126**(4): p. 041101.

130. Chen, H., et al., Ceramic tubular nanofiltration membranes with tunable performances by atomic layer deposition and calcination. Journal of Membrane Science, 2017. **528**: p. 95-102.

131. Shang, R., et al., Atmospheric pressure atomic layer deposition for tight ceramic nanofiltration membranes: Synthesis and application in water purification. Journal of Membrane Science, 2017. **528**: p. 163-170.

132. Vega, V., et al., Diffusive transport through surface functionalized nanoporous alumina membranes by atomic layer deposition of metal oxides. Journal of industrial and engineering chemistry, 2017. **52**: p. 66-72.

133. Dangwal, S., et al., ZIF-8 membranes supported on silicalite-seeded substrates for propylene/propane separation. Journal of Membrane Science, 2021. **626**: p. 119165.

134. Song, Z., et al., TiO2 nanofiltration membranes prepared by molecular layer deposition for water purification. Journal of Membrane Science, 2016. **510**: p. 72-78.

135. Xiao, Z., et al., Electrical and structural properties of p-type ZnO: N thin films prepared by plasma enhanced chemical vapour deposition. Semiconductor science and technology, 2005. **20**(8): p. 796.

136. Chen, H., et al., Investigation on hydrogenation of metal–organic frameworks HKUST-1, MIL-53, and ZIF-8 by hydrogen spillover. The Journal of Physical Chemistry C, 2013. **117**(15): p. 7565-7576.

137. Sholl, D.S. and R.P. Lively, Defects in metal–organic frameworks: challenge or opportunity? The journal of physical chemistry letters, 2015. **6**(17): p. 3437-3444.

138. Venna, S.R., J.B. Jasinski, and M.A. Carreon, Structural evolution of zeolitic imidazolate framework-8. Journal of the American Chemical Society, 2010. **132**(51): p. 18030-18033.

139. Venna, S.R. and M.A. Carreon, Highly permeable zeolite imidazolate framework-8 membranes for CO2/CH4 separation. Journal of the American Chemical Society, 2010. **132**(1): p. 76-78.

140. Cravillon, J., et al., Rapid room-temperature synthesis and characterization of nanocrystals of a prototypical zeolitic imidazolate framework. Chemistry of Materials, 2009. **21**(8): p. 1410-1412.

141. Tran, N.T., J. Kim, and M.R. Othman, Microporous ZIF-8 membrane prepared from secondary growth for improved propylene permeance and selectivity. Microporous and Mesoporous Materials, 2019. **285**: p. 178-184.

142. Yu, J., et al., ZIF-8 membranes with improved reproducibility fabricated from sputter-coated ZnO/alumina supports. Chemical Engineering Science, 2016. **141**: p. 119-124.

143. Tran, N.T., J. Kim, and M.R. Othman, Microporous ZIF-8 and ZIF-67 membranes grown on mesoporous alumina substrate for selective propylene transport. Separation and Purification Technology, 2020. **233**: p. 116026.

144. Liu, D., et al., Gas transport properties and propylene/propane separation characteristics of ZIF-8 membranes. Journal of membrane science, 2014. **451**: p. 85-93.

145. Ramu, G., M. Lee, and H.-K. Jeong, Effects of zinc salts on the microstructure and performance of zeolitic-imidazolate framework ZIF-8 membranes for propylene/propane separation. Microporous and Mesoporous Materials, 2018. **259**: p. 155-162.

146. Lee, M.J., et al., Ultrathin zeolitic-imidazolate framework ZIF-8 membranes on polymeric hollow fibers for propylene/propane separation. Journal of Membrane Science, 2018. **559**: p. 28-34.

147. Sun, J., C. Yu, and H.-K. Jeong, Propylene-selective thin zeolitic imidazolate framework membranes on ceramic tubes by microwave seeding and solvothermal secondary growth. Crystals, 2018. **8**(10): p. 373.

148. Hua, J., et al., Improved C3H6/C3H8 separation performance on ZIF-8 membranes through enhancing PDMS contact-dependent confinement effect. Journal of Membrane Science, 2021. **636**: p. 119613.

149. Sheng, L., et al., Enhanced C 3 H 6/C 3 H 8 separation performance on MOF membranes through blocking defects and hindering framework flexibility by silicone rubber coating. Chemical Communications, 2017. **53**(55): p. 7760-7763.

150. Torres Galvis, H.M. and K.P. de Jong, Catalysts for production of lower olefins from synthesis gas: a review. ACS catalysis, 2013. **3**(9): p. 2130-2149.

151. Alcheikhhamdon, Y., et al., Propylene-propane separation using Zeolitic-Imidazolate Framework (ZIF-8) membranes: Process techno-commercial evaluation. Journal of Membrane Science, 2019. **591**: p. 117252.

152. Li, J.-R., R.J. Kuppler, and H.-C. Zhou, Selective gas adsorption and separation in metal–organic frameworks. Chemical Society Reviews, 2009. **38**(5): p. 1477-1504.

153. Yeo, Z.Y., et al., An overview: synthesis of thin films/membranes of metal organic frameworks and its gas separation performances. RSC Advances, 2014. **4**(97): p. 54322-54334.

154. Wang, X., et al., Formation of continuous and highly permeable ZIF-8 membranes on porous alumina and zinc oxide hollow fibers. Chemical Communications, 2016. **52**(92): p. 13448-13451.

155. Li, W., et al., Ultrathin metal–organic framework membrane production by gel–vapour deposition. Nature communications, 2017. **8**(1): p. 1-8.

156. Reif, B., et al., Solvent-free transformation of spray coated ZnO layers to ZIF-8 membranes. Microporous and Mesoporous Materials, 2019. **276**: p. 29-40.

157. Cai, J., et al., A revisit to atomic layer deposition of zinc oxide using diethylzinc and water as precursors. Journal of Materials Science, 2019. **54**(7): p. 5236-5248.

158. Chernova, E., et al., Enhanced gas separation factors of microporous polymer constrained in the channels of anodic alumina membranes. Scientific reports, 2016. **6**(1): p. 1-8.

159. Wang, Y., et al., Growth of ZIF-8 membranes on ceramic hollow fibers by conversion of zinc oxide particles. Industrial & Engineering Chemistry Research, 2019. **58**(42): p. 19511-19518.

160. Lee, J.H., et al., Zeolitic imidazolate framework ZIF-8 films by ZnO to ZIF-8 conversion and their usage as seed layers for propylene-selective ZIF-8 membranes. Journal of Industrial and Engineering Chemistry, 2019. **72**: p. 374-379.

161. Patel, Y., et al., Development of nanoporous AAO membrane for nano filtration using the acoustophoresis method. Sensors, 2020. **20**(14): p. 3833.

162. Maghsodi, A., et al., Optimization of effective parameters in the synthesis of nanopore anodic aluminum oxide membrane and arsenic removal by prepared magnetic iron oxide nanoparicles in anodic aluminum oxide membrane via ultrasonic-hydrothermal method. Ultrasonics sonochemistry, 2018. **48**: p. 441-452.

163. Tuncel, D. and A. Ökte, Improved adsorption capacity and photoactivity of ZnO-ZIF-8 nanocomposites. Catalysis Today, 2021. **361**: p. 191-197.

164. Poinern, G.E.J., N. Ali, and D. Fawcett, Progress in nano-engineered anodic aluminum oxide membrane development. Materials, 2011. **4**(3): p. 487-526.

165. Prashanth, P., et al., Synthesis, characterizations, antibacterial and photoluminescence studies of solution combustion-derived α-Al2O3 nanoparticles. Journal of Asian Ceramic Societies, 2015. **3**(3): p. 345-351.

166. Gangwar, J., et al., Phase dependent thermal and spectroscopic responses of Al 2 O 3 nanostructures with different morphogenesis. Nanoscale, 2015. **7**(32): p. 13313-13344.

167. Hu, Y., et al., In situ high pressure study of ZIF-8 by FTIR spectroscopy. Chemical Communications, 2011. **47**(47): p. 12694-12696.

168. Cheetham, A.K., C. Rao, and R.K. Feller, Structural diversity and chemical trends in hybrid inorganic–organic framework materials. Chemical communications, 2006(46): p. 4780-4795.

169. Zhang, Z., et al., Improvement of CO2 adsorption on ZIF-8 crystals modified by enhancing basicity of surface. Chemical Engineering Science, 2011. **66**(20): p. 4878-4888.

170. Nordin, N.A.H.M., et al., Facile modification of ZIF-8 mixed matrix membrane for CO 2/CH 4 separation: synthesis and preparation. Rsc Advances, 2015. **5**(54): p. 43110-43120.

171. Hara, N., et al., ZIF-8 membranes prepared at miscible and immiscible liquid–liquid interfaces. Microporous and Mesoporous Materials, 2015. **206**: p. 75-80.

172. Okazaki, M. and S. Kimura, Scale formation on reverse-osmosis membranes. Journal of chemical engineering of Japan, 1984. **17**(2): p. 145-151.

173. Shah, M.N., et al., An unconventional rapid synthesis of high performance metal–organic framework membranes. Langmuir, 2013. **29**(25): p. 7896-7902.

174. Eum, K., et al., ZIF-8 membranes via interfacial microfluidic processing in polymeric hollow fibers: efficient propylene separation at elevated pressures. ACS applied materials & interfaces, 2016. **8**(38): p. 25337-25342.

175. Lee, M.J., H.T. Kwon, and H.K. Jeong, High-flux zeolitic imidazolate framework membranes for propylene/propane separation by postsynthetic linker exchange. Angewandte Chemie International Edition, 2018. **57**(1): p. 156-161.

176. James, J.B., et al., Postsynthetic modification of ZIF-8 membranes via membrane surface ligand exchange for light hydrocarbon gas separation enhancement. ACS Applied Materials & Interfaces, 2019. **12**(3): p. 3893-39.

VITA

Anil Ronte

Candidate for the Degree of

Doctor of Philosophy

Dissertation: ZEOLITIC IMIDAZOLE FRAMEWORK ZIF-8 MEMBRANES FOR ENHANCED PROPYLENE/PROPANE SEPARATION

Major Field: Chemical Engineering

Biographical:

Education:

Completed the requirements for the Doctor of Philosophy in Chemical Engineering at Oklahoma State University, Stillwater, Oklahoma in May, 2022.

Completed the requirements for the Master of Technology in Chemical Engineering at University College of Technology, Hyderabad, India in 2017.

Completed the requirements for the Bachelor of Technology in Chemical Engineering at Chaitanya Bharathi Institute of Technology, Hyderabad, India in 2014.

Experience:

Graduate Research and Teaching Assistant, Oklahoma State University (Aug 2018 – May 2022)
Research Assistant, CSIR-IICT, Hyderabad, India. (May 2017 – May 2018).

Professional Memberships:

American Institute of Chemical Engineers (AIChE).